DEVELOPMENT OF A DIRECT PHOTOCHEMICAL METHOD FOR THE GENERATION OF BIOMOLECULAR INTERFACES FOR APPLICATIONS IN LEUKOCYTE BIOLOGY

BY

CHRISTINE TOH HERMAN

DISSERTATION

Submitted in partial fulfillment of the requirements
for the degree of Doctor of Philosophy in Chemistry
in the Graduate College of the
University of Illinois at Urbana-Champaign, 2012

Urbana, Illinois

Doctoral Committee

Professor Ryan C. Bailey, Chair
Professor Paul J. Hergenrother
Professor Paul J. A. Kenis
Professor Scott K. Silverman
Professor Fei Wang

Abstract

Methods for generating surface-immobilized biomolecular patterns and gradients have provided invaluable insight into the molecular basis of numerous complex biological processes. Herein, we describe the development of a general, photochemical method for creating biointerface substrates presenting single- and multi-component biomolecular patterns and gradients. In our approach, the generation of a light density gradient across a photoactive benzophenone monolayer on glass results in covalent attachment of solution-phase biomolecules onto the surface. This simple, direct and molecularly general approach was used to generate surface-immobilized biomolecular gradient substrates for proof-of-principle biomolecular photopatterning demonstrations, as well as investigations of multi-parameter cell-substrate interactions and fundamental leukocyte biology studies. Substrates tailored to present P-selectin or E-selectin, which are proteins expressed on the inflamed endothelium, were applied to flow assays with neutrophils isolated from whole blood for investigating the effects of bromelain, an alternative anti-inflammatory treatment, on neutrophil recruitment *in vitro* under conditions of physiological shear stress. Beyond applications in leukocyte biology, this methodology for biomolecular substrate generation can serve as an enabling tool for investigating the molecular basis of cell migration and polarization in response to immobilized proteins, and for systematically addressing the combined effects of multiple stimuli, such as immobilized biomolecule density, mechanical cues, and shear stress on cell behavior.

Acknowledgements

This work was supported by the Camille and Henry Dreyfus Foundation, the Roy J. Carver Charitable Trust, the National Science Foundation Graduate Research Fellowship Program (NSF GRFP), and the National Institutes of Health National Research Service Award (NIH NRSA) through the National Center for Complementary and Alternative Medicine (NCCAM Award Number F31AT006286). The content is solely the responsibility of the authors and does not necessarily represent the official views of the National Center for Complementary & Alternative Medicine, the National Institutes of Health, or the National Science Foundation. This research was carried out in part in the Institute for Genomic Biology, Core Facilities, University of Illinois, as well as the Frederick Seitz Materials Research Laboratory Central Facilities, University of Illinois, which is partially supported by the U.S. Department of Energy under Grants DE-FG02-07ER46453 and DE-FG02-07ER46471.

I would like to thank my adviser, Professor Ryan C. Bailey, for his support, encouragement, and dedication to my research progress and professional development. I would also like to thank my thesis committee members: Professors Hergenrother, Kenis, Silverman, and Wang.

I would like to acknowledge the members of the Bailey Lab, past and present. I have had an awesome time working with such wonderful lab mates and friends. Special thanks to gradient project members: Teresa Martin, Madeline Michael, Ted Limpoco, Jessica Banks, Gregory Potts, and Aurora Turgeon.

A special thanks to my parents who have encouraged me since I was little to give my heart to whatever I do, and also to my husband and best friend, Geoffrey, for his love and support. I thank my siblings and all my extended family for their friendship and love. I'm also so thankful for all the friends I've made while studying at the University of Illinois.

I thank God for creating this mysterious universe and giving me the privilege of exploring it with the tools of science.

Table of Contents

Chapter 1

Introduction and Background

Cellular adhesive microenvironments are enormously complex and dynamic. The interplay between the density and spatial distribution of many distinct biomolecules determines the response and behavior of cells *in vivo*. To better understand the nature of these complex physiological processes that consist of interfacial recognition events, scientists have utilized expertise in molecular synthesis and design to control and influence the behavior of cells,[1] resulting in well-defined surfaces presenting biologically relevant ligands at distinct spatial locations.[3] Methods for the generation of substrates presenting biomolecules in a spatially controlled manner are therefore enabling tools for applications in fundamental biological studies, as well as biosensor systems, microarray technologies, and biointerface science. My doctoral research has focused on the development of a general method for creating single- and multi-component biomolecular pattern and gradient substrates for applications in leukocyte biology. The biomolecular patterns and gradients and their subsequent biological applications presented herein demonstrate the potential of the developed biointerface methodology to help shed light on the mechanism by which the activated endothelium recruits leukocytes to the blood vessel wall during the first steps of the inflammatory response (Figure 1.1).

This introductory chapter consists of an overview of the various components that make up this interdisciplinary work. An overview of the different strategies that have been developed to generate biomolecular substrates is presented, including the simple, direct and molecularly general approach that utilizes the photoactive properties of benzophenone (BP) to generate quantifiable surface-immobilized biomolecular patterns and gradients. Next, a brief review of the current molecular understanding of the process of leukocyte recruitment and inflammation is presented, including an introduction to bromelain, a natural anti-inflammatory therapeutic, which is the focus the biological applications of the described biomolecular substrate generation

methodology. Finally, the various *in vivo* and *in vitro* approaches that have been taken to study leukocyte recruitment is discussed, and a case is made for why the BP-mediated biomolecular substrate generation methodology is an enabling tool for investigating the molecular basis of leukocyte recruitment and investigating the potential mechanisms for bromelain's anti-inflammatory activity.

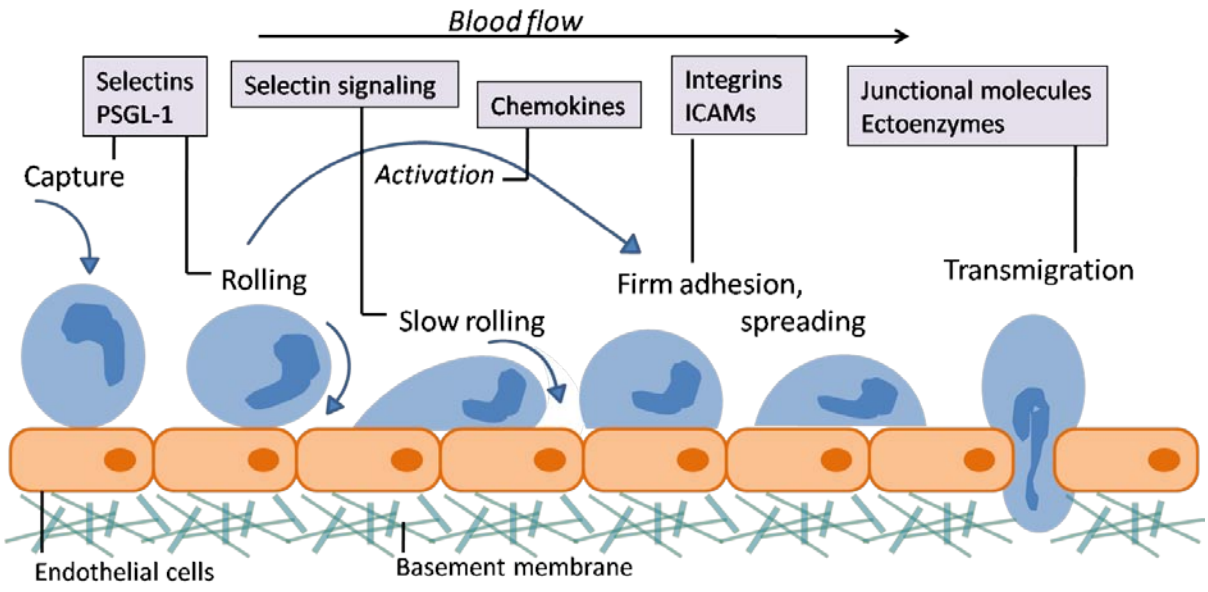

Figure 1.1 Schematic representation of the leukocyte adhesion cascade. Cytokine-activated endothelial cells present selectins, chemokines, and intercellular adhesion molecules (ICAMs) that enable leukocyte capture, rolling, and firm adhesion. Adapted from reference.[2]

1.1 Strategies for generating surface-immobilized biomolecular patterns and gradients

Numerous methods have been previously reported for the generation of substrates presenting immobilized biomolecules. These include the use of microfluidics followed by surface attachment,[4] electrochemical desorption of self-assembled monolayers on gold,[5] photochemical surface deprotection to reveal reactive functional groups,[6] and diffusion-guided surface adsorption.[7] Biomolecular gradients generated with these methods have been implemented in a variety of applications including biointerface science,[8] microarray technology,[9] biosensors,[10] microfluidics/point-of-care applications,[11] and nanotechnology.[12] Tools for generating substrates with immobilized biomolecules have been rapidly developing

due to a growing interest in exercising spatio-temporal control over protein patterns,[1] characterizing immobilized protein site density for quantitative biointerface studies,[13] and generating substrates presenting multiple ligands to model complex physiological environments and perform multi-parameter biological assays.[4a,5,14]

The ideal gradient generation approach is one that is simple, molecularly general, quantifiable, and easily extendable to create substrates with higher levels of biomolecular substrate complexity. Yet every gradient generation methodology has its inherent strengths and limitations. Some require prior chemical modification of biomolecules with non-native functional groups to enable site-specific immobilization. Conversely, others utilize native functional groups to execute covalent attachment, which offers increased biomolecular generality but often at the cost of random biomolecular orientation. Some techniques are limited to small-scale gradients (100s of microns), while others have the potential to generate gradients on the millimeter-scale. Finally, a handful of approaches have the potential to allow the controlled deposition of multiple different biomolecules onto a single surface, while others are limited to single-component substrates. (For an extensive review of the various approaches to gradient generation and surface immobilization of biomolecules, see references.[14a,14b])

The approach presented herein involves the use of light as a reagent, which allows facile control over the spatial distribution and surface density of immobilized biomolecules.[14c] Glass substrates functionalized to present the photocrosslinking molecule benzophenone (BP) are utilized to directly photoimmobilize multiple classes of biomolecules onto the surface as governed by spatially controlled incident photon flux and solution-phase biomolecule concentration.[14c] Others have shown alternative photochemical biomolecular patterning strategies, often based upon either a combination of photolithographic patterning and bioconjugation,[14d,15] or direct photochemical activation of the surface.[6,16] More relevant to this work, BP-modified substrates were previously used in the photoimmobilization of polymers[17] and biomolecules.[10b,18] However, these demonstrations were limited to generating substrates presenting a single biomolecule, with minimal applications in biological assays. This work represents the first demonstration of biomolecular photopatterning for applications in leukocyte biology and for the investigation of the mode of action of an anti-inflammatory therapeutic.

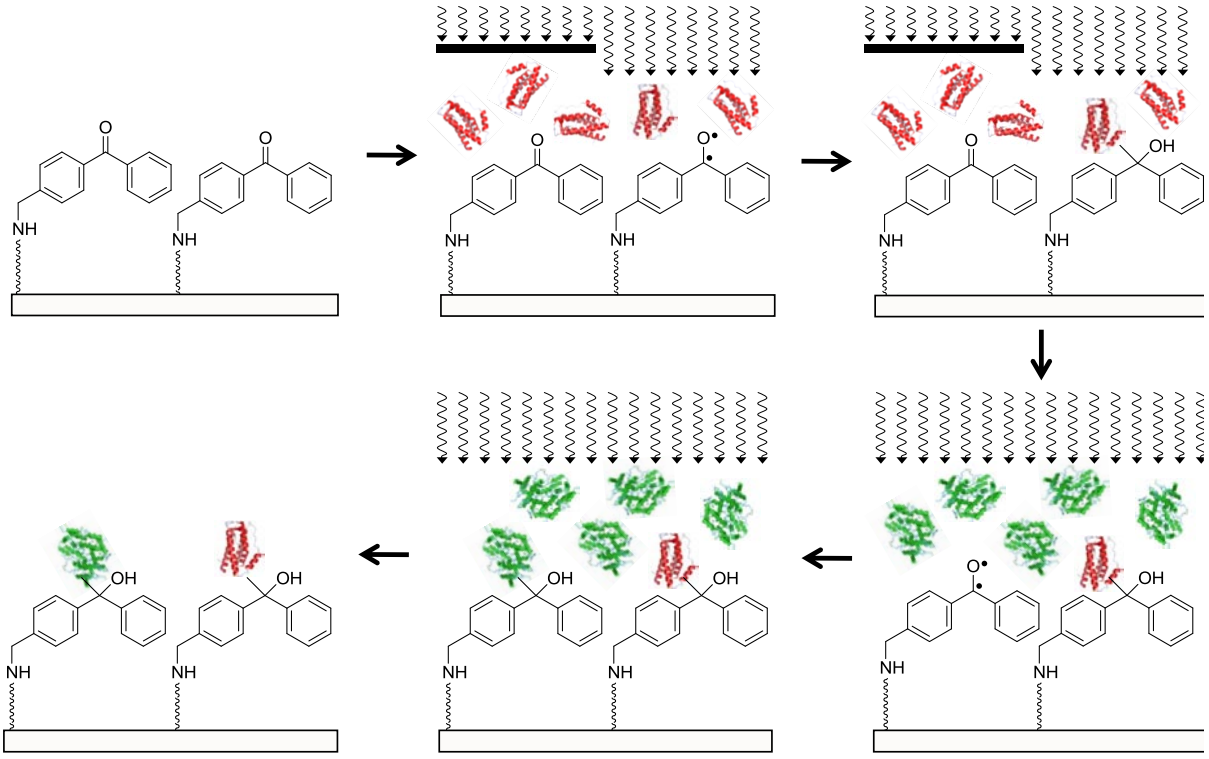

Figure 1.2 Schematic representation of the generation of multi-component biomolecular surface patterns and gradients via sequential exposures of benzophenone-modified substrates in the presence of different biomolecule solutions.

In my work with BP-modified substrates, biomolecular patterns and gradients are generated by immersing substrates in a solution containing the biomolecule of interest and exposing the substrate to light (350 – 365 nm), which results in the covalent attachment of biomolecules to the surface in a spatially controlled manner (Figure 1.2). When illuminated with UV light, BP undergoes an n→π* molecular transition, generating a triplet diradical that can result in the formation of a new C-C bond between the BP-modified substrate and the molecule of interest via a proton abstraction/radical recombination mechanism.[19] If an excited BP molecule does not abstract a proton from a neighboring molecule, it will relax back to the ground state, enabling re-excitation in the presence of a different biomolecule. In this manner, I have demonstrated that BP-based photoimmobilization is a versatile technique for generating multi-component gradients by sequential exposures in the presence of different biomolecule solutions, and that these surfaces can be used as *in vitro* models for biological studies.[14c] In choosing this

particular gradient generation approach, I envisioned that the overall simplicity, biomolecular generality, and capability to generate user-specified multi-component substrates for biointerface studies would make this a broadly applicable platform for researchers in need of model substrates presenting well-defined biomolecular patterns and gradients for biological applications.

Gradient substrates have a potential advantage over homogeneous substrates for applications in leukocyte flow assays, namely, the ability to yield high-content data by examining cell behavior in response to the presence of a variety of site densities on a single substrate. This approach is more efficient compared to the generation of numerous different substrates representing the different ligand densities under investigation. Additionally, the approach involves the covalent immobilization of biomolecules to the surface, which eliminates the risk of protein desorption due to disrupted non-covalent interactions. By pursuing the BP photopatterning approach to biomolecular substrate generation, I chose to forfeit the ability to control biomolecule orientation in exchange for biomolecular generality and overall simplicity.

In addition to the traits mentioned above, mechanical stiffness is another characteristic that is important to consider when choosing a material that will be used to model physiological environments. Several studies have shown that the mechanical properties of biointerfaces can have a dramatic effect on cell behavior.[20] In my work with BP-modified substrates, I have chosen to work with glass, which has a Young's modulus of 72 GPa at 20 °C. While the mechanical properties of the blood vessel wall cannot be described by a single Young's modulus, the three major components of the blood vessel, namely, elastin, smooth muscle and collagen, have Young's moduli of 0.1-1.0 MPa, 10-100 kPa, and 0.1-1.0 GPa, respectively.[21] Clearly, glass substrates have very different mechanical properties compared to the blood vessel. Traditionally, leukocyte biology researchers have utilized both glass and polystyrene for *in vitro* experiments and have verified that observations of leukocyte behavior on immobilized selectins on glass are representative of leukocyte behavior *in vivo,* which suggests that despite the differences in mechanical stiffness, glass substrates are suitable for *in vitro* leukocyte flow assays.[22] However, to be entirely certain of the physiological implications of biological studies performed on glass substrates, it will be necessary to confirm all *in vitro* observations with follow-up studies using mechanically similar materials *in vitro*, or in mouse models of inflammation.

The BP gradient generation methodology that has been developed satisfies the majority of the criteria for the ideal substrate for leukocyte flow assays and shows promise for future applications in leukocyte biology and beyond, as supported by research results presented in Chapters 2 and 3.

1.2 Overview of the biology underlying leukocyte recruitment and inflammation

Physiological processes involving numerous biological molecules sustain all forms of life, from microscopic single-celled prokaryotes to macroscopic multicellular organisms. Mammals' bodies are equipped with an immune system that is able to recruit white blood cells, or leukocytes, to the scene when viruses, bacteria and other potentially deadly intruders invade. The first step of this process, known as the inflammatory response, is the recruitment of leukocytes from the blood stream to the site of the injury or infection.[23]

Inflammation is a two-edged sword: Although it is essential for survival, when not properly regulated it can wreak havoc on the very being it was intended to protect.[24] Numerous diseases are correlated with improperly regulated inflammation, including rheumatoid arthritis, asthma, psoriasis, thrombotic disorders, and autoimmune disease.[24] Inflammation is also associated with increased risk of malignancy in cancer,[25] and studies suggest leukocytes found in the tumor microenvironment may assist in metastasis and immunosuppression.[26] A comprehensive understanding of the molecular underpinnings of the inflammatory response is essential for laying the groundwork to develop more effective therapeutic interventions.

To study inflammation, researchers have employed various biological techniques. Much of the *in vivo* biological work has centered around the generation of genetically engineered "knock-out" mice, which lack one of the proteins involved in the inflammatory response. Such studies have revealed what happens to the process of inflammation in the absence of individual components, and have led the research community to propose a mechanism for the leukocyte adhesion cascade (Figure 1.1).[2] Although aspects of the proposed mechanism remain topics of debate, the overall consensus in the field is that inflammation happens in several sequential steps. First, inflammatory cytokines, secreted by dying cells and bacteria, cause endothelial cells lining nearby blood vessels to express elevated levels of selectins,[27] which are able to recognize ligands on leukocytes. Selictins recruit leukocytes from the blood stream to the blood vessel

surface, causing them to roll along the blood vessel wall in the presence of physiological shear stress.[28] Prolonged leukocyte-endothelium interactions[29] give leukocytes the opportunity to interact with chemokines presented on the endothelial lining. When chemokines bind to leukocyte-expressed G-protein-coupled receptors (GPCRs),[30] downstream signaling cascades cause leukocyte-expressed integrins to undergo a conformational change, which gives leukocytes the ability to bind to intercellular adhesion molecules (ICAMs) on the endothelial lining.[31] Leukocytes firmly adhere to the blood vessel wall,[29] and finally, additional receptor-ligand interactions facilitate the process of diapedesis, which enables the leukocyte to pass through the blood vessel wall and follow chemical cues until it arrives at the site of the injury or infection.[2]

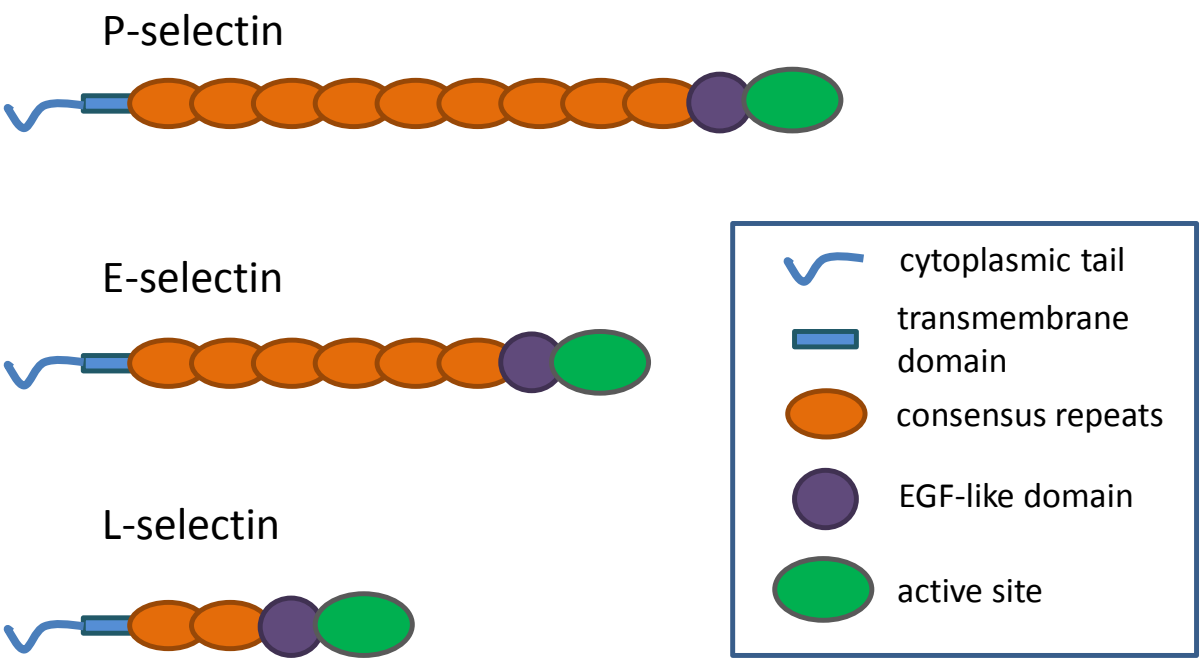

Figure 1.3 A schematic representation of the three selectins: P-, E-, and L-selectin. All three selectins have an N-terminal active site, composed of a lectin domain that enables calcium-dependent carbohydrate recognition, followed by a motif known as an epithelial growth factor (EGF) domain and a varying number of consensus repeats, a transmembrane domain, and a cytoplasmic tail.

The biological applications of the BP substrate generation methodology presented herein focuses on the first step of the leukocyte recruitment process: selectin-mediated leukocyte

rolling. Figure 1.3 presents a schematic representation of the three selectins: P-, E-, and L-selectin. P-selectin and E-selectin are expressed on the inflamed endothelium and play a central role during the initiation of an inflammatory response: When the endothelium receives distress signals from underlying tissue, P-selectin is the first biomolecule deployed as it is mobilized from intracellular storage pools, known as Weibel-Palade bodies, to the luminal surface of the endothelium.[32] The interaction between P-selectin and its primary leukocyte-expressed ligand, P-selectin glycoprotein ligand-1 (PSGL-1), supports neutrophil rolling along the surface of the blood vessel.[31a] E-selectin, which binds to PSGL-1 among other ligands,[33] is also presented on the endothelium during the inflammatory response, but its expression is largely controlled by translation (*i.e.*, it is not stored intracellularly),[34] and its presentation temporally lags behind that of P-selectin *in vivo.* L-selectin is expressed on most leukocytes and binds to ligands expressed on high endothelial venules (HEVs) of lymph nodes and an the endothelium, as well as to ligands on other leukocytes, in a process known as secondary tethering. P-selectin and E-selectin are the two major biomolecular players in inflammation because of their role in initiating the recruitment of leukocytes to interact with the blood vessel wall during inflammation. All three selectins have an N-terminal active site, composed of a lectin domain that enables calcium-dependent carbohydrate recognition, followed by a motif known as an epithelial growth factor (EGF) domain and a varying number of consensus repeats, a transmembrane domain, and a cytoplasmic tail (Figure 1.3).[35] All three selectins recognize sialylated and fucosylated oligosaccharides, most importantly a motif known as sialyl Lewis x (sLe^x), which is presented on several glycoproteins and glycolipids on leukocytes and some endothelial cells and is required for all selectins to bind to PSGL-1 and other selectin ligands. The role of selectins in the leukocyte adhesion cascade has been extensively reviewed.[36]

While the basic framework for understanding inflammation is in place, much remains unknown about the molecular details underlying this complex physiological process. The inherent complexity and redundancy of many receptors and ligands involved in the process pose challenges for studying the mechanism of inflammation, and also makes it difficult to develop therapeutics that are able to disrupt unwanted inflammation. Among the receptor-ligand interactions involved in the leukocyte adhesion cascade are selectins and their ligands,[37] chemokines and their receptors,[38] leukocyte integrins and their complementary intercellular adhesion molecules (ICAMs),[29] and endogenous anti-adhesive factors.[39] Given the number of

biomolecular players, it is reasonable to predict that multi-target therapeutics that are able to disrupt several receptor-ligand interactions simultaneously will be more effective than single-target treatments for unwanted inflammation.[40] Understanding the interplay between the various receptor-ligand interactions that occur during leukocyte recruitment will help lay the groundwork for the development of multi-target therapeutics, and this is the underlying motivation behind the biological investigations described in Chapter 3.

1.3 Bromelain—a natural multi-target anti-inflammatory therapeutic

Bromelain is a natural anti-inflammatory treatment that is currently used as an alternative or complementary treatment for treating inflammation.[41] This extract from pineapple stems contains cysteine proteases that are known to cleave multiple cell surface molecules involved in the adhesion and activation leukocytes.[42] Protein-based therapeutics are typically known to suffer from proteolytic degradation via enzymes in the digestive tract. However, bromelain taken by oral administration was found to be present at detectable levels in the blood plasma and exhibit proteolytic activity, with few adverse side effects.[43] While bromelain has been demonstrated to have anti-inflammatory, fibrinolytic, and anti-thrombotic effects in both *in vivo* and *in vitro studies*,[41,44] the mechanisms by which bromelain attenuates the recruitment of various leukocyte subsets remains poorly understood. Amongst the enzymes present in bromelain extract is stem bromelain, which was the focus of my studies and will be referred to as bromelain herein.

Bromelain (EC 3.4.22.32) has a molecular mass of 23,800 Da and is commercially available as a complex mixture with other components that are not completely characterized but include phosphatases, glucosidases, peroxidases, cellulases, glycoproteins and carbohydrates.[41] Bromelain has a broad substrate spectrum and is able to cleave substrates ranging from low molecular weight peptides to high molecular weight substrates such as fibrin, albumin and casein. Bromelain's substrate specificity is not fully characterized, but it has been found to cleave most efficiently at Arg-Arg sites of synthetic substrates[45] and to preferentially cleave glycyl, alanyl and leucyl bonds.[41] However, it is difficult to predict potential protein cleavage sites since natural proteins have been found to exhibit broader susceptibility to bromelain cleavage than that of synthetic substrates.[42]

In an attempt to understand the molecular basis of bromelain's anti-inflammatory properities, other research labs have investigated the effects of bromelain treatment on neutrophil migration in response to chemokines, which is the step in the leukocyte adhesion cascade immediately following leukocyte transmigration through the blood vessel wall.[42,46] In the first of these studies, performed under the direction of Laura P. Hale, neutrophils were isolated from whole blood, treated with bromelain, and analyzed for the expression of numerous ligands and receptors using flow cytometry.[42] Follow up studies were performed in the same lab to investigate how bromelain treatment affected neutrophils migration in response to IL-8 and fMLP, two known inducers of cell migration, both *in vitro* and in mouse models of inflammation.[42]

While others have investigated the effects of bromelain treatment on neutrophil migration, there are no previous studies on the effects of bromelain on selectin-mediated leukocyte rolling, the first step of the leukocyte adhesion cascade. In the work described in Chapter 4, I set out to fill this literature gap, motivated by the desire to shed additional light on potential mechanisms by which bromelain exerts its therapeutic benefits in inflammatory conditions. Such information will be useful to researchers and doctors interested in understanding bromelain's mode of action and developing more effective treatments for dysregulated inflammation.

1.4 *In vivo* and *in vitro* approaches to studying leukocyte recruitment

Mechanistic biological studies are extremely challenging to carry out *in vivo* due to the complexity of the physiological environment in which inflammation naturally occurs. In such a highly variable and difficult-to-control environment, it is essentially impossible to parse apart all the variables and determine which parameter (*e.g.*, protein expression level, rate of blood flow) causes which behavior (*e.g.*, cell rolling, cell adhesion). To further complicate matters, many of the receptor-ligand interactions involved in leukocyte recruitment are redundant and have functionally overlapping roles. This redundancy serves to confound studies involving knock-out mice, since engineered mice may find ways to adapt and compensate for the missing protein.[22a] To avoid the added complications that come with studies involving gene targeted disruption of specific ligands in mice, others have looked to commercially available function-blocking

antibodies to functionally remove specific proteins and observe the outcome. However, this approach comes with its own potential complications such as incomplete blocking or non-specific antibody binding.[22a]

The majority of *in vivo* mouse studies on inflammation are aimed at addressing questions regarding the role of a particular protein in leukocyte recruitment. However, questions regarding the interplay between different biomolecules involved in leukocyte recruitment are more challenging, if not impossible, to address with standard *in vivo* experiments because of the complexity inherent to living systems. Researchers have consequently looked to *in vitro* studies for answers to these questions.

Successful *in vitro* experiments require model systems[47] with properties that can be tuned by the experimenter to represent some aspect of a biological system. Two common approaches to generating model substrates for studying leukocyte recruitment include immobilizing a protein involved in inflammation on a surface, or generating monolayers of endothelial cells for use as blood vessel models. By having the ability to alter one or two parameters (*e.g.*, protein site density, flow rate) in a controlled and quantifiable manner, researchers can determine the relationship between the variable parameter and the subsequent observed leukocyte behavior. The ultimate goal of an *in vitro* model substrate for inflammation is not necessarily to mimic the *in vivo* biological environment, but to serve as a well-defined and easily controlled substrate that yields quantitative information about cause-and-effect relationships between substrate composition and cell behavior.

Leukocyte flow assays have indeed provided additional pieces to the complex puzzle of inflammation and have enhanced the current understanding of the mechanism underlying the process of leukocyte recruitment. For example, researchers led by Daniel A. Hammer have performed numerous biophysical studies to understand the molecular basis of selectin-ligand binding by using receptor-coated substrates and studying the interactions of ligand-coated microspheres with selectin-coated surfaces under various conditions.[48] Another team of researchers led by Rodger P. McEver used substrates presenting immobilized PSGL-1 to demonstrate the first *in vitro* observation of "catch bond" behavior, a phenomenon in which the

affinity between a receptor-ligand pair increases as shear stress increases up to a point of optimum shear stress, beyond which interactions convert to "slip bond" behavior.[49]

In addition to these examples, numerous other studies have shown that selectin-mediated rolling under conditions of physiological shear stress can be studied in an *in vitro* flow assay format, yielding new insights into the biophysical phenomena underlying the first step of leukocyte recruitment.[13a,50] However, the substrates employed as model substrates are typically made by non-specifically adsorbing proteins onto a surface,[48d,51] yielding substrates that are susceptible to changes over time.[1,14b] In addition, to probe the effect of surface density on cell behavior using this approach would require that numerous substrates be generated and that multiple separate experiments be performed in sequence. In other cases, researchers have used cytokine-stimulated endothelial cell monolayers[52] that express multiple ligands in a physiologically relevant manner. While there are certain advantages to using cell monolayers as a blood vessel model compared to surface-immobilized protein substrates, the primary downside of the approach is it offers little control over the site density of the ligands presented.

While typical model substrates present one biomolecule at a uniform site density, a handful of previous studies report the use of substrates with two biomolecules deposited on the surface at varying levels.[51,53] However, using non-specific adsorption to generate two-component substrates for experiments requires that numerous substrates be generated to represent all possible iterations of protein levels for each biological assay. This time- and resource-intensive approach is non-ideal for yielding information in a timely and efficient manner.

The ideal model substrate for *in vitro* leukocyte flow assays would therefore allow the researcher to:

1. Covalently attach biomolecules to the surface
2. Immobilize biomolecules in user-defined patterns and gradients
3. Control biomolecule orientation and/or quantify ligand site density
4. Immobilize multiple biomolecules on a single substrate

A method that meets these criteria would help remedy the short-comings of traditional approaches to the generation of model substrates for applications in leukocyte biology and

beyond. Such a technique would be of enormous value to the field of leukocyte biology in that it would enable new insights into the combined effect of biomolecular site density and other parameters on cell behavior in an efficient and resourceful manner. The BP photopatterning approach described herein satisfies the above criteria for model substrate generation, and thus holds promise for revealing new insights about the leukocyte adhesion cascade.

Beyond applications in leukocyte biology, a methodology for the generation of biomolecular surface gradients is of fundamental interest for *in vitro* assays enabling the investigation of cell migration and polarization in response to immobilized protein concentration,[4a,54] and for multi-parameter studies in cell biology that systematically address the combined effects of multiple stimuli, such as the density of multiple biomolecules, topography, and shear stress on cell behavior.[55] The focus of my doctoral research, and the focus of this manuscript, is on applications of the developed BP-mediated surface-immobilized gradient generation methodology in leukocyte biology.

1.5 Overview of work presented herein

This chapter presented an overview of strategies for biomolecular pattern and gradient generation, leukocyte recruitment and inflammation, bromelain, and approaches to studying leukocyte recruitment.

Chapter 2 describes the development of a molecularly general photochemical method that utilizes BP-functionalized surfaces to generate biomolecular patterns and gradients. The substrates generated present covalently immobilized biomolecules at defined and varied site densities. Data is presented that demonstrates the quantitative determination of biomolecule deposition, substrate versatility, retention of protein functionality, and ability to deposit multiple biomolecules onto the same surface, as well as preliminary demonstrations of cell adhesion and leukocyte flow assays on biomolecular patterns and gradients. These initial studies demonstrate that the BP approach to biomolecular substrate generation is an attractive methodology for a wide range of biomaterials and biointerface research applications that rely upon defined biomolecular interfaces.

Chapter 3 presents the generation of single- and multi-component substrates for multi-parameter leukocyte flow assays for the investigation of selectin-mediated rolling of two immortalized leukocyte model cell lines, HL-60 promyelocytes and Jurkat T lymphocytes. The results of these proof-of-principle investigations reveal the combined effect of immobilized protein site density and applied wall shear stress on cell rolling behavior, and shows that the described gradient generation approach yields well-defined substrates with the ability to present immobilized proteins over a large range of site densities. Data is presented that demonstrates the first application of two-component biomolecular substrates to probe the transition from rolling to adhesion of leukocytes under conditions of physiological shear stress. The findings show that BP biointerface substrates can be applied to the investigation of cell-substrate interactions in the context of multi-parameter leukocyte flow studies.

Chapter 4 presents the results of *in vitro* studies that help shed light on the molecular mechanism underlying the anti-inflammatory effects of bromelain, a multi-target anti-inflammatory therapeutic. A natural proteinase preparation isolated from pineapple stems, bromelain has been demonstrated to proteolytically alter multiple cell surface molecules involved in the adhesion and activation of certain leukocyte subsets[42] and is currently used as an alternative or complementary medication for treating inflammation.[41] Other research labs have investigated the effects of bromelain treatment on neutrophil migration in response to chemokines, but the investigation outlined in Chapter 4 represents the first to reveal that bromelain cleaves a ligand involved in selectin-mediated leukocyte rolling, the first step of the process of leukocyte recruitment. The findings from these investigations will be useful in the development of more effective treatments for dysregulated inflammation and the diseases associated with it.

Chapter 5 presents a summary of all this work and a detailed plan for future developments and applications of the BP gradient methodology in leukocyte biology.

1.6 References

1. M. Mrksich, *Chemical Society Reviews* **2000**, *29*, 267.
2. K. Ley, C. Laudanna, M. I. Cybulsky, S. Nourshargh, *Nature Reviews Immunology* **2007**, *7*, 678.
3. N. Sniadecki, R. Desai, S. Ruiz, C. Chen, *Annals of Biomedical Engineering* **2006**, *34*, 59.
4. a) R. C. Gunawan, E. R. Choban, J. E. Conour, J. Silvestre, L. B. Schook, H. R. Gaskins, D. E. Leckband, P. J. A. Kenis, *Langmuir* **2005**, *21*, 3061; b) S. K. W. Dertinger, X. Jiang, Z. Li, V. N. Murthy, G. M. Whitesides, *Proceedings of the National Academy of Sciences* **2002**, *99*, 12542; c) J. Park, D.-H. Kim, G. Kim, Y. Kim, E. Choi, A. Levchenko, *Lab on a Chip* **2010**, *10*, 2130.
5. S. T. Plummer, Q. Wang, P. W. Bohn, R. Stockton, M. A. Schwartz, *Langmuir* **2003**, *19*, 7528.
6. W. S. Dillmore, M. N. Yousaf, M. Mrksich, *Langmuir* **2004**, *20*, 7223.
7. a) L. J. Millet, M. E. Stewart, R. G. Nuzzo, M. U. Gillette, *Lab on a Chip* **2010**, *10*, 1525; b) C. J. Wang, X. Li, B. Lin, S. Shim, G.-l. Ming, A. Levchenko, *Lab on a Chip* **2008**, *8*, 227.
8. a) M. Mrksich, *Current Opinion in Chemical Biology* **2002**, *6*, 794; b) R. C. Gunawan, J. Silvestre, H. R. Gaskins, P. J. A. Kenis, D. E. Leckband, *Langmuir* **2006**, *22*, 4250.
9. a) T. Cha, A. Guo, X. Y. Zhu, *Proteomics* **2005**, *5*, 416; b) S. F. Kingsmore, *Nature Reviews Drug Discovery* **2006**, *5*, 310.
10. a) K. De Vos, J. Girones, S. Popelka, E. Schacht, R. Baets, P. Bienstman, *Biosensors and Bioelectronics* **2009**, *24*, 2528; b) Y. Jung, J. M. Lee, J.-w. Kim, J. Yoon, H. Cho, B. H. Chung, *Analytical Chemistry* **2009**, *81*, 936; c) X.-h. Liu, H.-k. Wang, J. N. Herron, G. D. Prestwich, *Bioconjugate Chemistry* **2000**, *11*, 755; d) A. L. Washburn, L. C. Gunn, R. C. Bailey, *Analytical Chemistry* **2009**, *81*, 9499.
11. R. Fan, O. Vermesh, A. Srivastava, B. K. H. Yen, L. Qin, H. Ahmad, G. A. Kwong, C.-C. Liu, J. Gould, L. Hood, J. R. Heath, *Nature Biotechnology* **2008**, *26*, 1373.
12. A. B. Braunschweig, F. Huo, C. A. Mirkin, *Nature Chemistry* **2009**, *1*, 353.

13. a) K. Moore, K. Patel, R. Bruehl, F. Li, D. Johnson, H. Lichenstein, R. Cummings, D. Bainton, R. McEver, *Journal of Cell Biology* **1995**, *128*, 661; b) D. M. Togashi, A. G. Ryder, G. Heiss, *Colloids and Surfaces B: Biointerfaces* **2009**, *72*, 219.

14. a) T. M. Keenan, A. Folch, *Lab on a Chip* **2008**, *8*, 34; b) L. S. Wong, F. Khan, J. Micklefield, *Chemical Reviews* **2009**, *109*, 4025; c) C. R. Toh, T. A. Fraterman, D. A. Walker, R. C. Bailey, *Langmuir* **2009**, *25*, 8894; d) N. P. Reynolds, J. D. Tucker, P. A. Davison, J. A. Timney, C. N. Hunter, G. J. Leggett, *Journal of the American Chemical Society* **2009**, *131*, 896.

15. a) S. Chen, L. M. Smith, *Langmuir* **2009**, *25*, 12275; b) N. Li, C.-M. Ho, *Lab on a Chip* **2008**, *8*, 2105; c) J. Y. Lee, S. S. Shah, C. C. Zimmer, G.-y. Liu, A. Revzin, *Langmuir* **2008**, *24*, 2232; d) W. C. Chang, D. W. Sretavan, *Langmuir* **2008**, *24*, 13048; e) K. M. Ainslie, T. A. Desai, *Lab on a Chip* **2008**, *8*, 1864; f) S. Waichman, M. Bhagawati, Y. Podoplelova, A. Reichel, A. Brunk, D. Paterok, J. Piehler, *Analytical Chemistry*, *82*, 1478.

16. a) C. Wendeln, S. Rinnen, C. Schulz, H. F. Arlinghaus, B. J. Ravoo, *Langmuir*, ASAP; b) E. W. L. Chan, M. N. Yousaf, *Molecular Biosystems* **2008**, *4*, 746; c) J. M. Belisle, J. P. Correia, P. W. Wiseman, T. E. Kennedy, S. Costantino, *Lab on a Chip* **2008**, *8*, 2164; d) M. A. Holden, S.-Y. Jung, P. S. Cremer, *Analytical Chemistry* **2004**, *76*, 1838.

17. a) O. Prucker, C. A. Naumann, J. Ruhe, W. Knoll, C. W. Frank, *Journal of the American Chemical Society* **1999**, *121*, 8766; b) G. K. Raghuraman, R. Dhamodharan, O. Prucker, J. Ruhe, *Macromolecules* **2008**, *41*, 873.

18. a) L. F. Rozsnyai, D. R. Benson, S. P. A. Fodor, P. G. Schultz, *Angewandte Chemie International Edition in English* **1992**, *31*, 759; b) E. Delamarche, G. Sundarababu, H. Biebuyck, B. Michel, C. Gerber, H. Sigrist, H. Wolf, H. Ringsdorf, N. Xanthopoulos, H. J. Mathieu, *Langmuir* **1996**, *12*, 1997; c) W. W. Shen, S. G. Boxer, W. Knoll, C. W. Frank, *Biomacromolecules* **2001**, *2*, 70; d) X. Cao, M. S. Shoichet, in *Journal of Biomaterials Science -- Polymer Edition, Vol. 13*, VSP International Science Publishers, **2002**, pp. 623; e) K. Abu-Rabeah, D. Atias, S. Herrmann, J. Frenkel, D. Tavor, S. Cosnier, R. S. Marks, *Langmuir* **2009**, *25*, 10384; f) N. Griep-Raming, M. Karger, H. Menzel, *Langmuir* **2004**, *20*, 11811; g) M. Y. Balakirev, S. Porte, M. Vernaz-Gris, M. Berger, J.-P. Arie, B. Fouque, F. Chatelain, *Analytical Chemistry* **2005**, *77*, 5474; h) T.

Konry, M. Bouhifd, S. Cosnier, M. Whelan, A. Valsesia, F. Rossi, R. S. Marks, *Biosensors and Bioelectronics* **2007**, *22*, 2230; i) S. Szunerits, N. Shirahata, P. Actis, J. Nakanishi, R. Boukherroub, *Chemical Communications* **2007**, 2793; j) L. Y. Hwang, H. Gotz, W. Knoll, C. J. Hawker, C. W. Frank, *Langmuir* **2008**, *24*, 14088; k) L. Marcon, M. Wang, Y. Coffinier, F. Le Normand, O. Melnyk, R. Boukherroub, S. Szunerits, *Langmuir* **2009**, *26*, 1075.

19. G. Dorman, G. D. Prestwich, *Biochemistry* **1994**, *33*, 5661.
20. a) J. Fu, Y.-K. Wang, M. T. Yang, R. A. Desai, X. Yu, Z. Liu, C. S. Chen, *Nature Methods* **2010**, *7*, 733; b) V. F. M. Segers, R. T. Lee, *Circulation Research* **2011**, *109*, 910; c) A. P. Balgude, X. Yu, A. Szymanski, R. V. Bellamkonda, *Biomaterials* **2001**, *22*, 1077.
21. F. L. Wuyts, V. J. Vanhuyse, G. J. Langewouters, W. F. Decraemer, E. R. Raman, S. Buyle, *Physics in Medicine and Biology* **1995**, *40*, 1577.
22. a) M. Sperandio, J. Pickard, S. Unnikrishnan, S. T. Acton, K. Ley, F. Minoru, in *Methods in Enzymology, Vol. 416*, Academic Press, **2006**, pp. 346; b) S. Hong, D. Lee, H. Zhang, J. Q. Zhang, J. N. Resvick, A. Khademhosseini, M. R. King, R. Langer, J. M. Karp, *Langmuir* **2007**, *23*, 12261.
23. C. S. Bonder, P. Kubes, in *Leukocyte Trafficking* (Eds.: A. Hamann, B. Engelhardt), WILEY-VCH Verlag GmbH &Co. KGaA, Weinhein, Germany, **2005**, pp. 14.
24. G. W. Schmid-Schonbein, *Annual Review of Biomedical Engineering* **2006**, *8*, 93.
25. A. Ekbom, C. Helmick, M. Zack, H. Adami, *New England Journal of Medicine* **1990**, *323*, 1228.
26. a) R. Negus, G. Stamp, J. Hadley, F. Balkwill, *American Journal of Pathology* **1997**, *150*, 1723; b) F. Balkwill, A. Mantovani, *The Lancet* **2001**, *357*, 539.
27. W. M. Becker, *The World of the Cell, 5th edition*, Benjamin/Cummings Publishing, Menlo Park, CA, **2002**.
28. a) M. Bevilacqua, E. Butcher, B. Furie, B. Furie, M. Gallatin, M. Gimbrone, J. Harlan, K. Kishimoto, L. Lasky, R. McEver, J. Paulson, S. Rosen, B. Seed, M. Siegelman, T. Springer, L. Stoolman, T. Tedder, A. Varki, D. Wagner, I. Weissman, G. Zimmerman, *Cell* **1981**, *67*, 233; b) L. Lasky, *Science* **1992**, *258*, 964; c) R. P. McEver, *Current Opinion in Immunology* **1994**, *6*, 75.

29. R. Alon, S. Feigelson, *Seminars in Immunology* **2002**, *14*, 93.

30. a) Y. Tanaka, D. H. Adams, S. Shaw, *Immunology Today* **1993**, *14*, 111; b) D. D. Patel, W. Koopmann, T. Imai, L. P. Whichard, O. Yoshie, M. S. Krangel, *Clinical Immunology* **2001**, *99*, 43.

31. a) M. Sperandio, *Febs Journal* **2006**, *273*, 4377; b) E. F. Plow, T. A. Haas, L. Zhang, J. Loftus, J. W. Smith, *Journal of Biological Chemistry* **2000**, *275*, 21785.

32. R. P. McEver, J. H. Beckstead, K. L. Moore, L. Marshall-Carlson, D. F. Bainton, *The Journal of Clinical Investigation* **1989**, *84*, 92.

33. a) Y. Katayama, A. Hidalgo, J. Chang, A. Peired, P. S. Frenette, *The Journal of Experimental Medicine* **2005**, *201*, 1183; b) P. Kotovuori, E. Tontti, R. Pigott, M. Shepherd, M. Kiso, A. Hasegawa, R. Renkonen, P. Nortamo, D. C. Altieri, C. G. Gahmberg, *Glycobiology* **1993**, *3*, 131; c) R. C. O. Zanardo, C. S. Bonder, J. M. Hwang, G. Andonegui, L. Liu, D. Vestweber, L. Zbytnuik, P. Kubes, *Blood* **2004**, *104*, 3766; d) X. Zou, V. R. Shinde Patil, N. M. Dagia, L. A. Smith, M. J. Wargo, K. A. Interliggi, C. M. Lloyd, D. F. J. Tees, B. Walcheck, M. B. Lawrence, D. J. Goetz, *American Journal of Physiology - Cell Physiology* **2005**, *289*, C415; e) E. Borges, G. Pendl, R. Eytner, M. Steegmaier, O. Zöllner, D. Vestweber, *Journal of Biological Chemistry* **1997**, *272*, 28786.

34. M. P. Bevilacqua, J. S. Pober, D. L. Mendrick, R. S. Cotran, M. A. Gimbrone, *Proceedings of the National Academy of Sciences of the United States of America* **1987**, *84*, 9238.

35. R. P. McEver, in *Leukocyte Recruitment, Endothelial Cell Adhesion Molecules, and Transcriptional Control: Insights for Drug Discovery* (Ed.: T. Collins), Kluwer Academic Publishers, Boston, **2001**, pp. 1.

36. a) R. P. McEver, *Current Opinion in Cell Biology* **2002**, *14*, 581; b) D. Vestweber, J. E. Blanks, *Physiological Reviews* **1999**, *79*, 181.

37. K. Sean Eardley, P. Cockwell, *Kidney International* **2005**, *68*, 437.

38. M. Thelen, *Nature Immunology* **2001**, *2*, 129.

39. E. Y. Choi, E. Chavakis, M. A. Czabanka, H. F. Langer, L. Fraemohs, M. Economopoulou, R. K. Kundu, A. Orlandi, Y. Y. Zheng, D. A. Prieto, C. M. Ballantyne, S. L. Constant, W. C. Aird, T. Papayannopoulou, C. G. Gahmberg, M. C. Udey, P.

Vajkoczy, T. Quertermous, S. Dimmeler, C. Weber, T. Chavakis, *Science* **2008**, *322*, 1101.

40. W.-H. Boehncke, M. P. Schön, *Trends in Pharmacological Sciences* **2003**, *24*, 49.
41. H. R. Maurer, *Cellular and Molecular Life Sciences* **2001**, *58*, 1234.
42. L. P. Hale, P. K. Greer, G. D. Sempowski, *Clinical Immunology* **2002**, *104*, 183.
43. J. V. Castell, G. Friedrich, C. S. Kuhn, G. E. Poppe, *American Journal of Physiology - Gastrointestinal and Liver Physiology* **1997**, *273*, G139.
44. a) D. J. Fitzhugh, S. Shan, M. W. Dewhirst, L. P. Hale, *Clinical Immunology* **2008**, *128*, 66; b) L. P. Hale, *International Immunopharmacology* **2004**, *4*, 255; c) L. P. Hale, P. K. Greer, C. T. Trinh, M. R. Gottfried, *Clinical Immunology* **2005**, *116*, 135; d) J. E. Onken, P. K. Greer, B. Calingaert, L. P. Hale, *Clinical Immunology* **2008**, *126*, 345; e) E. R. Secor Jr, W. F. Carson Iv, M. M. Cloutier, L. A. Guernsey, C. M. Schramm, C. A. Wu, R. S. Thrall, *Cellular Immunology* **2005**, *237*, 68.
45. A. D. Rowan, D. J. Buttle, A. J. Barrett, *Archives of Biochemistry and Biophysics* **1988**, *267*, 262.
46. J. E. Onken, P. K. Greer, B. Calingaert, L. P. Hale, *Clinical Immunology* **2008**, *126*, 345.
47. B. R. Peterson, M. Mrksich, *Current Opinion in Chemical Biology* **2007**, *11*, 579.
48. a) S. K. Bhatia, D. A. Hammer, *Langmuir* **2002**, *18*, 5881; b) D. K. Brunk, D. A. Hammer, *Biophysical Journal* **1997**, *72*, 2820; c) A. O. Eniola, P. J. Willcox, D. A. Hammer, *Biophysical Journal* **2003**, *85*, 2720; d) A. W. Greenberg, D. K. Brunk, D. A. Hammer, *Biophysical Journal* **2000**, *79*, 2391.
49. T. Yago, J. Wu, C. D. Wey, A. G. Klopocki, C. Zhu, R. P. McEver, *Journal of Cell Biology* **2004**, *166*, 913.
50. a) D. A. Hammer, D. K. Brunk, in *Tissue Engineering Methods and Protocols*, **1999**, pp. 543; b) T. Yago, A. Leppanen, H. Y. Qiu, W. D. Marcus, M. U. Nollert, C. Zhu, R. D. Cummings, R. P. McEver, *Journal of Cell Biology* **2002**, *158*, 787; c) U. Schaff, P. E. Mattila, S. I. Simon, B. Walcheck, *Journal of Leukocyte Biology* **2008**, *83*, 99; d) M. B. Lawrence, D. F. Bainton, T. A. Springer, *Immunity* **1994**, *1*, 137; e) U. H. von Andrian, S. R. Hasslen, R. D. Nelson, S. L. Erlandsen, E. C. Butcher, *Cell* **1995**, *82*, 989.
51. E. Woolf, I. Grigorova, A. Sagiv, V. Grabovsky, S. W. Feigelson, Z. Shulman, T. Hartmann, M. Sixt, J. G. Cyster, R. Alon, *Nature Immunology* **2007**, *8*, 1076.

52. G. Cinamon, V. Grabovsky, E. Winter, S. Franitza, S. Feigelson, R. Shamri, O. Dwir, R. Alon, *Journal of Leukocyte Biology* **2001**, *69*, 860.
53. J. A. DiVietro, M. J. Smith, B. R. E. Smith, L. Petruzzelli, R. S. Larson, M. B. Lawrence, *Journal of Immunology* **2001**, *167*, 4017.
54. A. Lagunas, J. Comelles, E. Martinez, J. Samitier, *Langmuir* **2010**, *26*, 14154.
55. J. Y. Park, S. Takayama, S.-H. Lee, *Integrative Biology* **2010**, *2*, 229.

Chapter 2

Direct Biophotolithographic Method for Generating Substrates with Multiple Overlapping Biomolecular Patterns and Gradients

Notes and Acknowledgements

This chapter has been reproduced from the original papers, titled "Direct Biophotolithographic Method for Generating Substrates with Multiple Overlapping Biomolecular Patterns and Gradients" (Toh, C. R.; Fraterman, T. A.; Walker, D. A.; Bailey, R. C. *Langmuir* **2009**, *25*, 8894-8898) and "Quantitative Photochemical Immobilization of Biomolecules on Planar and Corrugated Substrates: A Versatile Strategy for Creating Functional Biointerfaces" (Martin, T. A.; Herman, C. T.; Limpoco, F. T.; Michael, M. C.; Potts, G. K.; Bailey, R. C. *ACS Applied Materials & Interfaces* **2011**, 3, 3762-3771). It has been reproduced here with permission from the American Chemical Society © 2009 and 2011. The original documents can be accessed online at http://pubs.acs.org/doi/abs/10.1021/la9019537 and http://pubs.acs.org/doi/abs/10.1021%2Fam2009597.

We acknowledge funding for this work from the Roy J. Carver Charitable Trust, the Camille and Henry Dreyfus Foundation, and 3M, via a non-tenured faculty grant. C.T.H. acknowledges support from a National Science Foundation Graduate Research Fellowship. This research was carried out in part in the Institute for Genomic Biology, Core Facilities, University of Illinois, as well as the Frederick Seitz Materials Research Laboratory Central Facilities, University of Illinois, which is partially supported by the U.S. Department of Energy under Grants DE-FG02-07ER46453 and DE-FG02-07ER46471. T. A. Martin contributed contact angle measurements and cell patterning images acquired with fluorescence microscopy; F. T. Limpoco contributed the AFM data; G. K. Potts contributed the PSGL-1 patterning.

2.1 Introduction

Cellular adhesive environments are composed of many distinct biomolecules whose density and spatial distribution determine the response of cells. To better understand the nature of these complex interfacial recognition events and subsequent processes, scientists have utilized expertise in molecular synthesis, design, and control to influence the behavior of cells,[1] resulting in well-defined surfaces presenting biologically relevant ligands at distinct spatial locations.[2] Particularly challenging to fabricate are surface-immobilized gradients in which the density of a specific biomolecule is spatially varied in a continuous (rather than digital) manner. However, *in vivo*, numerous biomolecules are involved in defining adhesive environments. Thus, a further challenge exists in generating multi-component, overlapping surface gradients wherein the surface density of multiple biomolecules is spatially controlled.

On a broader level, there is a growing interest in surface chemical approaches for the generation of substrates presenting patterned biomolecules for applications in biointerface science,[3] microarray technology,[4] biosensors,[5] microfluidics and point-of-care applications,[6] and nanotechnology.[7] Biomolecular patterning tools have been rapidly developing due to a growing interest in exercising spatio-temporal control over protein patterns,[1] characterizing immobilized protein site density for quantitative biointerface studies,[8] and generating substrates presenting multiple ligands to model complex physiological environments.[9] The most advantageous patterning approaches are those that are simple, molecularly general, quantifiable, and easily extendable to create substrates with higher levels of biomolecular complexity.

Several approaches have been developed to generate substrates presenting immobilized biomolecules. Surface-immobilized biomolecular gradients can be formed by first generating chemical gradients on surfaces, via chemical or photochemical modification of surface functional groups[10] or the manipulation of self-assembled monolayers[9e,11] followed by the conjugation of biomolecules via various chemical functionalities. Alternatively, biomolecular gradients can be created in solution by controlled mixing in microfluidic networks followed by direct transfer to a uniform surface.[3b,12] Surface gradients generated via these approaches have proven to be exceedingly valuable in investigating biological processes such as cell polarity,[12a] migration and metastasis,[3b,11b,13] wound healing,[14] and neuronal guidance.[12b,12c] However, many of these

enabling approaches require complicated microfluidic designs, have limits on the number of components incorporated, or require specific and often non-native chemical functionalities, which can limit their general applicability to different classes of biomolecules (peptides, proteins, carbohydrates, etc.). Other groups have developed biomolecular patterning strategies based upon either a combination of photolithographic patterning and bioconjugation[15] or direct photochemical activation of the surface.[10,16] More relevant to this work, benzophenone-modified substrates were previously used in the photoimmobilization of polymers[17] and biomolecules.[5b,18]

In this report, a direct, biomolecularly general method for creating overlapping, multicomponent patterns and surface gradients is described. The approach, outlined in Scheme 2.1, involves the spatially selective photochemical activation of benzophenone (BP) monolayers in the presence of a solution-phase biomolecule. Upon illumination with 365 nm light, BP undergoes an $n \rightarrow \pi^*$ transition to form a transient diradical that can covalently attach proximal biomolecules to the surface via insertion into a C−H bond.[19] Excited BP molecules that fail to undergo C−H insertion relax back to the ground state whereby they can be re-excited in the presence of a different biomolecule solution, allowing for the creation of overlapping patterns and gradients. Because of the general reactivity of BP towards ubiquitous C−H bonds, this method represents a general approach for direct surface bioconjugation. Other groups have taken a similar approach to using BP to generate biomolecular patterns and gradients, but instead of attaching unmodified biomolecules to BP-modified substrates, they attach BP to the biomolecule and use light to attach the BP-labeled biomolecule to the surface.[20] However, this approach is susceptible to biomolecular cross-linking in solution and multilayer formation because the reaction is not confined to the surface.

In my work with BP-modified substrates, biomolecular patterns are generated by immersing substrates in a solution containing the biomolecule of interest and exposing the substrate to light through a photomask (350 – 365 nm), which results in the covalent attachment of biomolecules to the surface in a spatially controlled manner (Scheme 2.1). I describe the first application of BP photochemistry to generate surface-immobilized biomolecular patterns and gradients with the ability to attach both proteins and carbohydrates.

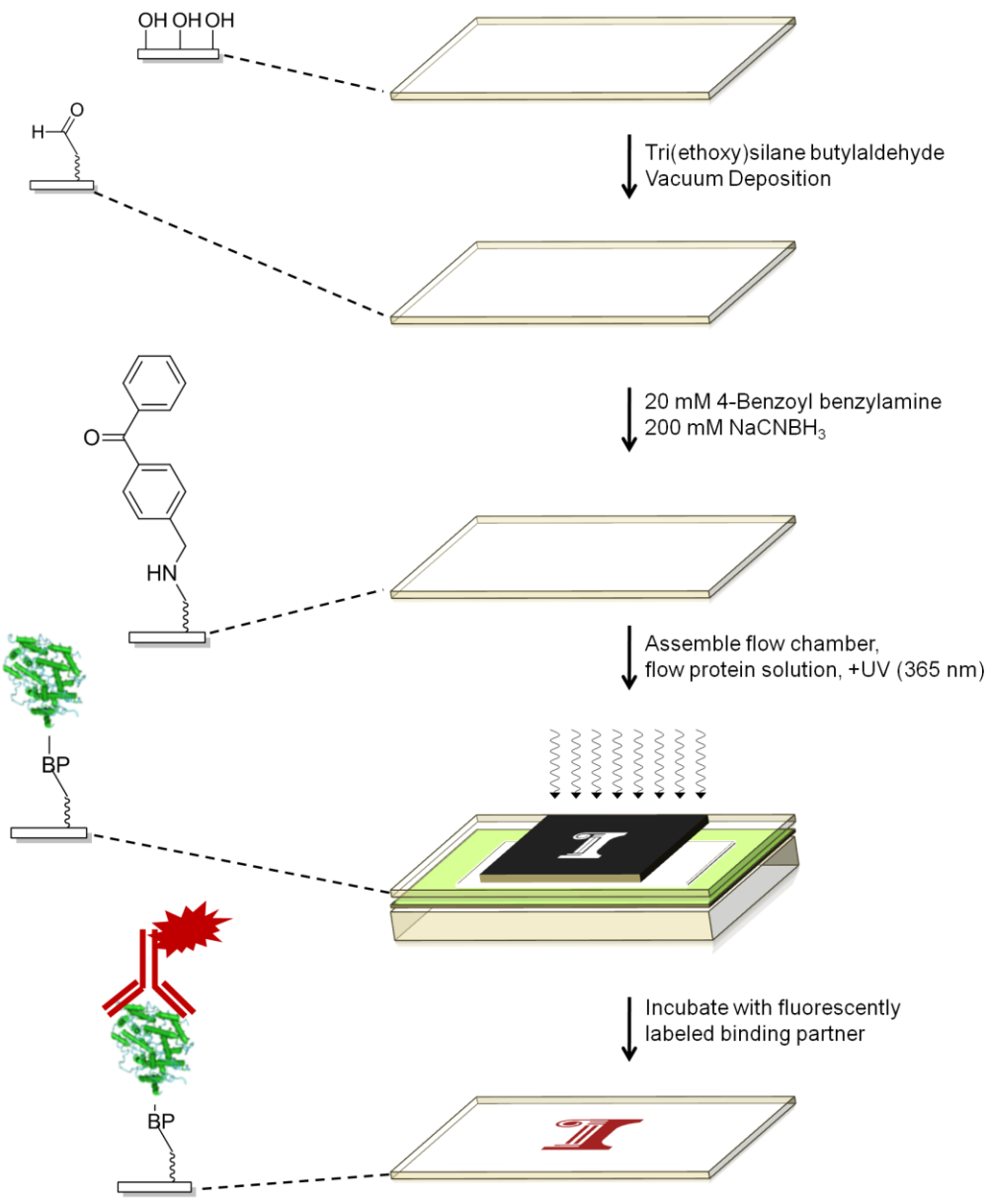

Scheme 2.1 A schematic diagram showing the preparation of BP-modified substrates and subsequent biomolecule photoimmobilization. Glass microscope slides are cleaned, silanized and functionalized with BP. A biomolecule is introduced to the substrate followed by exposure to UV light (~365 nm), resulting in the formation of new C-C bonds between the surface and the biomolecules. The resulting biomolecular patterns are visualized with a fluorescently labeled binding partner.

The BP photopatterning methodology was applied to create substrates that present one or two discrete biomolecules in patterns and gradients, and demonstrate, via a radioimmunoassay, that this methodology affords quantitative control over the density of biomolecule deposition immobilized onto the underlying substrate. Subsequent ligand-binding assays and cell adhesion experiments showed that specific ligand recognition occurs and that cells adhere selectively to immobilized capture ligands, indicating that the photopatterned molecules are not rendered biologically inactive. These results demonstrate that BP-based photoimmobilization is a versatile technique for generating multi-component patterns and gradients by sequential exposures in the presence of different biomolecule solutions, and that these surfaces can be applied as *in vitro* models for biological studies.[21] Together with the molecular generality afforded by the C-H bond insertion mechanism, the advantages of this direct photochemical attachment methodology, such as quantitative deposition, retention of protein functionality, and the ability to deposit multiple biomolecules onto the same surface, make this approach attractive for a wide range of biomaterials research applications that rely upon defined biomolecular interfaces and the creation of substrates that serve as models of complex physiological microenvironments

2.2 Results and Discussion

I have developed a straight-forward and versatile technique for generating photopatterned biomolecular substrates that are suitable for probing receptor-ligand interactions and for biointerface studies. BP-modified substrates are assembled into a flow chamber and exposed to UV light in the presence of a biomolecular solution to generate patterns or gradients (Scheme 2.1). The resulting patterns are visualized by recognition with a fluorescently labeled antibody, a native ligand, or by selective cell adhesion.

2.2.1 Chemical characterization of BP-modified substrates

BP-modified substrates were prepared and characterized after each step by water contact angles (Table 2.1). Freshly cleaned substrates were extremely hydrophilic, giving an unmeasurable contact angle as reported in the literature.[22] Following vapor phase silanization, the water contact angle increased to 44.8 (±1.9)°, indicating an increase in hydrophobicity due to the addition of the monolayer onto the glass substrate. These values are within the range of values reported in the literature for aldehyde-functionalized surfaces.[9f,23] Subsequent attachment

of BP further increased the hydrophobicity of the surface, giving a water contact angle of 53.4 (±1.1)°. After protein conjugation to the BP-modified surface, a ~20° decrease in contact angle is observed, which is consistent with literature reports.[15c] Given the significant changes in the relative hydrophobicity measured during each step of this procedure, water contact angle measurements were routinely used to verify the success of each chemical modification step.

	Glass	Aldehyde silane	BP functionalization	Post-Protein Conjugation
Contact Angle (H_2O)	0°	44.8 ± 1.9°	53.4 ± 1.1°	30.2 ± 2.1°
RMS Roughness (AFM)	352 pm	915 pm	833 pm	775 pm
Chemical Structure	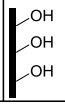	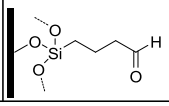	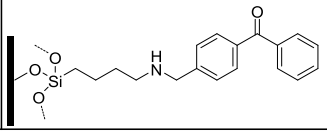	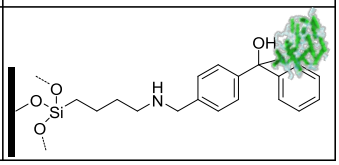

Table 2.1 Surface characterization of BP-modified substrates. Surfaces were characterized using contact angle goniometry and AFM to determine changes in hydrophobicity and surface roughness. Contact angle data represent the average of *n*=9 substrates (± standard deviation) from two batches of slides made on the same day. AFM analysis was performed on BP-modified silicon after each reaction and the RMS roughness was determined.

In order to confirm that the derivatization procedure did not lead to significant changes in substrate topography, the surface roughness following each chemical and biochemical functionalization step was monitored using atomic force microscopy (Table 2.1). Through the entire surface functionalization procedure and subsequent photoimmobilization of a representative protein, the root mean squared (rms) roughness of the substrates increased slightly, from 352 pm for the clean glass surface to 775 pm for the protein-modified substrate, revealing no dramatic changes in surface topography.[24]

2.2.2 Generation of substrates presenting biomolecular patterns and gradients

I first demonstrated the ability to create single-component protein patterns with biotinylated lectin Concanavalin A (ConA-biotin) on BP-modified glass substrates. After

introducing the solution-phase protein to a BP-modified substrate, the substrate was illuminated through a 500-μm square photomask pattern followed by visualization with a fluorescently labeled binding partner, as shown in Figure 2.1a. I extended the protocol to generate two-component biomolecular patterns by sequentially exposing the same substrate in the presence of two different biomolecules. More specifically, the BP surface was illuminated through the photomask in the presence of mannan, followed by rotation of the mask ~45° and exposure in the presence of P-selectin. The resulting overlapping patterns were visualized with two spectrally distinct fluorescently labeled binding partners (Figure 2.1b). To my knowledge, the resulting two-component substrate is the first example of overlapping patterns of carbohydrates and proteins on the same substrate.

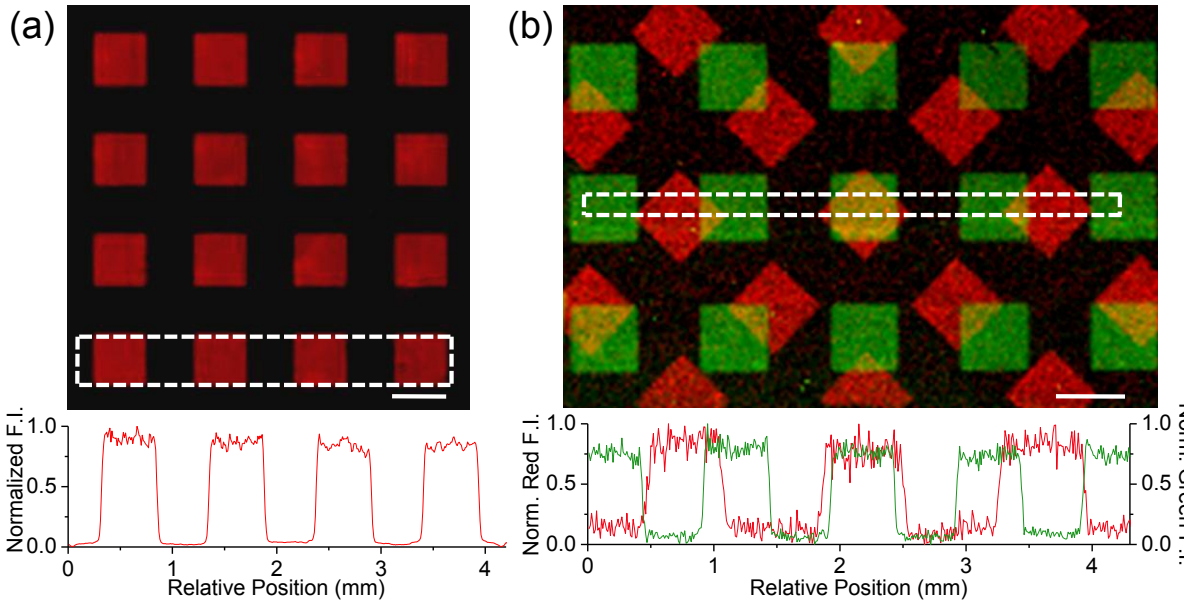

Figure 2.1 Demonstration of direct photoimmobilization of proteins and carbohydrates on BP-modified glass substrates: (a) biotinylated ConA and (b) overlapping patterns of glycoprotein P-selectin (red) and polysaccharide mannan (green). Dashed lines indicate areas in the fluorescence line scans. F.I. stands for fluorescence intensity. Scale bars: 500 μm.

Upon the basis of the digital patterning results shown in Figure 2.1, it was reasonable to believe that gradients of biomolecules on the surface could be generated by continuously varying

the spatial exposure across the surface during illumination. In addition to the spatial exposure to UV light, the relative amount of surface attachment can also be controlled by adjusting the concentration of solution-phase biomolecule. Figure 2.2a demonstrates both of these levels of control in the fabrication of one-component continuous surface gradients of ConA-biotin by positioning a programmable shutter in between the light source and the substrate. Illumination and linear movement of the shutter were initiated simultaneously so that a gradient in light exposure was created across the substrate. Gradient profiles at three different ConA-biotin concentrations show the relationship between solution-phase biomolecule concentration and the slope of the resulting gradient.

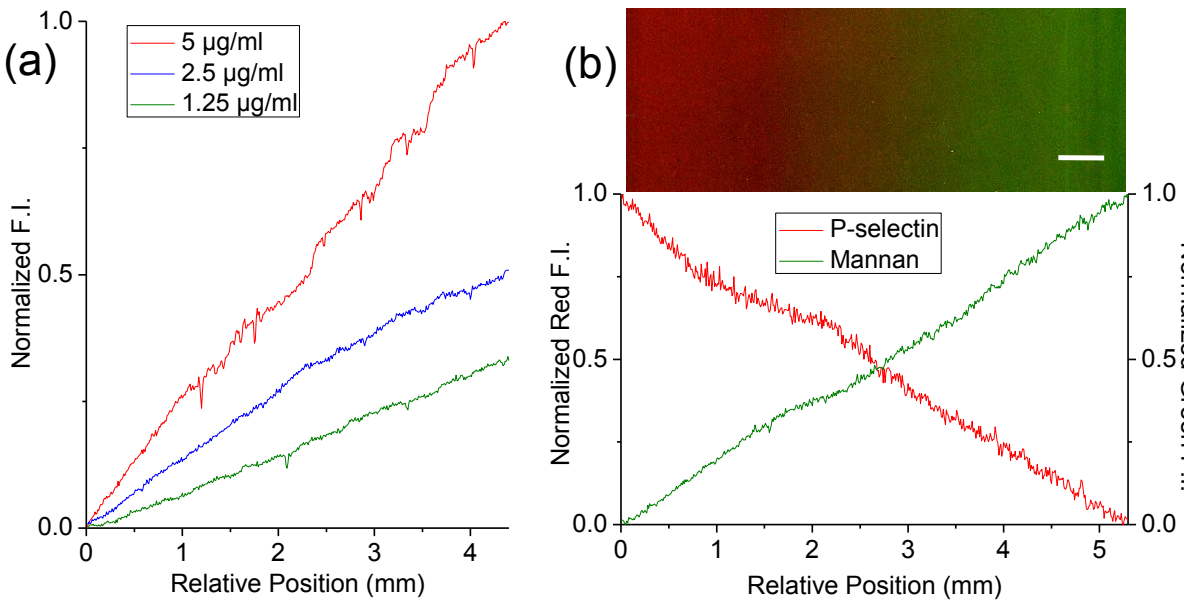

Figure 2.2 Demonstration of control over gradient profile and biomolecular generality of the photochemical approach: (a) biotinylated ConA gradient slope can be controlled by varying the biomolecular concentration during photoimmobilization and (b) a single substrate displaying two overlapping gradients of P-selectin (red) and mannan (green). F.I. stands for fluorescence intensity. Scale bar: 500 µm.

Similarly to the two-component patterning demonstration, parallel overlapping gradients of P-selectin (red) and mannan (green) were fabricated by sequential exposures with 180° shutter

reorientation, as shown in Figure 2.2b. I was also able to generate two-component perpendicular gradients by rotating the shutter by 90°, as shown for mannan and P-selectin in Figure 2.3. Notably, the photochemical approach allows the immobilized biomolecule concentration to be varied along the direction of flow. A diagonal line drawn from bottom left to top right across Figure 2.3a gives an identical profile to that of Figure 2.2b, whereas the diagonal from top left to bottom right shows both components varied together from high to low concentration. These results suggest that the simplicity and versatility provided by the BP-patterning methodology will allow the facile construction of complex, overlapping gradient substrates that will find utility in future studies of cell−substrate interactions.

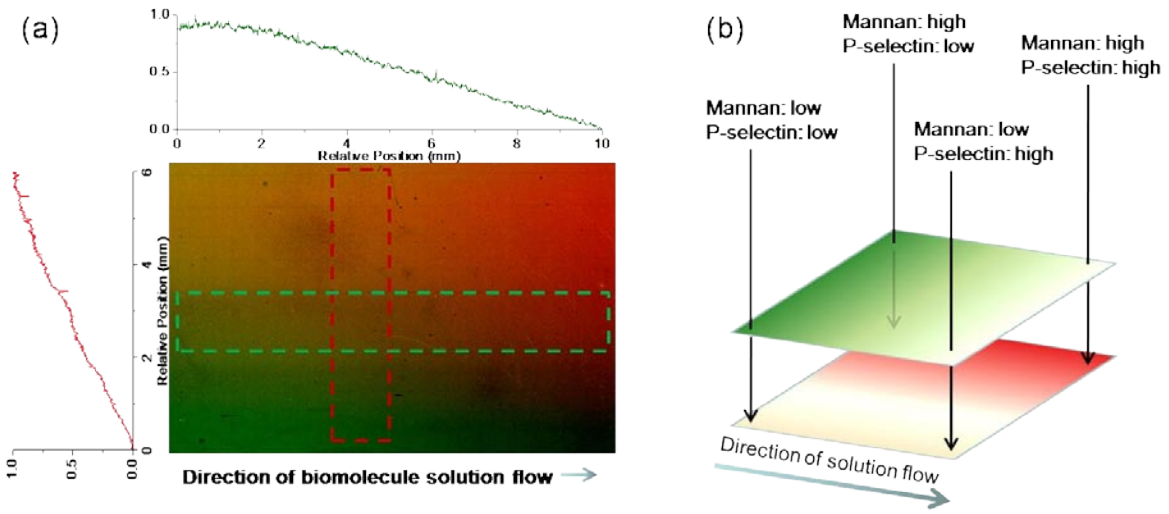

Figure 2.3 Two-component biomolecular gradients on BP-modified substrates with perpendicular gradient profiles yield substrates that present different ratios of two components in various regions. (a) Fluorescence image and line scans of overlapping gradients of mannan (green) and P-selectin (red), parallel and perpendicular to the direction of solution flow, respectively. Dashed lines indicate areas in fluorescence line scans. (b) Illustration of how perpendicular gradients substrates present numerous "microenvironments" with different relative ratios of the two components on a single substrate.

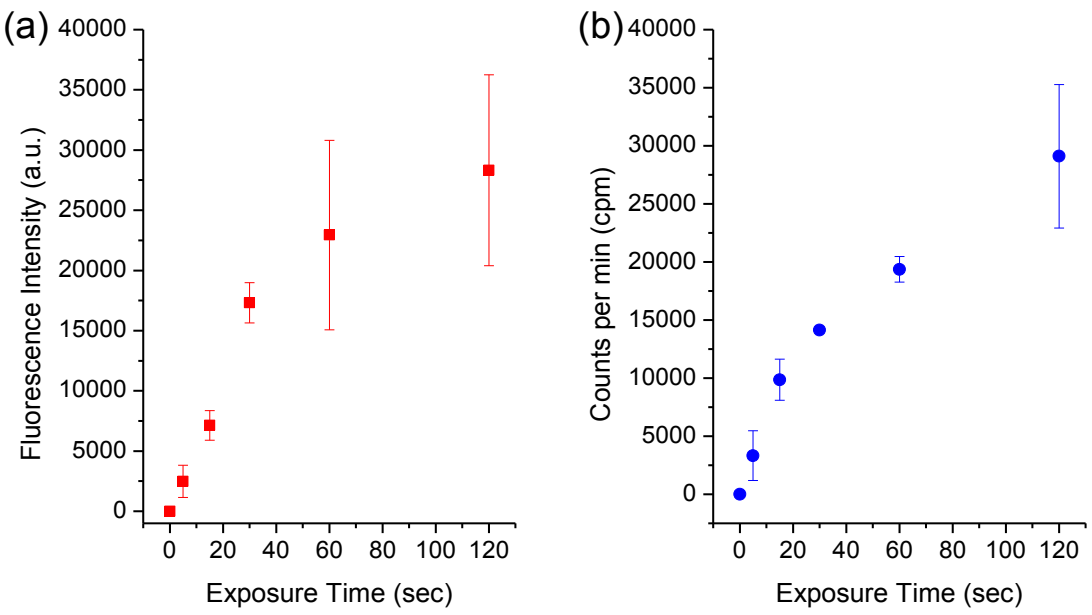

Figure 2.4 Protein loading is positively correlated with UV exposure time. Biotinylated ConA (5 µg/mL) was uniformly photopatterned onto BP-modified substrates for 5, 15, 30, 60, or 120 sec. The signal from subsequent (a) fluorescence analysis and (b) radioimmunoassays shows that signal increases with increasing UV exposure time (~365 nm, 17 mW/cm^2). Control substrates were employed to account for nonspecific binding of antibodies. Data points represent the average of *n*=3-4 (± 95% C.I.).

2.2.3 Quantitative determination of protein site density

Determining the site density of ligands as a function of UV exposure time allows substrates to be tailored to present specific concentrations of ligands for subsequent applications. Substrates were patterned to present uniform ConA-biotin over a range of site densities. The resulting F.I. data were plotted as a function of exposure time (Figure 2.4). Protein site density was quantified by incubating substrates with a saturating concentration of [^{125}I]-labeled streptavidin. Calibration plots were made using known concentrations of [^{125}I]-labeled streptavidin, and the resulting radioactivity (CPM) for each concentration of [^{125}I]-labeled streptavidin was plotted as CPM vs. number of molecules (data not shown). Using the calibration

plot, and knowing the analysis area, the site density (molecules/μm^2) was determined for each exposure time. Since fluorescence measurements are considerably more convenient to perform on substrates compared to radioiummunoassays, site density was plotted against the F.I. for each time point to establish a correlation to convert from fluorescence to loading density (Figure 2.5). Increasing the exposure time results in higher densities of immobilized ligands on the substrate, with a maximum loading value, under the patterning conditions used, observed at approximately 200 molecules/μm^2.

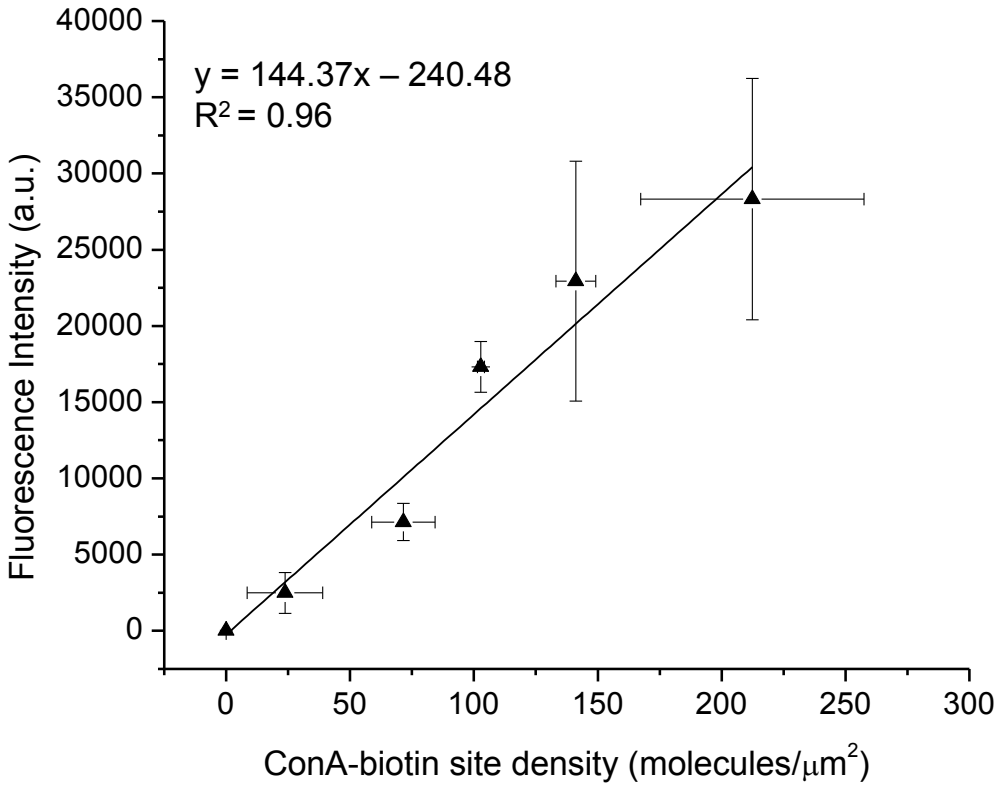

Figure 2.5 Results from fluorescence-radioactivity correlation studies. Data from the biotinylated ConA radioimmunoassay (Figure 2.4a,b) were converted from units of CPM to site density using the linear regression from a standard curve generated from known amounts of [^{125}I]-labeled Streptavidin (Figure 2.4c). Plotting fluorescence intensity (F.I.) as a function of ConA-biotin site density allows data from future fluorescence analyses to be converted to protein site density.

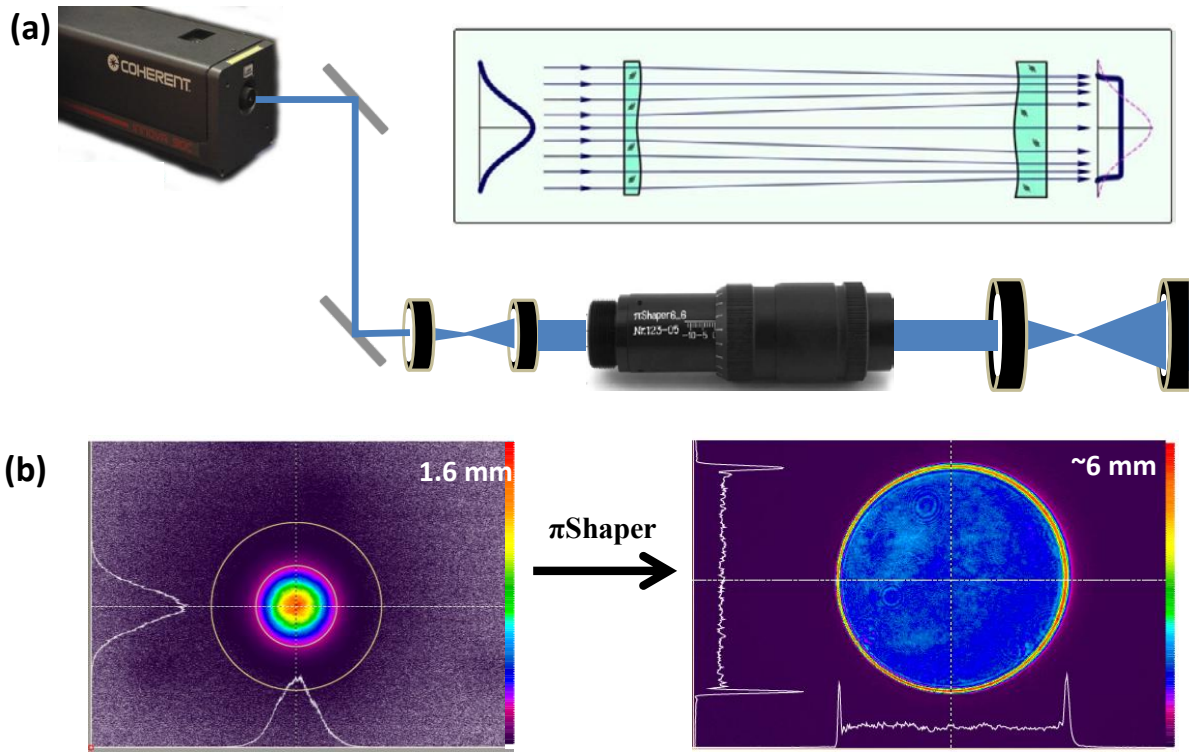

Figure 2.6 The optical configuration used to generated an expanded, homogenized beam of collimated light (λ= 351.1-363.8 nm). (a) The unmodified Coherent Ar ion laser beam has a Gaussian profile. As the beam is expanded and passed through a set of refractive optics, the Gaussian profile is converted to a flat-top, while retaining collimation. Optics I and II make up the Keplerian telescope that expands the beam four-fold to have the appropriate diameter to enter the πShaper. Optics III and IV make up the Keplerian telescope that expand the beam an additional three-fold, resulting in the optimized field of light for photopatterning applications. Lens I, plano-convex, f = 25.4 mm; Lens II, plano-convex, f = 100 mm; Lens III, plano-convex, f = 50 mm; Lens IV, plano-convex, f = 150 mm. (b) A beam profiling camera was used to acquire images of the beam before and after passing through the πShaper.

2.2.4 New light source for photopatterning applications

One of the limitations of the initial photopatterning setup came from the diffuse LED light source. Due to light scatter, I observed that patterns had increasingly higher "background" levels (immobilized protein in areas that were not directly exposed to light) with longer

illumination times, limiting the signal-to-noise (S/N) ratio that could be obtained (data not shown). For the same reason, the maximum difference in F.I. observed across a gradient was consistently a factor of 2 to 3. This would severely limit future investigations of cell-substrate interactions over a wide range of immobilized ligand densities, since gradients presenting ligands over a broad range of surface densities would be unattainable.

To solve this problem, I obtained an Ar ion laser (351.1-363.8 nm), which has a highly collimated output. Collimated light is composed of parallel light rays that disperse slowly with distance. I envisioned this would decrease unwanted light scatter during photopatterning and minimize background protein attachment, enabling the generation of gradients presenting a broader range of site densities. An instrument known as a πShaper (MT Berlin) was used in conjunction with several optical components to convert the Gaussian profile to a homogeneous or "flat-top" output and expand the beam for large-area photopatterning (Figure 2.6). This new laser setup enabled us to generate patterns with a S/N ratio of ~15, compared to ~2 with the UV

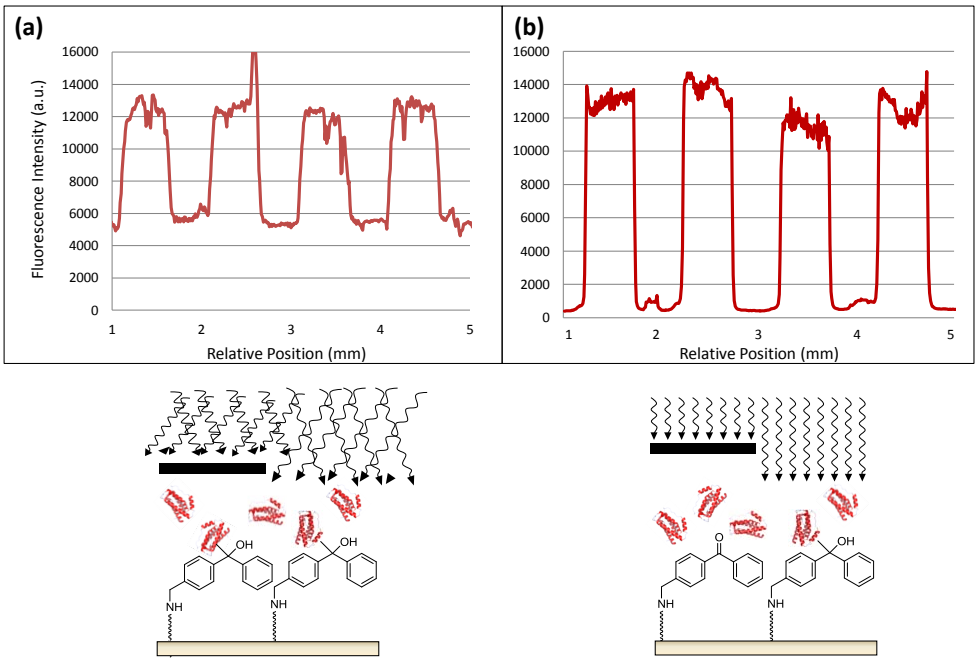

Figure 2.7 Switching light sources from the UV LED to the laser+πShaper enabled an increase in S/N ratio from 2 to ~15. Presumably, the increase in S/N is the result of switching from a diffuse light source, which leads to high background immobilization due to light scatter (left), to a collimated light source that minimizes background immobilization (right).

LED light source (Figure 2.7).

2.2.5 Demonstration of immobilized protein function: ligand recognition and cell patterning

Common applications of substrates presenting immobilized biomolecules include recognition of native ligands and cell adhesion studies. It is therefore important to verify that the photoimmobilization process, which involves exposure to UV light (λ = 351.1-363.8 nm), does not physically damage biomolecules such that they can no longer be recognized by appropriate receptors on the surface of cells. To demonstrate the ability of photopatterned proteins to retain their specific ligand-binding properties, I generated substrates presenting photopatterned P-selectin in an array of circles and squares (Figure 2.8). P-selectin is a glycoprotein involved in leukocyte tethering on the endothelial lining of blood vessels and HL-60 cells are known to express PSGL-1, a receptor for P-selectin.[8a] The resulting images suggest that P-selectin is able to bind specifically to both soluble PSGL-1 (Figure 2.8a) and cell surface-bound PSGL-1 expressed on HL-60 promyelocytic cells (Figure 2.8b). HL-60 cells, which were fluorescently labeled for visualization purposes, specifically adhere to the square patterns of P-selectin and not

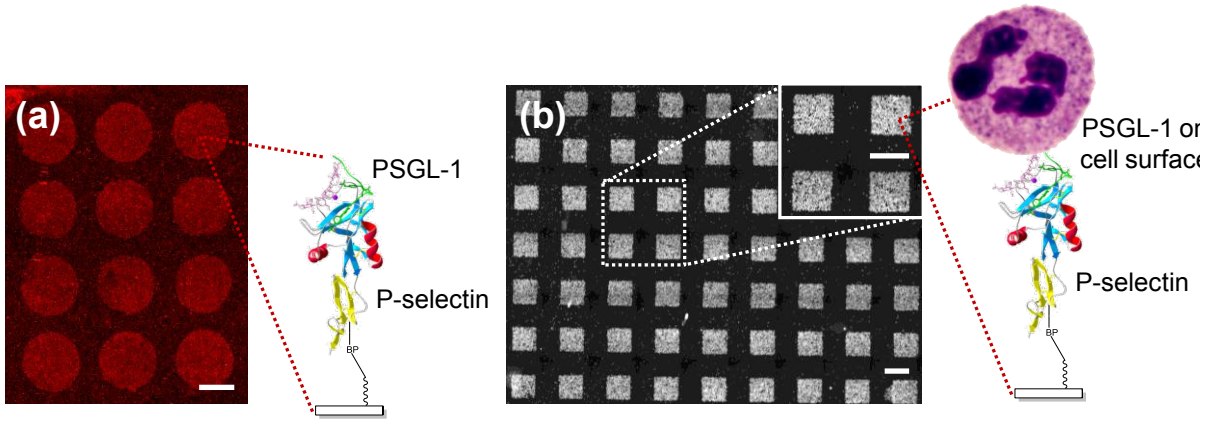

Figure 2.8 Native ligand recognition demonstrated with photopatterned glycoprotein P-selectin. (A) P-selectin was immobilized onto BP-modified substrates in 800-μm circles. Fluorescence images were obtained by incubating substrates with PSGL-1. (B) HL-60 promyelocytes, which express PSGL-1 on their surface, selectively adhere to 500-μm squares of photoimmobilized P-selectin on BP-modified substrates, as visualized by fluorescent cell labeling and microscopy. Scale bars: 500 μm.

to the surrounding background, thereby demonstrating the integrity of the photoimmobilized biomolecule and suggesting a general utility of the BP attachment scheme to creating cell-compatible biointerfaces.

The interaction of HL-60 cells with photochemically generated gradients of P-selectin was also investigated. As shown in Figure 2.9a, the number of immobilized cells correlates with the amount of immobilized P-selectin, as the degree of HL-60 attachment decreases from left to right down a P-selectin gradient. Control experiments showing no cell adhesion were carried out

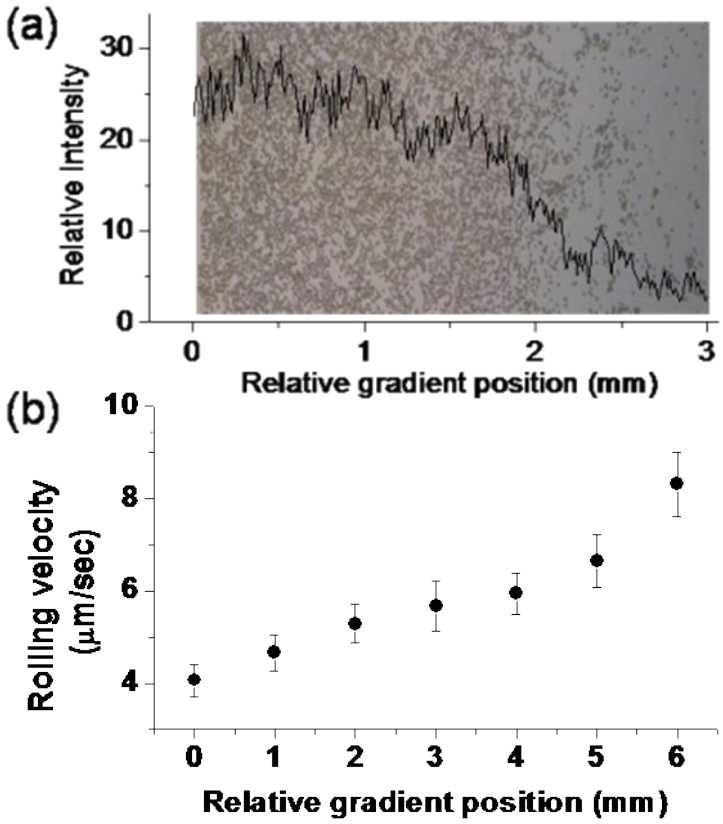

Figure 2.9 HL-60 cells adhere to and roll on immobilized P-selectin gradient substrates. (a) Optical micrograph of HL-60 cells seeded onto a 3-mm surface gradient of P-selectin overlaid with the corresponding line scan showing the gradient in the number of immobilized cells. (b) Plot of HL-60 cell rolling velocity versus position on a 6-mm P-selectin gradient. The wall shear stress was 0.24 dyn/cm^2. Error bars represent the 95% confidence intervals determined for n = 44, 44, 46, 40, 45, 39, and 49 cells at positions 0−6 mm, respectively.

on nonspecific protein surfaces as well as on surfaces presenting no protein ligands (data not shown). As a further demonstration of the utility of photochemically generated biomolecular gradients as cell adhesive models, I investigated the rolling behavior of HL-60 cells as they were flowed perpendicularly over a P-selectin surface gradient (Figure 2.9b). The observed range of rolling velocities and the correlation between adhesion and the amount of immobilized P-selectin is consistent with previous reports.[25] HL-60 cells were not observed to adhere to or roll on surfaces of photoimmobilized nonspecific proteins or plain BP-modified substrates. This proof-of-principle demonstration of leukocyte rolling on BP-modified substrates presenting photoimmobilized P-selectin demonstrate the potential of the BP photopatterning approach for fundamental applications in leukocyte biology.

2.3 Conclusion

In this work, I generated BP-modified substrates and characterized each surface modification step. I applied the methodology to create multi-component patterns of both proteins and carbohydrates. Furthermore, I employed a modified radioimmunoassay technique to establish the quantitative nature of biomolecular immobilization, which can be optimized by adjusting the UV exposure time. The data presented herein show that BP-modified substrates can be used to make spatially confined protein patterns and show that photopatterned biomolecules retain their ability to recognize their native ligands and to be recognized by native cellular receptors. An alternative to conventional gradient generation methods, this simple surface-modification approach requires only a UV light source and translation stage, provides molecularly general direct covalent attachment, and allows the patterning of multiple biomolecules into patterns and gradients. I also demonstrated the potential of BP-modified substrates to be applied to studying cell-substrate interactions, by performing a leukocyte flow assay to demonstrate leukocyte rolling on immobilized P-selectin gradients.

2.4 Materials and Methods

All chemicals were purchased from Sigma-Aldrich (St. Louis, MO) and used as received, unless otherwise noted.

2.4.1 Preparation of BP-modified substrates

Glass microscope slides (Fisher Scientific) were cleaned with Piranha solution (4:1 (v:v) concentrated H_2SO_4 : 30% H_2O_2).[26] Substrates were rinsed extensively with water (ELGA LabWater Reservoir, Veolia Water Systems) and absolute ethanol (Decon Laboratories), and dried under a stream of nitrogen. Slides were baked in an oven at 120 ºC for 1 hr, cooled to room temperature, and positioned upright along the wall of a vacuum dessicator, with 100 µL of 3-(triethoxysilyl)butyl aldehyde (Gelest) placed in the center of the chamber. Vacuum was applied to the sealed chamber and vacuum deposition of silane onto the glass slides was allowed to occur for 2.5 hr. Slides were then cured at 120 ºC for 1 hr, soaked in absolute ethanol for 30 min, rinsed with absolute ethanol, and dried under a stream of nitrogen. Successful silanization was determined via measurement of water contact angles (Ramê-Hart Goniometer).

Slides were then incubated in the dark for 4 hr at rt in the presence of 20 mM 4-benzoyl benzylamine hydrochloride (Matrix Scientific) and 200 mM $NaCNBH_3$ in a solution of 4:1 DMF:MeOH, followed by immersion in aldehyde-blocking buffer (0.1 M Tris, 200 mM ethanolamine, pH 7.0) for 1 hr at room temperature. Slides were rinsed thoroughly with water, DMF, methanol, and ethanol, dried under a stream of nitrogen. The resulting BP-modified substrates were stored in a dessicator in the dark until further use.

2.4.2 AFM analysis of surface roughness

AFM measurements were performed using an MFP-3D microscope (Asylum Research). Substrates were prepared as described above, except silicon wafers were used instead of glass microscope slides. Changes in the surface roughness of the substrates after each chemical treatment were monitored by obtaining 1 × 1 µm topographic images in AC mode using a silicon probe with <10 nm tip radius and a cantilever nominal force constant of 40 N/m (BudgetSensors). Roughness values were calculated from the root mean square of the height amplitudes after the images were corrected for sample tilt using the MFP-3D imaging analysis and statistical software.

2.4.3 Generation of biomolecular patterns and gradients on BP-modified substrates: UV LED

The following biomolecules were used in photoimmobilization studies: biotinylated Concanavalin A (ConA-biotin), purchased from Vector Laboratories; mannan isolated from

Saccharomyces cerevisiae; recombinant human P-selectin (CHO cell-derived), purchased from R&D Systems; and fibronectin (FN), purchased from Invitrogen. Protein stock solutions were prepared by resuspending lyophilized protein in the recommended buffer solutions (1x PBS for proteins) to a concentration of 1 mg/mL. Aliquots were stored frozen at -20 ºC until further dilutions in the respective buffers were freshly prepared to yield solutions of 5 μg/ml for photopatterning applications. A solution of mannan was prepared by diluting lyophilized powder to a final concentration of 20 mg/ml in purified water for photopatterning applications.

A rectangular parallel-plate flow chamber (GlycoTech) was assembled with a BP-modified glass substrate separated by a silicone gasket of 127 μm thickness, 6 cm length, and 1 cm width. Vacuum was applied to hold together the substrate-chamber assembly. Appropriate connectors and tubing for the solution inlet and outlet were assembled, and a syringe pump (Harvard Apparatus) was utilized to pull biomolecule solutions through the chamber. Prior to irradiation with UV light, the biomolecule solution was flowed through the chamber at a rate of 3 mL/min. During UV irradiation, biomolecular solution flow was stopped, or biomolecule solutions were flowed at a rate of 10 μL/min. Illumination for data shown in all figures was performed at 3 mW/cm^2 through the back of the substrate with a CF2000 UV LED source (365 nm, Clearstone Technologies), with the exception of Figures 2.7b and 2.8a, in which case illumination was performed with the laser+πShaper setup. For gradient generation, an opaque shutter connected to a computer-controlled translation stage (ThorLabs Opto dc driver) was programmed to move at a velocity of 0.1 mm/s for protein immobilization and 0.02 mm/s for carbohydrate immobilization, with total light exposure determined by the size of the desired gradient. Following illumination, substrates were immersed in an appropriate rinse solution and sonicated on ice. The following rinse solutions were utilized: for ConA-biotin, 0.5% Tween 20 in HEPES buffer; for mannan, 0.5 mg/mL sodium dodecyl sulfate in Dulbecco's PBS buffer; and for P-selectin, 0.5% Tween 20 and 1% BSA in Dulbecco's PBS buffer with $Ca^{2+}$and Mg^{2+}.

2.4.4 Setting up new light source: Ar ion laser with refractive beam optics

The optical configuration used to generated an expanded, homogenized beam of collimated light is shown in Figure 2.6. I obtained an Argon ion laser (Coherent Innova 90-4, Laser Innovations), which has a UV output (λ = 351.1-363.8 nm) and a Gaussian profile with a

diameter of approximately 1.5 mm (at $1/e^2$), as determined with a laser beam-profiling camera (Ophir-Spiricon). I placed mirrors in line with the beam to direct it through the πShaper, which consists of a set of refractive beam optics. As the beam passes through the πShaper, the Gaussian profile is converted to a flat-top. Lenses I and II (plano-convex, f = 25.4 mm; and plano-convex, f = 100 mm, respectively, positioned approximately 125 mm apart) make up the Keplerian telescope that expands the beam four-fold, from a diameter of 1.5 mm to 6 mm, such that it has the appropriate diameter to enter the πShaper. Lenses III and IV (plano-convex, f = 50 mm; and plano-convex, f = 150 mm, respectively, positioned approximately 200 mm apart) make up the Keplerian telescope that expand the beam an additional three-fold, from a diameter of 6 mm to 18 mm, resulting in the optimized field of light for photopatterning applications. The πShaper was mounted on an x,y,z-translation stage which enabled it to be positioned precisely in line with the beam. All other optics were mounted with stationary lens mounts that were positioned directly in line with the beam. At each step of the setup, and prior to each photopatterning application, the profile of the beam was measured with the laser camera and modifications to the positions of optics and the πShaper were made until a flat-top output of the desired intensity was achieved.

2.4.5 Generation of biomolecular patterns and gradients: laser + πShaper

For data presented in Figures 2.7b and 2.8a, the BP-modified substrate in the assembled device was positioned face-down (allowing for illumination through the back of the glass substrate) beneath the UV output of the laser+πShaper setup. The laser light was homogenized using refractive beam-shaping optics (π-Shaper), as described above. The laser power was adjusted to give a final illumination intensity of 14 mW/cm^2 at the substrate. For photopatterning of biomolecules, a chromium-coated glass photomask with 500-μm square features separated by 500 μm, or a relief mask presenting 800-μm circles with 200-μm spacing, was placed onto the back of the substrate and irradiated for the following times: 5 min for ConA-biotin and 1 min for P-selectin.

Following UV exposure, the flow chamber assembly was immersed in a rinse solution and the substrate was separated from the flow chamber device. The following rinse solutions were utilized: 0.5% (v/v) Tween 20 in PBS buffer for substrates presenting ConA-biotin and

fibronectin; and 0.5% (v/v) Tween 20 and 1% (w/v) BSA in Dulbecco's PBS with Ca^{2+} and Mg^{2+} for substrates presenting P-selectin.

2.4.6 Fluorescence imaging of substrates presenting photoimmobilized biomolecules

Photopatterned substrates were blocked with 1% BSA in PBS or HEPES overnight followed by incubation with fluorescently labeled binding partners and visualization with a fluorescence slide scanner (GenePix 4000B, MDS Analytical Technologies) to obtain fluorescence intensity line scans. For the visualization of immobilized ConA-biotin, substrates were incubated for 1 h in a solution of streptavidin−AlexaFluor647 conjugate (0.05 μg/mL, Invitrogen) in 1% BSA/HEPES. For substrates with two-component mannan and P-selectin immobilization, slides were incubated for 1 hr in a solution of ConA-biotin (0.1 μg/mL), streptavidin−Cy3 conjugate (0.05 μg/mL, Invitrogen), mouse anti-human P-selectin (0.5 μg/mL, R&D Systems, clone 9E1), and AlexaFluor647-conjugated rabbit anti-mouse IgG (1 μg/mL, Invitrogen) in 1% BSA/HEPES. Substrates presenting P-selectin for native-ligand binding studies were incubated overnight in a solution containing: native ligand PSGL-1 (8 μg/mL, F_c chimera, R&D Systems), mouse anti-human IgG (4 μg/mL, Abnova), and AlexaFluor647-conjugated goat anti-mouse IgG (2 μg/mL, Invitrogen), in 1% BSA/PBS with Ca^{2+} and Mg^{2+}. Substrates were rinsed in PBS, water, dried under a stream of nitrogen, and imaged on a fluorescence slide scanner. The specific ligand-binding ability of P-selectin is demonstrated by the fact that incubation in the same solution lacking PSGL-1 results in baseline fluorescence levels in the resulting images (data not shown).

2.4.7 Quantitative determination of immobilized protein site density

To determine protein loading on BP-modified substrates under various photoimmobilization conditions, a radioimmunoassay using an [^{125}I]-labeled binding partner was performed to analyze photopatterned protein substrates. In an effort to establish a relationship between the site density from the radioimmunoassay and the fluorescence intensity (F.I.), identical substrates were created and analyzed in parallel using both fluorescence and immunological methods, and the resultant data were correlated. A rectangular parallel-plate flow chamber was assembled with a BP-modified glass substrate (as described above). The assembled device was positioned face-down, allowing for illumination through the back of the substrate

beneath the UV LED array source, which was configured to an output of power of 17 mW/cm^2. A total of 8 substrates were prepared for each of the following six irradiation time points in the presence of ConA-biotin (5 μg/mL): 5, 15, 30, 60, and 120 sec. BP-modified substrates that never contacted ConA-biotin were used as controls. Four of the eight replicates at each exposure time were analyzed for F.I., as described above. The remaining four replicates were subjected to a radioimmunoassay for site density quantitation.

[^{125}I]-labeled streptavidin was generated by a standard protein iodination technique. Streptavidin (10 mg/mL, Pierce) was placed into the bottom of tube pre-coated with Pierce Iodination Reagent, along with ^{125}I (5 μCi/μg, in 10^{-8} M NaOH, Perkin-Elmer), followed by incubation at room temperature for 10 min with shaking. The solution was then purified using a Bio-Spin 6 purification column (Bio-Rad). The percentage of excess ^{125}I remaining in the protein solution was determined following a standard protocol for thin layer chromatography on Whatman filter paper.[27] The concentration of material obtained after purification was determined using a Bradford assay. Slides presenting ConA-biotin were incubated with saturating concentrations of [^{125}I]-labeled SA (0.05 μg/mL) in 1% BSA/PBS for 1 hr, rinsed in PBS, purified water, and dried under a stream of nitrogen. Slides were cut into four pieces and each piece placed into a scintillation tube with 1 mL of scintillation fluid (ScintiSafe Econo 1, Fisher Scientific). The radioactivity count for all the sample tubes was determined using a scintillation counter (Beckman LS 6500 Liquid Scintillation Counter, Beckman Coulter), and reported in units of counts per min (CPM). The number of radioactive molecules bound per area (molecules/μm^2) was then determined by comparison of the CPM obtained from the slides to a standard curve of [^{125}I]-labeled streptavidin standards of known concentration. Plots of F.I. vs. exposure time, and CPM vs. exposure time were combined to establish a correlation between F.I. and the density of immobilized biomolecules.

2.4.8 Cell adhesion and rolling studies

HL-60 cells (gift from the Hergenrother group at UIUC, or purchased from ATCC) were cultured in RPMI 1640 supplemented with penicillin (100 U/mL), streptomycin (100 μg/mL), and 10% fetal bovine serum (SCS Cell Media Facility, UIUC). Photopatterned P-selectin substrates were prepared as described above. Substrates were rinsed and soaked overnight in

PBS containing 0.2% Pluronic F127 and 1% BSA. Substrates were then rinsed three times in water and placed into a cell culture dish (100 mm x 20 mm). Cells were fluorescently labeled using AlexaFluor488 carboxylic acid succinimidyl ester (Invitrogen) and seeded onto substrates in PBS at a concentration of 5 x 10^6 cells/mL and incubated at 4 ºC for 2 hr. The solution was aspirated off and the substrates were rinsed in PBS to remove non-specifically bound cells. The resulting patterns of cells were visualized using a fluorescence microscope (Leica DM 6000 Upright Microscope, Leica Microsystems).

For cell patterning demonstrations, photopatterned P-selectin gradient substrates were prepared as described, rinsed and sonicated for 30 min in 0.2% Pluronic F127 in PBS, and blocked overnight in 0.2% Pluronic F127 and 1% BSA in PBS. Cells were seeded onto substrates at 5 × 10^6 cells/mL in PBS and incubated at 4 °C for 2 hr. Nonadhered cells were aspirated off after gentle rinsing with PBS, and the resulting cell gradients were imaged using an optical microscope (Zeiss 40C Invertiskop, Carl Zeiss Inc.).

For HL-60 cell rolling studies, a 6-mm P-selectin gradient was prepared as described and assembled with the parallel plate flow chamber. Cells were resuspended in cell media at 5 × 10^5 cells/mL and flowed through the chamber at 50 μL/min, yielding an applied shear stress of 0.24 dyn/cm^2. Shear stress was calculated using the equation $T = 6\mu Q/a^2 b$, where μ is the apparent viscosity of the media, Q is the volumetric flow rate, a is the height of the flow chamber, and b is the width of the flow chamber. Cell rolling videos were recorded with a digital camera, and the velocity of rolling cells was determined with ImageJ (National Institutes of Health).

2.5 References

1. M. Mrksich, *Chemical Society Reviews* **2000**, *29*, 267.
2. N. Sniadecki, R. Desai, S. Ruiz, C. Chen, *Annals of Biomedical Engineering* **2006**, *34*, 59.
3. a) M. Mrksich, *Current Opinion in Chemical Biology* **2002**, *6*, 794; b) R. C. Gunawan, J. Silvestre, H. R. Gaskins, P. J. A. Kenis, D. E. Leckband, *Langmuir* **2006**, *22*, 4250.
4. a) T. Cha, A. Guo, X. Y. Zhu, *Proteomics* **2005**, *5*, 416; b) S. F. Kingsmore, *Nature Reviews Drug Discovery* **2006**, *5*, 310.
5. a) K. De Vos, J. Girones, S. Popelka, E. Schacht, R. Baets, P. Bienstman, *Biosensors and Bioelectronics* **2009**, *24*, 2528; b) Y. Jung, J. M. Lee, J.-w. Kim, J. Yoon, H. Cho, B. H. Chung, *Analytical Chemistry* **2009**, *81*, 936; c) X.-h. Liu, H.-k. Wang, J. N. Herron, G. D. Prestwich, *Bioconjugate Chemistry* **2000**, *11*, 755; d) A. L. Washburn, L. C. Gunn, R. C. Bailey, *Analytical Chemistry* **2009**, *81*, 9499.
6. R. Fan, O. Vermesh, A. Srivastava, B. K. H. Yen, L. Qin, H. Ahmad, G. A. Kwong, C.-C. Liu, J. Gould, L. Hood, J. R. Heath, *Nature Biotechnology* **2008**, *26*, 1373.
7. A. B. Braunschweig, F. Huo, C. A. Mirkin, *Nature Chemistry* **2009**, *1*, 353.
8. a) K. Moore, K. Patel, R. Bruehl, F. Li, D. Johnson, H. Lichenstein, R. Cummings, D. Bainton, R. McEver, *Journal of Cell Biology* **1995**, *128*, 661; b) D. M. Togashi, A. G. Ryder, G. Heiss, *Colloids and Surfaces B: Biointerfaces* **2009**, *72*, 219.
9. a) B. D. Ratner, S. J. Bryant, *Annual Review of Biomedical Engineering* **2004**, *6*, 41; b) R. Ganesan, K. Kratz, A. Lendlein, *Journal of Materials Chemistry* **2010**, *20*, 7322; c) E. Beurer, N. V. Venkataraman, A. Rossi, F. Bachmann, R. Engeli, N. D. Spencer, *Langmuir*; d) R. C. Gunawan, E. R. Choban, J. E. Conour, J. Silvestre, L. B. Schook, H. R. Gaskins, D. E. Leckband, P. J. A. Kenis, *Langmuir* **2005**, *21*, 3061; e) S. T. Plummer, Q. Wang, P. W. Bohn, R. Stockton, M. A. Schwartz, *Langmuir* **2003**, *19*, 7528; f) A. Pulsipher, N. P. Westcott, W. Luo, M. N. Yousaf, *Journal of the American Chemical Society* **2009**, *131*, 7626.
10. a) W. S. Dillmore, M. N. Yousaf, M. Mrksich, *Langmuir* **2004**, *20*, 7223; b) E. W. L. Chan, M. N. Yousaf, *Molecular Biosystems* **2008**, *4*, 746.
11. a) B. M. Lamb, D. G. Barrett, N. P. Westcott, M. N. Yousaf, *Langmuir* **2008**, *24*, 8885; b) L. Liu, B. D. Ratner, E. H. Sage, S. Jiang, *Langmuir* **2007**, *23*, 11168.

12. a) R. T. Petty, H. W. Li, J. H. Maduram, R. Ismagilov, M. Mrksich, *Journal of the American Chemical Society* **2007**, *129*, 8966; b) C. J. Wang, X. Li, B. Lin, S. Shim, G.-l. Ming, A. Levchenko, *Lab on a Chip* **2008**, *8*, 227; c) S. K. W. Dertinger, X. Jiang, Z. Li, V. N. Murthy, G. M. Whitesides, *Proceedings of the National Academy of Sciences* **2002**, *99*, 12542.

13. S.-J. Wang, W. Saadi, F. Lin, C. M.-C. Nguyen, N. L. Jeon, *Experimental Cell Research* **2004**, *300*, 180.

14. M. J. Kipper, H. K. Kleinman, F. W. Wang, *Analytical Biochemistry* **2007**, *363*, 175.

15. a) N. P. Reynolds, J. D. Tucker, P. A. Davison, J. A. Timney, C. N. Hunter, G. J. Leggett, *Journal of the American Chemical Society* **2009**, *131*, 896; b) S. Chen, L. M. Smith, *Langmuir* **2009**, *25*, 12275; c) N. Li, C.-M. Ho, *Lab on a Chip* **2008**, *8*, 2105; d) J. Y. Lee, S. S. Shah, C. C. Zimmer, G.-y. Liu, A. Revzin, *Langmuir* **2008**, *24*, 2232; e) W. C. Chang, D. W. Sretavan, *Langmuir* **2008**, *24*, 13048; f) K. M. Ainslie, T. A. Desai, *Lab on a Chip* **2008**, *8*, 1864; g) S. Waichman, M. Bhagawati, Y. Podoplelova, A. Reichel, A. Brunk, D. Paterok, J. Piehler, *Analytical Chemistry*, *82*, 1478.

16. a) C. Wendeln, S. Rinnen, C. Schulz, H. F. Arlinghaus, B. J. Ravoo, *Langmuir*, ASAP; b) J. M. Belisle, J. P. Correia, P. W. Wiseman, T. E. Kennedy, S. Costantino, *Lab on a Chip* **2008**, *8*, 2164; c) M. A. Holden, S.-Y. Jung, P. S. Cremer, *Analytical Chemistry* **2004**, *76*, 1838.

17. a) O. Prucker, C. A. Naumann, J. Ruhe, W. Knoll, C. W. Frank, *Journal of the American Chemical Society* **1999**, *121*, 8766; b) G. K. Raghuraman, R. Dhamodharan, O. Prucker, J. Ruhe, *Macromolecules* **2008**, *41*, 873.

18. a) L. F. Rozsnyai, D. R. Benson, S. P. A. Fodor, P. G. Schultz, *Angewandte Chemie International Edition in English* **1992**, *31*, 759; b) E. Delamarche, G. Sundarababu, H. Biebuyck, B. Michel, C. Gerber, H. Sigrist, H. Wolf, H. Ringsdorf, N. Xanthopoulos, H. J. Mathieu, *Langmuir* **1996**, *12*, 1997; c) W. W. Shen, S. G. Boxer, W. Knoll, C. W. Frank, *Biomacromolecules* **2001**, *2*, 70; d) X. Cao, M. S. Shoichet, in *Journal of Biomaterials Science -- Polymer Edition, Vol. 13*, VSP International Science Publishers, **2002**, pp. 623; e) K. Abu-Rabeah, D. Atias, S. Herrmann, J. Frenkel, D. Tavor, S. Cosnier, R. S. Marks, *Langmuir* **2009**, *25*, 10384; f) N. Griep-Raming, M. Karger, H. Menzel, *Langmuir* **2004**, *20*, 11811; g) J. D. Jeyaprakash, S. Samuel, J. Ruhe, *Langmuir*

2004, *20*, 10080; h) M. Y. Balakirev, S. Porte, M. Vernaz-Gris, M. Berger, J.-P. Arie, B. Fouque, F. Chatelain, *Analytical Chemistry* **2005**, *77*, 5474; i) T. L. Delaney, D. Zimin, M. Rahm, D. Weiss, O. S. Wolfbeis, V. M. Mirsky, *Analytical Chemistry* **2007**, *79*, 3220; j) T. Konry, M. Bouhifd, S. Cosnier, M. Whelan, A. Valsesia, F. Rossi, R. S. Marks, *Biosensors and Bioelectronics* **2007**, *22*, 2230; k) S. Szunerits, N. Shirahata, P. Actis, J. Nakanishi, R. Boukherroub, *Chemical Communications* **2007**, 2793; l) L. Y. Hwang, H. Gotz, W. Knoll, C. J. Hawker, C. W. Frank, *Langmuir* **2008**, *24*, 14088; m) L. Marcon, M. Wang, Y. Coffinier, F. Le Normand, O. Melnyk, R. Boukherroub, S. Szunerits, *Langmuir* **2009**, *26*, 1075.

19. a) R. S. Davidson, *Chemical Communications* **1966**, 575; b) N. J. Turro, *Modern Molecular Photochemistry*, University Science Books, Mill Valley, **1991**; c) G. Dorman, G. D. Prestwich, *Biochemistry* **1994**, *33*, 5661.
20. a) C. L. Hypolite, T. L. McLernon, D. N. Adams, K. E. Chapman, C. B. Herbert, C. C. Huang, M. D. Distefano, W.-S. Hu, *Bioconjugate Chemistry* **1997**, *8*, 658; b) C. B. Herbert, T. L. McLernon, C. L. Hypolite, D. N. Adams, L. Pikus, C. C. Huang, G. B. Fields, P. C. Letourneau, M. D. Distefano, W.-S. Hu, *Chemistry & Biology* **1997**, *4*, 731; c) D. N. Adams, E. Y.-C. Kao, C. L. Hypolite, M. D. Distefano, W.-S. Hu, P. C. Letourneau, *Journal of Neurobiology* **2005**, *62*, 134.
21. C. R. Toh, T. A. Fraterman, D. A. Walker, R. C. Bailey, *Langmuir* **2009**, *25*, 8894.
22. H. Barhoumi, A. Maaref, N. Jaffrezic-Renault, *Langmuir* **2010**, *26*, 7165.
23. A. Pulsipher, M. N. Yousaf, *Langmuir* **2009**.
24. S. A. Alang Ahmad, L. S. Wong, E. ul-Haq, J. K. Hobbs, G. J. Leggett, J. Micklefield, *Journal of the American Chemical Society* **2009**, *131*, 1513.
25. a) C. Dong, X. X. Lei, *Journal of Biomechanics* **2000**, *33*, 35; b) M. B. Lawrence, G. S. Kansas, E. J. Kunkel, K. Ley, *Journal of Cell Biology* **1997**, *136*, 717.
26. M. B. Lawrence, T. A. Springer, *Cell* **1991**, *65*, 859.
27. C. S. R. Gooden, in *Diagnostic and Therapeutic Antibodies* (Eds.: A. J. T. George, C. E. Urch), Humana Press, Inc., New Jersey, **2000**, pp. 339.

Chapter 3

Probing Dynamic Cell-Substrate Interactions using Photochemically Generated Surface-Immobilized Gradients: Application to Selectin-Mediated Leukocyte Rolling

Notes and Acknowledgements

This chapter has been reproduced from the original paper "Photochemically Generated Surface-Immobilized Gradients: Application to Selectin-Mediated Leukocyte Rolling" (Herman, C. T.; Potts, G. K.; Michael, M. C.; Tolan, N. V., Bailey, R. C. *Integrative Biology* **2011**, 3, 779-791). It has been reproduced here with permission from the Royal Society of Chemistry © 2011. The paper can be accessed at http://pubs.rsc.org/en/Content/ArticleLanding/2011/IB/c0ib00151a.

This work was supported by grants from the Roy J. Carver Foundation and the Camille and Henry Dreyfus Foundation. CTH was supported by predoctoral fellowships from the National Science Foundation and the National Institutes of Health (NCCAM NRSA, Award Number F131AT006286-01). The content is solely the responsibility of the authors and does not necessarily represent the official views of the National Center for Complementary & Alternative Medicine, the National Institutes of Health, or the National Science Foundation.

We are grateful to the following individuals for their contributions to this work: Kathryn Carlson for help with radioimmunoassays; Geoffrey L. Herman for assistance with ImageJ data analysis; Dr. Barbara Pilas for assistance with flow cytometry; Dr. Alexei Lagoutchev for assistance with the π-shaper; Professor Fei Wang for providing HL-60 cells. Gregory K. Potts and Madeline C. Michael assisted in the analysis of leukocyte rolling data.

3.1 Introduction

Numerous cellular processes depend on a cell's ability to sense and respond to biomolecular gradient cues. Embryonic development, neuronal guidance, angiogenesis, wound healing, inflammation, and cancer/metastasis are among the complex physiological phenomena that are regulated and/or guided by spatial variation in the concentrations of ligands encountered either in the solution phase or presented as immobilized gradients within the cellular microenvironment (*i.e.*, adjacent cells or the extracellular matrix).[1] In order to experimentally parse out the detailed contributions of immobilized ligand density on cell behavior, substrates that present biomolecular gradients on surfaces are of fundamental interest for *in vitro* assays that enable the investigation of cell migration and polarization in response to immobilized protein concentration.[2] Of even greater interest are *in vitro* platforms that enable multi-parameter studies that systematically address the combined effects of multiple stimuli, such as the density of multiple biomolecules, topography, or shear stress, amongst others, on cell behavior.[3]

Many approaches have been developed to generate biomolecular surface gradients, including the use of microfluidics followed by surface attachment,[2a,4] electrochemical desorption of self-assembled monolayers on gold,[5] photochemical surface deproctection to reveal reactive functional groups,[6] and diffusion-guided surface adsorption.[7] Each of these techniques have inherent strengths and limitations, as detailed in Chapter 1.

The approach involves surface functionalization of glass to present a well-known photocrosslinking molecule, benzophenone (BP).[8] Solutions containing the biomolecule of interest are introduced to the substrate through a flow chamber and immobilized as UV light (351.1-363.8 nm) induces the formation of new C-C bonds between the BP molecules on the surface and the proteins. This approach was previously shown by our lab to be useful for the generation of single- and multi-component geometric patterns and spatial concentration gradients composed of both proteins and carbohydrates.[9] In choosing this particular gradient generation approach, I reasoned that the overall simplicity, biomolecular generality, and capability to generate complex, multi-component substrates for biointerface studies would make this a broadly applicable platform for researchers from many different fields possessing varying degrees of

familiarity with the advanced surface chemistries and microfabrication techniques utilized in other gradient generation methodologies.

As a proof-of-principle demonstration of this technique, I was interested in applying surface-immobilized gradients to achieve a better understanding of the process of leukocyte recruitment, the first step in the inflammatory response. Over the past several decades, numerous biomolecules involved in leukocyte trafficking have been identified and characterized. Among these are a family of molecules known as selectins, which are membrane-bound glycoproteins presented on leukocytes (L-selectin) and inflamed endothelial cells (P-selectin, E-selectin).[10] The role of selectins is to mediate the initial flow-dependent tethering and rolling of leukocytes on vascular surfaces.[11] Following selectin-mediated rolling, additional biomolecular interactions take place with other endothelial-expressed proteins and enzymes that ultimately lead to leukocyte arrest, diapedesis and migration through the tissue to the site of injury or infection.[12] Properly regulated inflammatory and immune responses are essential for health and survival, but if left unchecked, can result in a variety of diseases such as rheumatoid arthritis, asthma, psoriasis, Crohn's disease, thrombotic disorders, and autoimmune disease.[13] A more complete understanding of the molecular basis of leukocyte recruitment could lead to the development of more effective therapeutics for dysregulated inflammation.

Previous studies have shown that selectin-mediated rolling under conditions of physiological shear stress can be studied in an *in vitro* flow assay format, yielding new insights into the biophysical phenomena underlying the first step of leukocyte recruitment.[14] *In vitro* leukocyte flow assays, however, typically employ surfaces presenting non-specifically adsorbed proteins[15,16] that are susceptible to changes over time,[17] or utilize confluent endothelial cell monolayers[18] that express multiple relevant ligands but offer little control over ligand site density.

As schematically illustrated in Figure 3.1, substrates presenting photochemically immobilized gradients of P-selectin and PSGL-1 were generated, characterized, and employed in leukocyte flow assays to determine how various selectin-ligand interactions affect the rolling behavior of two leukocyte cell lines, HL-60 promyelocytes and Jurkat T lymphocytes. Cells were perfused across substrates presenting immobilized protein under conditions of physiological wall

shear stress. Videos were acquired at several positions across the gradient surface and analyzed to assess the combined effect of protein site density and wall shear stress on the number and velocity of rolling cells. By analyzing cell behavior at each combination of site density and shear stress, the interplay between immobilized protein density and shear stress was observed. This simple gradient generation approach will allow for the interrogation of the complex mechanisms involved in the biological processes involved in leukocyte rolling *in vivo* and further elucidate the interplay between substrate composition and environmental conditions.

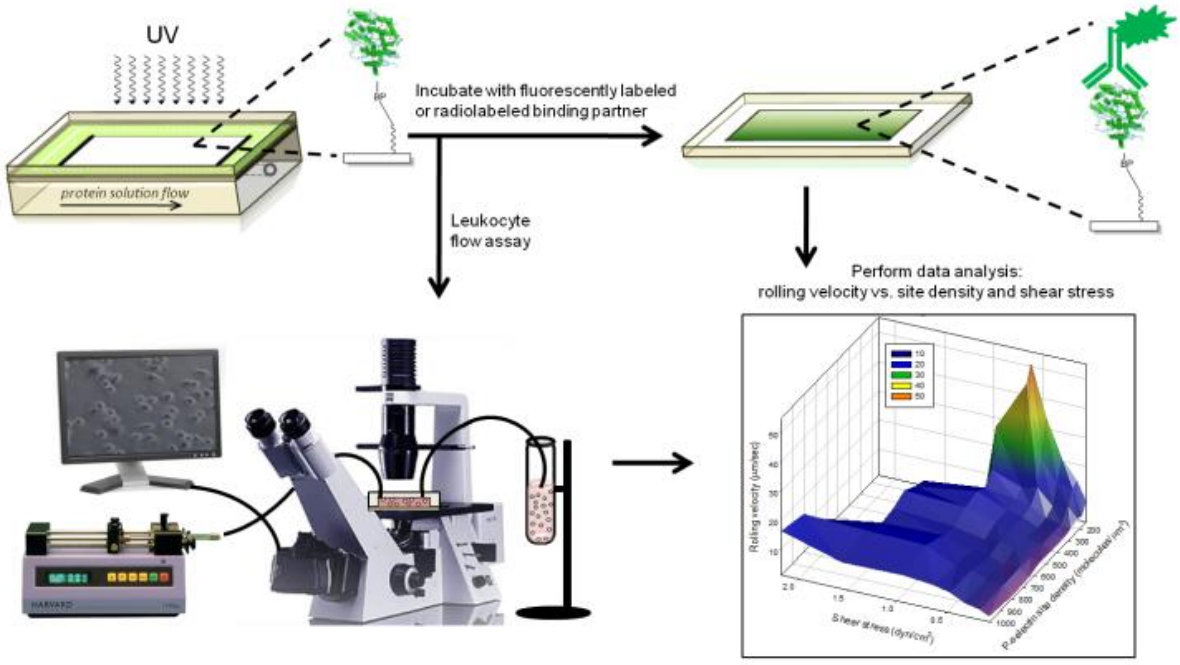

Figure 3.1 A schematic representation of the process by which surface-immobilized gradients on benzophenone (BP)-modified substrates are generated, characterized, and applied to multi-parameter leukocyte flow investigations.

In this study, I describe a facile, molecularly general method for generating model substrates that present covalently immobilized biomolecules at defined and varied site densities. Furthermore, I demonstrate that gradient substrates presenting proteins over a wide range of site densities allow data-rich information to be collected from a single substrate in a short time. This presents an additional advantage over previous approaches which utilize substrates limited to a

single homogeneous presentation of a protein of interest and require multiple substrates to probe the concentration dependence of leukocyte rolling.

3.2 Results and Discussion

In this proof-of-principle study, I demonstrate that surface-immobilized biomolecular gradients generated using BP-modified substrates can be tailored to present protein site densities in a controlled manner and can be applied to leukocyte flow assays. Previous reports of leukocyte flow assays have typically employed substrates that present adsorbed proteins at a uniform site density. The advantages of utilizing photochemically immobilized protein gradients over adsorbed protein substrates are increased biomolecule attachment stability (due to a covalent linkage of proteins to the surface) and the ability to present ligands at controllably varied site densities on a single substrate. This provides a more direct route to conducting comprehensive investigations to assess the effects of various combinations of shear stress and site density on cell behavior using a single substrate, compared to many different substrates that each present only a single immobilized density. In this way, large amounts of data can be acquired from a single experiment, minimizing the amount of materials and time that are required for a multi-parameter analysis of selectin-mediated rolling.

	H_2O Contact Angle, Batch 1	H_2O Contact Angle, Batch 2	H_2O Contact Angle, Batch 3	Average of 3 batches
TESA silanization	48.0 (±1.4)	42.7 (±1.1)	45.2 (±2.6)	45.2 (±2.6)
+BP	57.5 (±7.7)	59.6 (±0.9)	57.3 (±3.9)	58.1 (±3.9)

Table 3.1 Summary of contact angles following silanization with TESA and functionalization with benzophenone (BP). The contact angles reported for each batch are the average (± standard deviation) of at least four substrates.

3.2.1 Characterization of BP-modified substrates

Three batches of BP-modified substrates were generated (Table 3.1). Following each chemical derivatization, substrates were characterized with contact angle goniometry. The

contact angle after silanization was 45.2 (± 2.6)°. After functionalization with BP, the contact angle increased to 58.1 (± 3.9)°.

Conditions for generation of one-component gradients used in Jurkat cell flow assays						
Protein	**concentration (μg/mL)**	**power (mW/cm^2)**	**total exposure time (sec)**	**gradient size (mm)**	**size of gradient used in assay (mm)**	**# positions analyzed in assay**
P-selectin	5	14	24	4.8	2.4	8
PSGL-1	10	14	24	4.8	3	7

Conditions for generation of one-component gradients used in HL-60 cell flow assays						
Protein	**concentration (μg/mL)**	**power (mW/cm^2)**	**total exposure time (sec)**	**gradient size (mm)**	**size of gradient used in assay (mm)**	**# positions analyzed in assay**
P-selectin	10	14	30	4.8	4.2	10
PSGL-1	10	14	24	4.8	4.2	7

Table 3.2 Summary of gradient generation conditions used to generate one-component gradients of P-selectin and PSGL-1.

3.2.2 Quantitative determination of immobilized protein site densities

Data from radioimmunoassays and fluorescence assays are plotted to show the relationship between F.I. and site density, as shown in Figure 3.2. Under the conditions used, I observed that the relationship between the F.I. and corresponding radioactivity signal (converted from cpm to site density using a standard curve) was linear for each set of immobilized protein substrates. The reported site densities are an estimate based on the ability of antibodies to detect the proteins. For simplicity, I assume a 1:1 binding relationship between the [^{125}I]-labeled secondary polyclonal antibody (pAb) and primary monoclonal antibody (mAb), which likely results in an overestimate of protein loading, since each primary mAb might be recognized by multiple secondary [^{125}I]-labeled pAbs. I also assume a 1:1 binding relationship between the

primary mAb and the immobilized surface proteins, although each primary mAb has two antigen binding sites. Overall, the effective site density is probably lower than that determined from the radioimmunoassay since proteins are randomly orientated on the surface and therefore not all are able to be recognized by cellular receptors. However, similar methods and assumptions have been previously made for substrates used in quantitative selectin-ligand assays.[19]

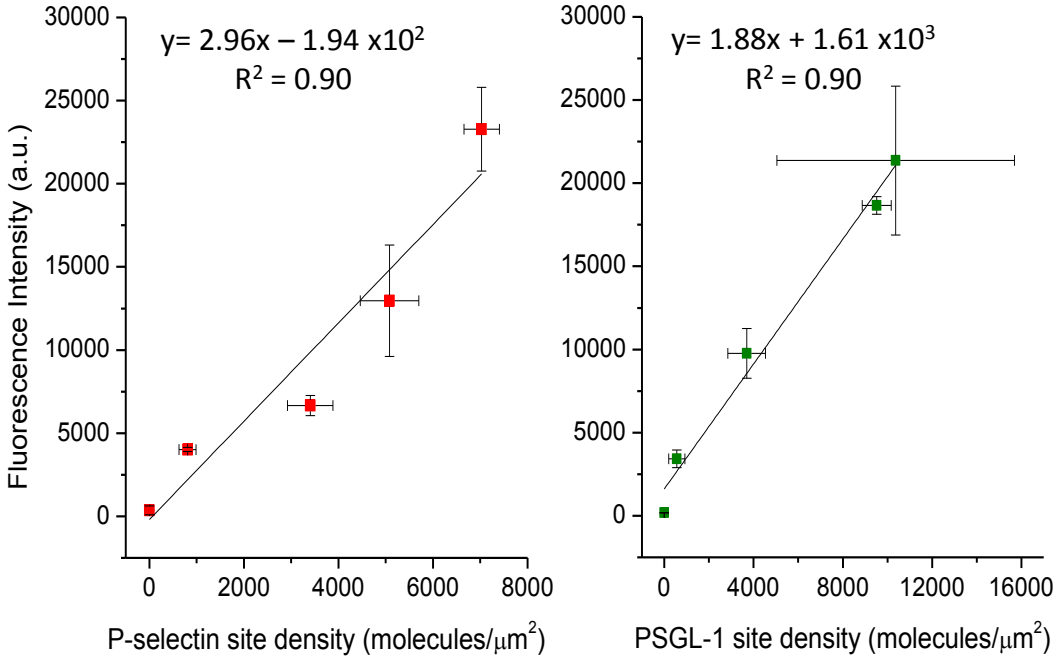

Figure 3.2 The relationship between fluorescence intensity and site density was determined for photoimmobilized P-selectin (red) and PSGL-1 (green) on BP-modified substrates. Substrates were generated in triplicate via flood UV exposures (four different exposure times ranging from 10 to 180 sec) in the presence of protein solution, resulting in homogeneous substrates presenting a wide range protein site density levels. Fluorescence measurements were acquired after incubating substrates with fluorescently labeled antibodies. For site density determination, substrates were incubated with saturating concentrations of primary monoclonal antibody (mAb) and [^{125}I]-labeled secondary polyclonal antibody (pAb). Control substrates were used to account for non-specific mAb and pAb binding. Data is plotted as the average (± 95% C.I.) for n=3 substrates.

Substrates for Jurkat cell flow assays		
P-selectin site density	standard deviation	approximation
(molecules/μm^2)		
2392.03	364.52	2400
2180.13	502.35	2200
1782.28	525.53	1800
1384.13	396.81	1400
1026.76	311.67	1000
669.1	92.73	650
425.96	28.84	450
182.81	12.38	180

Substrates for HL-60 cell flow assays		
P-selectin site density	standard deviation	approximation
(molecules/μm^2)		
958.43	87.69	1000
770.42	152.76	800
657.79	130.43	650
545.16	102.76	550
448.74	84.59	450
352.32	61.69	350
286.76	50.21	280
221.19	0.73	220
182.78	22.78	180
144.37	17.99	140

PSGL-1 site density	standard deviation	approximation
(molecules/μm^2)		
5899.34	1313.66	6000
4646.76	777.97	5000
3927.47	712.62	4000
3424.61	721.77	3500
2581.96	544.16	2500
1739.31	365.04	1800
836.41	175.5436	800

PSGL-1 site density	standard deviation	approximation
(molecules/μm^2)		
4339.32	1032.91	4500
3860.19	971.11	4000
3470.98	767.19	3500
2697.33	738.54	2500
1718.97	516.5	1500
1125.06	397.79	1000
123.08	84.66	100

Table 3.3 Summary of data and respective approximations from one-component gradients of P-selectin and PSGL-1 on BP-modified substrates. Protein site density was determined by converting data from fluorescence assays to site density using data from fluorescence-radioactivity correlation studies (see Figure 3.2).

3.2.3 Generation and characterization of linear one-component gradients

The goal in preparing one-component gradient substrates for leukocyte flow assays was to incorporate biomolecules that are known to be involved in the initial steps of leukocyte recruitment. The first step of leukocyte recruitment is rolling along the endothelium, which is facilitated by selectin-ligand interactions. In these studies, I generated and characterized one-component gradients of P-selectin and PSGL-1 and applied them to leukocyte flow assays. Conditions for gradient generation were optimized by adjusting protein concentration, exposure time and light intensity, to yield linear slopes encompassing a large range of protein site densities, which are detailed below. The plots in Figure 3.3 show linescans from two or three replicate substrates for each protein. The conditions utilized for P-selectin and PSGL-1 gradients were optimized for each protein. For clarity, I report the values as approximations of the precisely determined values (Table 3.3). Gradient substrates made in parallel with those used in

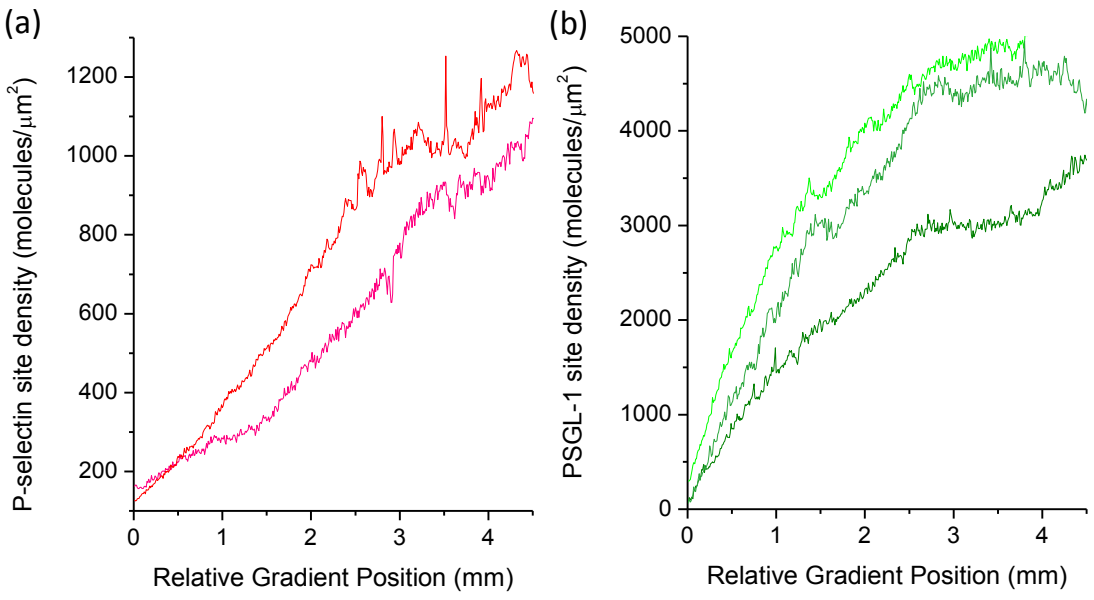

Figure 3.3 Linescans for one-component gradient substrates prepared for flow assays with HL-60 cells. BP-modified substrates present immobilized (a) P-selectin and (b) PSGL-1 on BP-modified substrates. Gradients were characterized in a fluorescence assay and fluorescence data was converted to site density using the results from the fluorescence-radioactivity correlation studies.

cell rolling experiments were characterized in a fluorescence assay and the results converted to site density using the appropriate linear relationship between F.I. and site density for each protein. The average site density at various positions along the gradient was determined for a region the size of the field of view of a 20x microscope objective.

3.2.4 Leukocyte flow assays

It is well-established that interactions between the selectins (P-, E-, and L-selectin) and their respective ligands facilitate leukocyte rolling, both *in vitro* and *in vivo*.[11d] P-selectin is responsible for initiating tethering and rolling of leukocytes on the blood vessel endothelium,[20] while L-selectin is expressed on most leukocytes and is able to bind to ligands on the endothelium[21] as well as to PSGL-1 presented on other cells.[22] This latter process is known as secondary tethering and enables rolling leukocytes to recruit additional leukocytes to the inflamed endothelium. In these studies, I generated substrates presenting varied site densities of P-selectin and PSGL-1 and applied them to leukocyte flow assays.

HL-60 cells were found to tether to and roll on P-selectin substrates over a wide range of site densities and wall shear stresses. Jurkat cells also tethered to and rolled on immobilized P-selectin, as well as PSGL-1, over a range of site densities and shear stresses. HL-60 cell rolling was not observed on PSGL-1 substrates (data not shown), which is consistent with literature reports that show low L-selectin expression on HL-60 cells.[23]

In general, I found that a minimum level of wall shear stress, commonly referred to as the shear threshold,[15,24] was required for selectin-mediated cell rolling to be initiated and sustained, and was also affected by the underlying site density of immobilized protein. A lack of cell rolling under a particular set of conditions is represented by the absence of that data point. In all cases, data from three replicate substrates is plotted as the average (±SEM), unless otherwise noted. Alongside each 2D plot, the average rolling velocities and cell flux are plotted in 3D surface plots (without error bars for clarity) to present the combined effects of site densities and shear stress on cell rolling velocity as an interaction landscape.

Neither cell type was found to interact with BSA-blocked BP-modified substrates, confirming that leukocyte rolling on gradient substrates were indeed the result of specific

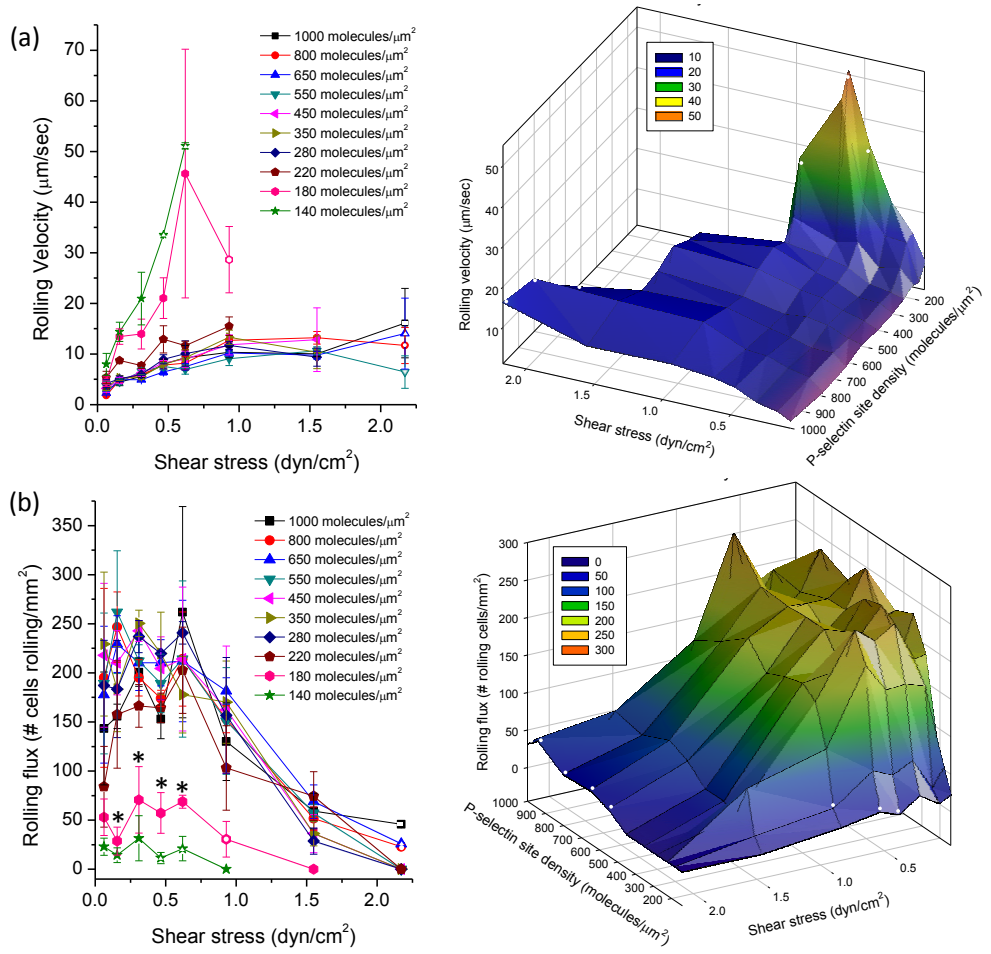

Figure 3.4 Results from initial attachment assays of HL-60 cells on immobilized P-selectin. HL-60 cells were perfused over one-component P-selectin gradient substrates at shear stresses ranging from 0.062 to 2.17 dyn/cm^2. 2D data plots and 3D surface plots show the average cell (a) rolling velocity and (b) rolling flux plotted as a function of shear stress and P-selectin site density. At low site densities (140 and 180 molecules/μm^2), rolling velocity increased sharply as a function of shear stress, while at all higher site densities analyzed, the rolling velocity leveled off beyond 0.93 dyn/cm^2. At site densities of 140 and 180 molecules/μm^2, significantly fewer rolling cells were observed compared to at higher site densities (p<0.05), while increasing the site density from 280 to 1000 molecules/μm^2 had no significant effect on rolling flux at shear stresses ≥ 0.16 dyn/cm^2. The mean rolling velocity or rolling flux was determined for each substrate, and the means from three substrates were averaged and plotted as the average (±SEM). Open data points represent the average (±range) of n=2 substrates.

interactions with the immobilized protein of interest. When Jurkat cells were incubated with a function-blocking mAb against L-selectin (10 μg/mL), cell rolling on immobilized PSGL-1 substrates was absent under all conditions of wall shear stress investigated. Additionally, when P-selectin substrates were incubated with a function-blocking mAb (20 μg/mL), cell rolling for both cell types was completely eliminated (data not shown).

3.2.4.1 P-selectin-mediated rolling of HL-60 cells

P-selectin substrates for HL-60 flow assays presented site densities ranging from 140 to 1000 molecules/μm^2 (Figure 3.3a). Cell rolling was observed over the entire range of site densities and the shear threshold was met starting at a shear stress of 0.062 dyn/cm^2 (10 μL/min). I found that as site density decreased, cell rolling occurred over a smaller range of shear stresses. At site densities of 140 and 180 molecules/μm^2, cell rolling was observed from the shear threshold value up to 0.62 and 0.93 dyn/cm^2, respectively, while at site densities $\geq$ 280 molecules/μm^2, cell rolling was observed up to 2.17 dyn/cm^2 (Figure 3.4a). Above 2.17 dyn/cm^2, HL-60 cell rolling was not observed at any of the site densities analyzed.

Rolling velocity data for HL-60 cells on P-selectin gradient substrates are represented in a 3D surface plot (Figure 3.4a), showing the combined effect of site density and shear stress on rolling velocity. Decreasing the site density from 220 to 140 molecules/μm^2 resulted in an increase in the average rolling velocity, which I presume is because a lesser number of receptor-ligand interactions leads to faster rolling. I speculate that saturation of cell surface-expressed PSGL-1 occurs above 220 molecules/μm^2, resulting in an average cell rolling velocity that is not significantly affected by shear stress. Overall, HL-60 cell rolling velocity increased as shear stress increased, and the effect was most pronounced at lower site densities.

Figure 3.4b shows the effect of shear stress and site density on cell rolling flux. Consistent with the cell rolling velocity data presented in Figure 3.4a, increasing the site density above 220 molecules/μm^2 at a given shear stress did not significantly affect rolling flux. The effect of shear stress at a given site density, however, exhibited the following trend: At site densities of 220 molecules/μm^2 and higher, rolling flux remained constant from 0.062 dyn/cm^2 to 0.93 dyn/cm^2, above which it dropped until cells were no longer observed to roll. Conversely, at the lowest site densities analyzed (140 and 180 molecules/μm^2), rolling flux was unaffected by

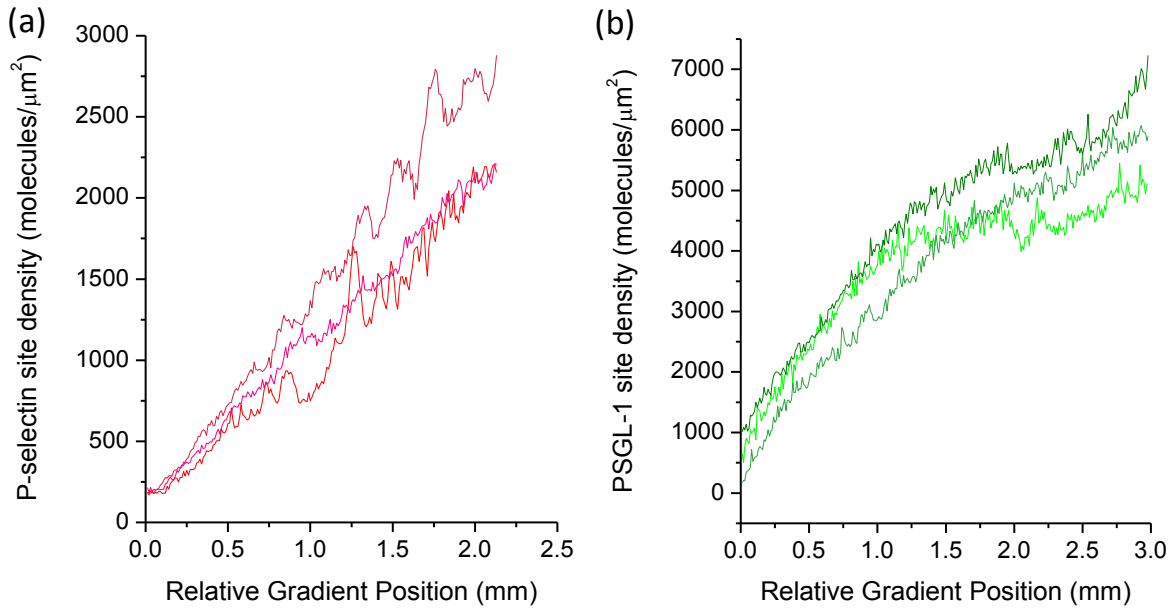

Figure 3.5 One-component gradients of (a) P-selectin and (b) PSGL-1 on BP-modified substrates were generated and characterized by converting data from fluorescence assays to site density using the results from fluorescence-radioactivity correlation studies (Figure 3.2). For substrates used in Jurkat flow assays, immobilized protein site densities ranged from approximately 180 to 2400 and 800 to 6000 molecules/μm^2 for P-selectin and PSGL-1, respectively.

increasing shear stress up to 0.93 and 1.55 dyn/cm^2, respectively, above which cells were no longer observed to roll. Overall, fewer cells (~3-fold less) were found to roll on the lowest site densities analyzed (140 and 180 molecules/μm^2), compared to at site densities ≥ 280 molecules/μm^2.

3.2.4.2 P-selectin-mediated rolling of Jurkat T cells

P-selectin-mediated cell rolling was also assessed for Jurkat T cells. P-selectin substrates for Jurkat flow assays presented site densities ranging from 140 to 1000 molecules/μm^2 (Figure 3.5a). Many trends were similar to those observed with HL-60 cells, including an overall positive

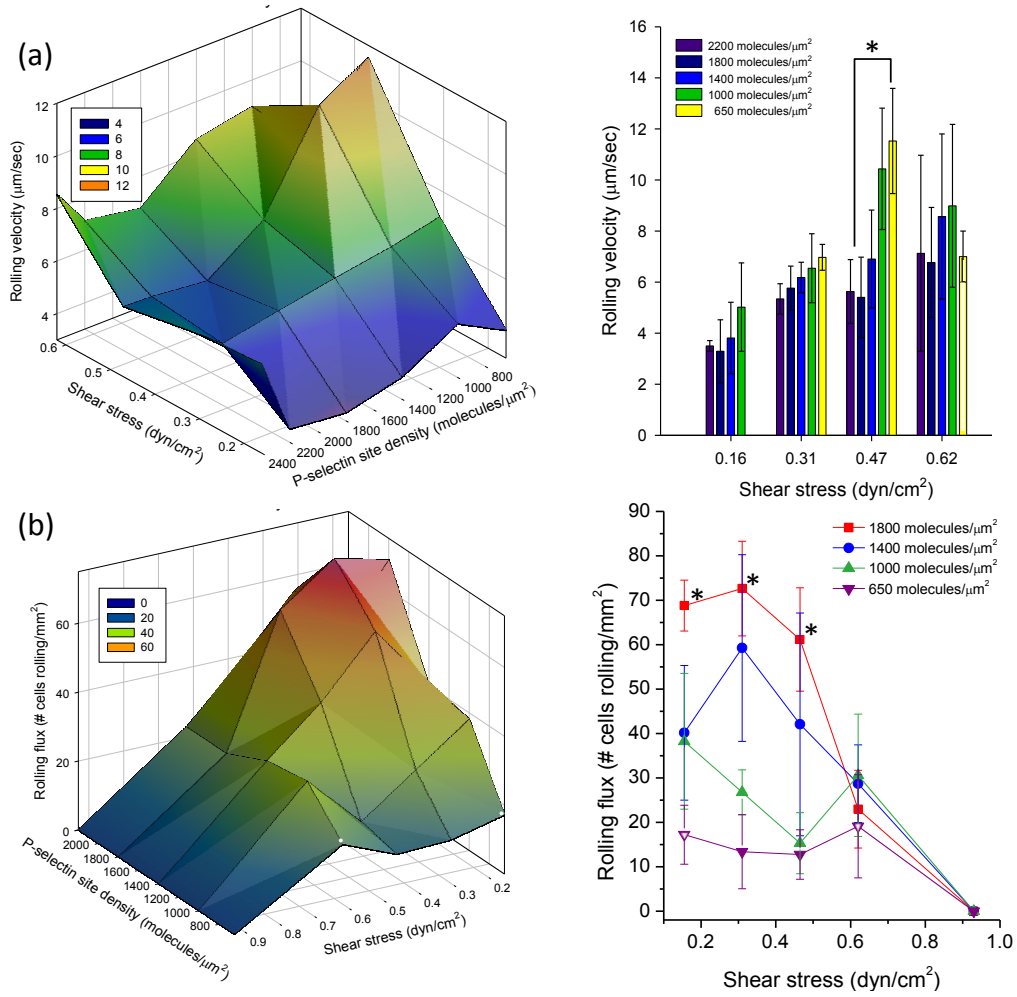

Figure 3.6 Results from initial attachment assays of Jurkat cells on immobilized P-selectin. (a) A 3D surface plot of rolling velocity as a function of shear stress and P-selectin site density reveals that increasing shear stress resulted in an overall increase in rolling velocity. However, the velocity of rolling cells at a given shear stress was largely unaffected by increasing site density, except at 0.47 dyn/cm^2, in which case rolling velocity was higher at a site density of 650 molecules/μm^2 compared to 1800 or 2200 molecules/μm^2 (*, p<0.05). (b) Rolling flux was greatest at higher site densities and lower shear stresses and decreased with increasing shear stress, except at the lowest site densities analyzed (650 and 1000 molecules/μm^2) at which rolling flux was steady over the range of shear stresses under which cell rolling was observed. The mean rolling velocity or rolling flux was determined for each substrate, and the means from three substrates were averaged together and plotted as the average (±SEM). Open data points represent the average (±range) of n=2 substrates.

correlation between cell rolling velocity and shear stress (Figure 3.6a), and an inverse correlation between shear stress and rolling flux (Figure 3.6b). However, at a given shear stress, rolling velocity was largely unaffected by increasing site density, except at 0.47 dyn/cm^2, at which cells rolled at a significantly higher rolling velocity at 650 molecules/μm^2 compared to at 1800 or 2200 molecules/μm^2 as illustrated in Figure 3.6 (p<0.05). Notably, the range of average rolling velocities for Jurkats on P-selectin is smaller and lower than that of HL-60 cells (approximately 3 - 12 μm/sec for Jurkat cells, compared to 1 - 50 μm/sec for HL-60 cells).

Similar to HL-60 cells, the number of rolling Jurkat cells on immobilized P-selectin decreased with increasing shear stress and, under certain shear stress conditions, increased with site density. More specifically, the number of rolling cells on a P-selectin site density of 1800 molecules/μm^2 was significantly higher than on 650 molecules/μm^2 in the range of 0.16 to 0.47 dyn/cm^2 (p<0.05). At shear stresses greater than 0.47 dyn/cm^2, increasing site density had no effect on rolling flux (Figure 3.6b).

3.2.4.3 PSGL-1-mediated Jurkat cell rolling

To probe L-selectin-mediated rolling of Jurkat cells, substrates presenting immobilized PSGL-1 ranging from 800 to 6000 molecules/μm^2 were utilized in leukocyte flow assays with Jurkat cells. On PSGL-1, the shear threshold for rolling was found to be 0.31 dyn/cm^2, compared to 0.16 dyn/cm^2 on P-selectin. Overall, average Jurkat cell rolling velocities on PSGL-1 were approximately 20-fold higher than on immobilized P-selectin (98.11-227.94 μm/sec on PSGL-1, compared to 2.40-11.91 μm/sec on P-selectin). This is consistent with previous reports which describe L-selectin-mediated rolling velocities are much higher that P- or E-selectin-mediated cell rolling due to differences in receptor-ligand kinetics.[25] The average rolling velocity decreased with increasing site density at a given wall shear stress, and increasing shear stress above 0.47 dyn/cm^2 had no significant effect on rolling velocity at a given site density (Figure 3.7a). At positions presenting PSGL-1 at site densities from 2500 to 6000 molecules/μm^2, cell rolling was observed from 0.31 to 1.55 dyn/cm^2, while at a site density of 1800 molecules/μm^2, rolling was observed from 0.16 to 0.93 dyn/cm^2. Comparatively, P-selectin-mediated Jurkat cell rolling occurred over a smaller range of shear stresses: Cell rolling was observed from 0.16 to

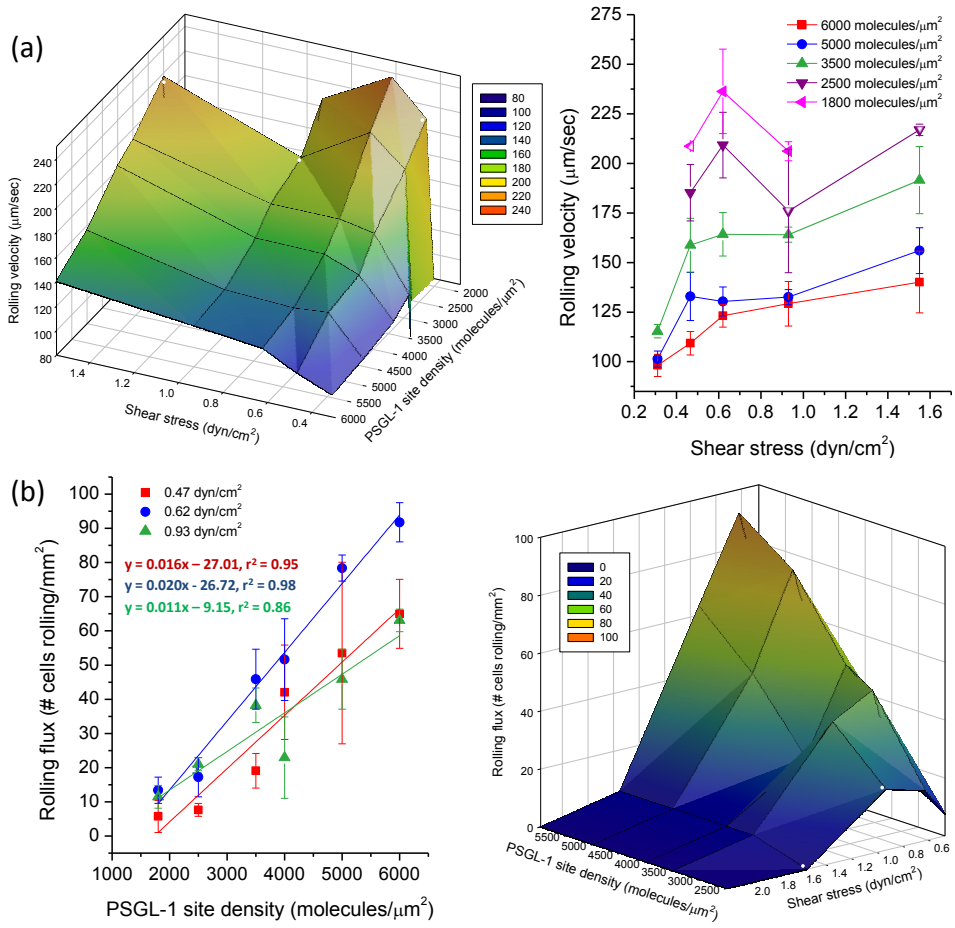

Figure 3.7 Results from initial attachment assays of Jurkat cells on immobilized PSGL-1. (a) Overall, cell rolling velocity was highest at lower site densities. At site densities ≥3500 molecules/μm^2, rolling velocity increased with increasing shear stress up to 1.55 dyn/cm^2. As site density decreased below 3500 molecules/μm^2, the range of shear stresses at which cell rolling occurred decreased, and increasing the shear stress had no effect on the rolling velocity. (b) The rolling flux of cells was affected by site density in a manner that was dependent on the shear stress. Linear regression and correlation analyses reveal that at 0.62 dyn/cm^2, the rolling flux increased most sharply as site density increased compared to at all other shear stresses analyzed. At all site densities analyzed, rolling flux increased as shear stress increased from 0.47 to 0.62 dyn/cm^2, and decreased thereafter. The mean rolling velocity or rolling flux was determined for each substrate, and the means from three substrates were averaged together and plotted as the average (±SEM). Open data points represent the average (±range) of n=2 substrates.

0.62 dyn/cm^2 on site densities ranging from 1000 to 2200 molecules/μm^2, and from 0.31 to 0.62 dyn/cm^2 on a site density of 650 molecules/μm^2 (Figure 3.7).

Data presented in Figure 3.6b show that Jurkat cell rolling flux on immobilized PSGL-1 substrates increased linearly as a function of site density in a manner that was dependent on the applied shear stress. This is evidenced by the slopes of the linear regression analyses of rolling flux vs. PSGL-1 site density. In all cases, a positive correlation was found (p<0.05, r^2= 0.95, 0.98, and 0.86 for 0.47, 0.62, and 0.93 dyn/cm^2, respectively), showing that Jurkat cell rolling flux on PSGL-1 increased with increasing site density at a given shear stress. Interestingly, the slope of the linear fit was highest for data collected at 0.62 dyn/cm^2, revealing that at this level of shear stress, site density had a greater effect on rolling flux compared to higher or lower shear stresses (0.47 or 0.93 dyn/cm^2).

3.2.4.4 HL-60 cell rolling and adhesion on two-component substrates of ICAM-1 and P-selectin

BP-modified substrates were tailored to present two biomolecules, intercellular adhesion molecule-1 (ICAM-1, R&D Systems) and P-selectin, and were utilized to investigate the effect of ICAM-1 density on cell rolling and adhesion (Figure 3.8). Briefly, a BP-modified substrate as assembled into the flow chamber and a solution of ICAM-1 (5 μg/mL) was introduced into the chamber. A relief mask with an array of circles (800-μm diameter, 200-μm spacing) was placed on the substrate, and a 5-mm gradient was generated over the array mask by programming the shutter to move a total of 5 mm over the duration of the UV exposure (12 sec, 14 mW/cm^2, as discussed above). PBS was flowed through the chamber to rinse out residual protein solution (400 μL/min for 3 min), then a solution of P-selectin (1.25 μg/mL) was introduced into the chamber and was photopatterned through the array mask for 5 sec (14 mW/cm^2).

In this manner, substrates were tailored to present a gradient of an adhesive protein, ICAM-1, amidst a uniform density of P-selectin. Substrates were characterized in a fluorescence immunoassay (Figure 3.8) and were utilized in leukocyte flow assays. HL-60 cells were flowed over the substrate at a shear stress of 0.23 dyn/cm^2, and the total numbers of rolling and adherent cells were determined as a function of ICAM-1 ligand density. At low levels of ICAM-1, the majority of cells are found to roll on the substrate, with less than 30% of interacting cells leading to firm adhesion. At high levels of ICAM-1, the majority of interacting cells are found to

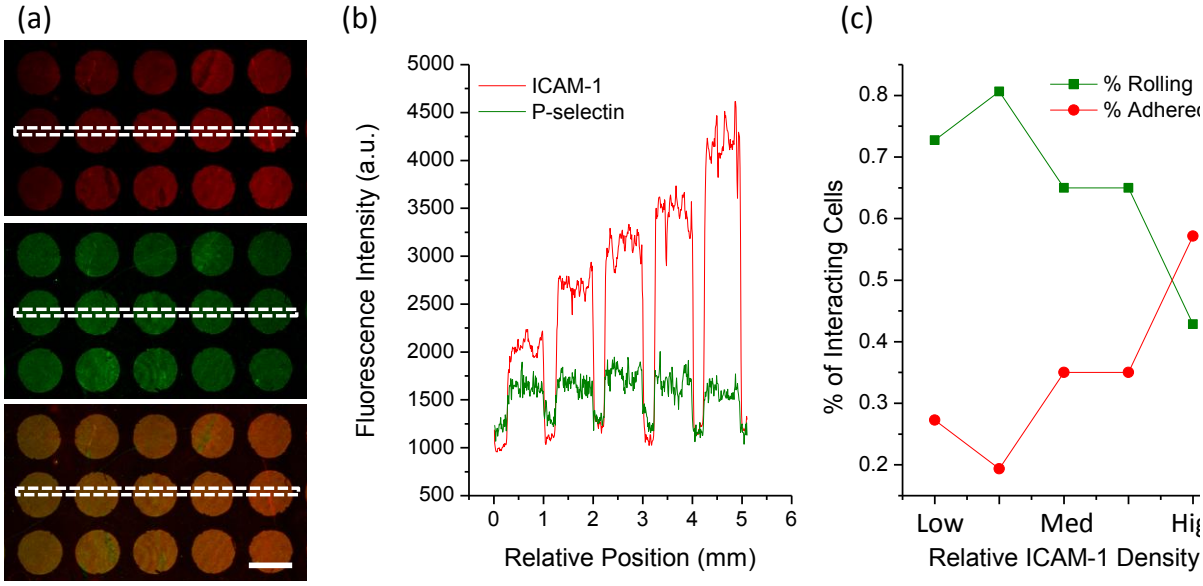

Figure 3.8 Substrates presenting ICAM-1 and P-selectin in an 800-µm circle array were characterized and utilized in leukocyte flow assays to assess the interplay of rolling and adhesion. (a) A fluorescence image of the two-component gradient substrate (top: ICAM-1, Cy5, red; middle: P-selectin, Cy3, green; bottom: overlay), and (b) the corresponding fluorescence linescans. (c) A greater percentage of cells are found to adhere to the substrate in areas with high levels of ICAM-1, under conditions of shear stress (0.23 dyn/cm^2). Data points represent the total percentage of rolling and adhered cells in three different rows of circles on a representative substrate. Scale bar: 800 µm.

convert to firm adhesion. On substrates presenting comparable levels of ICAM-1 in the absence of P-selectin, no cells were found to interact with the substrate (data not shown), which is consistent with previous literature reports that demonstrate that selectin-mediated rolling is a prerequisite for ICAM-1-mediated cell adhesion.[26]

3.2.5 Summary

In these studies, biomolecular gradient generation was performed on two different days for flow assays involving HL-60 cells and Jurkat cells. The range of protein site densities presented on the substrates generated for this study is comparable to the values that have been

previously reported in the literature for applications in leukocyte flow assays. Specifically, Brunk and Hammer[19] report microsphere rolling on E-selectin substrates ranging from 1400 to 3500 molecules/μm^2 and Alon, *et al.*[27] used P- and E-selectin substrates of 500 and 650 molecules/μm^2 for investigating T cell rolling. Important insights have been gleaned from these previous studies conducted at densities comparable to those generated in this paper.

I found that both HL-60 and Jurkat cells rolled on immobilized P-selectin gradients, while only Jurkat cells rolled on immobilized PSGL-1, consistent with literature reports of low L-selectin expression on HL-60 cells.[24] In addition, other trends observed in the cell rolling velocity and rolling flux data presented here are consistent with previous reports. For example, Lawrence, *et al.* studied HL-60 cell rolling on immobilized P-selectin[24] and observed, similar to these findings, that rolling flux is enhanced by increasing fluid shear up to a certain level, above which it decreases until cell rolling ceases to occur. In another study, Alon, *et al.* analyzed HL-60 cell rolling on an uncharacterized substrate of immobilized P-selectin up to wall shear stress levels of approximately 3 dyn/cm^2, observing a plateau in rolling velocity as shear stress was increased.[27] This is similar to the results for HL-60 cells rolling at P-selectin site densities of $\geq$ 280 molecules/μm^2. Additionally, for each selectin-ligand interaction probed, I found that a minimum shear threshold level was required in order for cells to roll on the surface, and that the threshold level was different for each protein, and in some cases for each ligand site density.

As noted in the literature,[11d] an interesting characteristic of selectin-mediated rolling, as opposed to rolling mediated by immobilized antibodies, is the ability to maintain near-constant cell rolling velocities even as cells are subjected to increasing levels of shear stress. Observed in both *in vivo*[28] and *in vitro*[29] studies, this is understood to be the result of an "automatic braking system," which comes from a combination of cellular features (*i.e.*, deformability and extrusion of membrane tethers) and certain molecular features of selectins and their corresponding ligands.[11d] When a cell comes into contact with a surface, there are repulsive forces that may be overcome by increasing shear stresses, enabling increased bond formation. In the data presented here, this trend is most clearly seen in initial attachment assays for HL-60 cells on P-selectin (at site densities $\geq$280 molecules/μm^2). Rolling velocities were seen to plateau instead of increasing linearly in proportion to increasing shear stress (Figure 3.4a). Although rolling velocity was not affected by increasing shear stress from 0.93 to 2.17 dyn/cm^2, the number of rolling cells

decreased over this range of shear stresses (Figure 3.4b). It appears, then, that shear stress affects the ability of HL-60 cells to tether to P-selectin in order to initiate rolling. However, once cells are rolling, shear stress does not affect the velocity at which they will roll. Initial attachment assays assessed the ability of cells to tether to the surface and initiate rolling in the presence of a given shear stress. The data suggests that the velocity of cells rolling on P-selectin remains constant over a wide range of wall shear stresses when the cells initiate rolling at each level of shear stress evaluated (Figure 3.4a).

For P-selectin-mediated Jurkat rolling, only at higher site densities (≥1400 molecules/μm^2) did the rolling velocity of cells plateau with increasing shear stress (Figure 3.6). PSGL-1-mediated Jurkat cell rolling velocities (Figure 3.7a) show this same trend at site densities ≥ 3500 molecules/μm^2.

I also found that HL-60 and Jurkat cells show differences in cell rolling behavior on immobilized P-selectin substrates. Comparing data in Figure 3.6b and Figure 3.4b, it is seen that Jurkat rolling flux on P-selectin was lower than that of HL-60 cells (maximum of 75 rolling cells/mm^2 for Jurkat cells, compared to 250 rolling cells/mm^2 for HL-60 cells). Additionally, Jurkat cell rolling on immobilized P-selectin was limited to a smaller range of shear stresses compared to HL-60 cells. The differences in the trends between data from HL-60 cells and Jurkat cell flow assays are likely due to the fact that Jurkat cells express an improperly glycosylated form of PSGL-1[30] that results in a weaker receptor-ligand interaction that is correspondingly less stable when challenged with increasing levels of shear stress, compared to HL-60 cells that express fully functional PSGL-1.

Data from initial attachment assays of Jurkat cells on immobilized PSGL-1 suggest that there are optimal levels of shear stress that enable cells to more sensitively respond to differences in protein site density (Figure 3.7b). This is demonstrated by the fact that the dependence of rolling flux on site density at a shear stress of 0.62 dyn/cm^2 was greater than at 0.47 or 0.93 dyn/cm^2. This demonstrates that there is a dynamic relationship between the combination of shear stress and site density on the observed cell rolling flux.

There are numerous other reports that utilize both leukocytes and leukocyte models (*i.e.*, bioconjugated microspheres) in flow assays to better understand the biophysical phenomena

underlying leukocyte recruitment. Various selectin-ligand interactions have been studied using ligand-coated microspheres in flow assays.[15,31] Selectin- or ligand-transfected cell lines,[24] and various leukocyte subsets isolated from blood samples including T cells[27,32] and neutrophils[26,33] have been assessed for their ability to roll on selectin-coated substrates. These *in vitro* approaches are complementary to *in vivo* studies and have the unique ability to provide a quantitative assessment of leukocyte recruitment (mediated by numerous different receptor-ligand interactions) under well-defined experimental conditions. In this way, *in vitro* approaches have contributed to a clearer understanding of the complex physiological processes underlying the inflammatory response.

In addition to probing leukocyte interactions on substrates presenting one biomolecule at a time, I have demonstrated the potential for this gradient methodology platform to generate substrates presenting two biomolecules, and the subsequent application of these substrates to leukocyte flow assays (Figure 3.8). Substrates were tailored to present a gradient of ICAM-1 amidst a uniform background of P-selectin. Leukocyte flow assays that probed the ability of HL-60 cells to interact with the substrates through rolling and firm adhesion revealed that higher levels of ICAM-1 resulted in a greater percentage of adhered cells.

It is widely accepted that selectin-mediated rolling is a necessary first step to integrin-mediated adhesion through interactions with intercellular adhesion molecules.[26] Immobilized chemokines are often involved in this process, as they serve to activate expression of integrins on the cell surface,[26,34] but some reports show that selectin-ligand interactions are sufficient for integrin activation.[35] These findings are consistent with these reports, since cells failed to roll or adhere on substrates presenting ICAM-1 alone (data not shown), yet are able to roll and adhere upon substrates presenting both P-selectin and ICAM-1. Substrates that present multiple relevant ligands are valuable for their ability to probe the interplay between multiple biomolecular interactions that occur simultaneously *in vivo*.[31b,36]

The gradient generation approach described herein offers a means of streamlining the investigation of the interplay between ligand site density and applied shear stress, and their combined effects on rolling behavior by enabling the creation of high-information-content substrates that present many different underlying ligand conditions that can be assayed in a

single experiment. Large-scale continuous gradients, such as those shown in Figures 3.3 and 3.5, have potential for applications in high-throughput multi-parameter analyses of cell-substrate interactions which would otherwise be more time- and labor-intensive due to the need to make multiple different substrates, each presenting different, uniform densities of the ligand(s) of interest. On the other hand, gradient arrays, such as those in Figure 3.8, can be tailored to present adhesive ligands in a manner that mimics an inflammatory site in a blood vessel wall, which can be on the order of 100s of μms in size,[37] allowing the combined effects of biomolecule ligand density and feature size on the complete leukocyte recruitment process to be investigated.

This is the first demonstration of the generation and quantitative characterization of biomolecular surface gradients presenting a wide range of surface-immobilized protein site densities, and their subsequent application in a comparative study of rolling behavior of leukocyte cell lines. I have assessed the combined effects of immobilized site density and shear stress on the resulting velocity and flux of rolling cells, demonstrating that this methodology is capable of generating gradient substrates for applications in rapid multi-parameter leukocyte flow investigations. Finally, although this manuscript is focused solely on leukocyte rolling assays, the general methodology of photochemical gradient generation will likely be of utility to a wide number of researchers interested in understanding biochemically complex cell-substrate interactions.

3.3 Conclusion

Model substrates presenting biochemical cues immobilized in a controlled and well-defined manner are of great interest for their applications in biointerface studies that elucidate the molecular basis of cell receptor-ligand interactions. This chapter presents a simple gradient generation approach that produces rationally controlled and quantifiable substrates, requiring only BP-modified glass substrates, protein solutions, and UV light. Immobilized proteins are shown to retain their function, as demonstrated by the ability of leukocytes to engage them in biologically relevant behaviors. This simple, direct and molecularly general approach to generating surface-immobilized biomolecular gradients produces substrates that are quantifiable and facilitate multi-parameter investigations of cell-substrate interactions.

Gradient substrates have an advantage over homogeneous substrates for applications in leukocyte flow assays due to their ability to yield high-content data by probing numerous combinations of shear stress and immobilized site density in a single set of experiments. This approach is more efficient compared to generating numerous separate sets of substrates for each combination of ligands and parameters under investigation. Additionally, covalent immobilization of biomolecules eliminates the risk of protein desorption due to disrupted non-covalent interactions. This methodology will be used to perform more comprehensive studies of selectin-mediated rolling of primary neutrophils and neutrophil models. Future work will also involve the generation of more complex substrates that simultaneously present multiple ligands in order to probe synergistic biomolecular interactions that control leukocyte rolling. These studies will be part of an effort to fully illuminate the cooperative effects of biomolecular interactions that facilitate leukocyte tethering, rolling, and adhesion to the endothelium during an inflammatory response. In addition to clear applications in leukocyte biology, this technique is well-suited to construct models for many cell-biomaterial interfaces that are defined by multiple modes of biomolecular interaction. This facile gradient generation methodology will enable biological studies that may lead to new insights into the biophysical phenomena and molecular mechanism underlying complex physiological processes such as leukocyte recruitment and the inflammatory response.

3.4 Materials and Methods

3.4.1 Preparation of BP-modified substrates

All chemicals were purchased from Sigma-Aldrich, unless otherwise noted. Glass microscope slides were cleaned with piranha solution (3:1 v/v concentrated H_2SO_4:30% H_2O_2).[38] Slides were functionalized with 4-(triethoxysilyl)butyl aldehyde (Gelest) via vacuum deposition under reduced pressure for 2.5 hr at rt. Following silanization, slides were cured at 120 °C for 1 hr, soaked in absolute ethanol for 30 min, and dried under a stream of nitrogen. Slides were then incubated in a solution of 20 mM 4-benzoyl benzylamine hydrochloride (Matrix Scientific) and 200 mM $NaCNBH_3$ in a 4:1 DMF:MeOH solution for 4 hr at rt. Remaining unreacted aldehyde groups were blocked by immersion in aldehyde blocking buffer (200 mM ethanolamine, 0.1 M Tris, pH 7) for 1 hr, followed by rinsing in DMF, methanol, and ethanol, and drying under a

stream of nitrogen. After each step, contact angle goniometry (Ramé-Hart) was used to confirm that the chemical functionalization was successful. The resulting BP-modified substrates were stored in a dessicator in the dark until use.

3.4.2 Quantitative determination of immobilized protein density

A standard method for quantifying immobilized protein site density on a surface involves incubating the substrate with a saturating concentration of radiolabeled antibody followed by analysis in a scintillation counter. A calibration curve of known standards is generated and used to convert the signal to a measure of site density (the number of antibodies bound per area), assuming 1:1 binding between the radiolabeled antibody and the antigen.[14b,19] A similar method was employed to determine the site density of proteins (P-selectin or PSGL-1) covalently attached to BP-modified substrates, as previously described.[9b] Traditional radioimmunoassays are designed to determine the average site density of a substrate presenting a homogeneous layer of a single protein. Because the end goal was to determine site densities at various positions along immobilized protein gradient substrates, I needed a way to correlate data from fluorescence images with the site density data from the radioimmunoassays. To address this challenge, substrates presenting a homogeneous site density of protein were generated and split into two groups: one for fluorescence analysis and one for radioactivity analysis. The results from both studies were correlated to determine the relationship between fluorescence intensity (F.I.) and site density for each protein. In this way, gradient substrates were quantified by converting data from fluorescence analyses to site density using the standard curves from the fluorescence-radioactivity correlation studies.

Solutions of P-selectin and PSGL-1 (R&D Systems) were freshly diluted from concentrated stocks (2 mg/mL) into PBS with Ca^{2+} and Mg^{2+} to a final concentration of 5 μg/mL. A BP-modified substrate was assembled into a rectangular parallel-plate flow chamber (GlycoTech) with a silicone gasket (127 μm thickness). The inlet and outlets tubes of the chamber were assembled to allow solution flow to be controlled by a syringe pump (Harvard Apparatus). Protein solutions were flowed through the chamber at 3 mL/min until filled (about 200 μL required), then flow was stopped. A UV LED (365 nm, 17 mW/cm^2, Clearstone Technologies) was employed to perform flood exposures of each substrate for various times (10,

30, 40, 60, 120, 180 sec) in the presence of each protein solution. Following protein photoimmobilization, the flow chamber was disassembled and substrates transferred to a solution of 1% BSA/0.5% Tween 20/PBS with Ca^{2+} and Mg^{2+} for 1 hr, and blocked in 1% BSA in PBS with Ca^{2+} and Mg^{2+} for an additional 1 hr. For each set of exposure conditions, six replicates were generated, three of which were subjected to fluorescence analysis, and three of which were analyzed for radioactivity and site density quantification.

Substrate characterization via fluorescence required primary unlabeled mAbs (R&D Systems), and AlexaFluor647-labeled secondary mAbs (Invitrogen). For radioimmunoassays, an unlabeled secondary goat anti-mouse IgG/M polyclonal antibody (pAb, Amersham Biosciences), was iodinated with ^{125}I (Perkin Elmer) using IODO-gen reagent (Pierce). [^{125}I]-labeled pAb was purified using Bio-spin 6 columns (Bio-rad) to remove excess ^{125}I, and characterized by thin layer chromatography to determine the specific activity and % free ^{125}I (0.69 μCi/μg, 4.42% free ^{125}I).[39] For fluorescence analysis, substrates were incubated with the appropriate primary mAb (1 μg/mL) and AlexaFluor647-labeled secondary mAb (0.05 μg/mL) in 1% BSA/PBS overnight at rt. They were then rinsed in PBS and H_2O, dried under a stream of nitrogen, and analyzed using a fluorescence slide scanner (GenePix 4000B, MDS Analytical Technologies). For radioactivity analysis and quantification, substrates were incubated with their respective primary mAbs (20 μg/mL) in BSA/PBS at rt overnight, followed by incubation with [^{125}I]-labeled secondary pAb (30 μg/mL) in BSA/PBS at room temperature for 30 min. Slides were then rinsed with PBS and water, dried under nitrogen, and cut into 1 x 2.5 cm pieces for analysis in a scintillation counter (LS 6500 Multi-Purpose Scintillation Counter, Beckman Coulter). Standards of [^{125}I]-labeled secondary pAb were used to generate a standard curve, which was used to convert all radioactivity measurements to the number of molecules immobilized on the surface. This correlation assumes a 1:1 binding interaction between the primary antibody and the immobilized antigen, and also between the primary and secondary antibodies. Knowing the area of each substrate analyzed, the F.I. data was plotted as a function of site density (molecules/μm^2) and linear regression analyses were performed to determine the linear fit for each set of data. The calibration curves, which were determined separately for P-selectin and PSGL-1, were used to convert all F.I. data from subsequent gradient substrates to units of site density (molecules/μm^2).

3.4.3 Generation of surface-immobilized gradients

For the creation of protein gradient substrates, an Ar ion laser (Coherent Innova 90-4, Laser Innovations, 351.1-363.8 nm) was employed for UV exposures and photoimmobilization. To enable large-area exposures with uniform illumination, the input Gaussian beam was converted to a flat-top output using a refractive beam shaper (π-Shaper, MT-Berlin), and expanded to a 1x1 cm^2 exposure area with a beam-expanding telescope optic configuration. The profile of the input and output beams were characterized with a laser beam profiling camera (Ophir-Spiricon) to ensure that the beam was homogeneous across the exposure field. The laser power was adjusted to a final illumination intensity of 14 mW/cm^2 at the substrate.

In order to create a gradient of light exposure across the BP-modified substrate, a shutter was attached to a programmable translation stage (ThorLabs Opto DC Driver) and positioned between the light source and the substrate. Illumination and linear movement of the shutter were initiated simultaneously so that the substrate was exposed to a gradient in light exposure.

The shutter was programmed to move 4.2 mm over a defined period (24-30 sec) while the substrate was exposed to the expanded and homogenized laser light. A BP-modified substrate was assembled in the flow chamber that was positioned beneath the shutter. After protein solutions were introduced into the chamber, UV exposure and shutter movement were initiated simultaneously. Following photoattachment, the flow chamber was immersed in a solution of 0.5% Tween 20 in PBS with Ca^{2+} and Mg^{2+}, the substrate was detached, and the same rinsing and blocking steps were performed as described above.

Six replicate gradient substrates were generated for each protein; three were analyzed with fluorescence to determine site densities as detailed above, and the other three utilized in leukocyte flow assays. Conditions for incubation with fluorescently labeled binding partners and the fluorescence scanner settings were the same as described above. Fluorescence data were converted to units of site density in molecules/μm^2, via the fluorescence-radioactivity correlation data. Substrates that were prepared for subsequent cell rolling studies were stored in BSA/PBS solution overnight.

3.4.4 Cell culture

HL-60 promyelocytes were obtained from Prof. Fei Wang (University of Illinois) and Jurkat T lymphocytes were purchased from the American Type Culture Collection (ATCC). Cells were cultured in RPMI 1640 medium supplemented with penicillin (100 U/mL), streptomycin (100 μg/mL), and 10% heat-inactivated fetal bovine serum (SCS Cell Media Facility, UIUC). Cells were passaged in order to maintain densities between 0.1 x 10^6 and 1.0 x 10^6 cells/mL.

3.4.5 Leukocyte flow assays

Figure 3.1 shows the schematic of the setup that was employed for the leukocyte flow assays. Gradient substrates were assembled into the parallel-plate flow chamber while immersed in PBS with Ca^{2+} and Mg^{2+} to prevent drying out of the substrate which could result in protein denaturation. The tubing was connected to a syringe pump to control fluid flow and the chamber was positioned on top of an optical microscope (Zeiss 40C Invertiskop, Carl Zeiss Inc.). Cells were counted, pelleted for 5 min at 500 rcf, rinsed with HBSS with Ca^{2+} and Mg^{2+}, and resuspended in 0.5% human serum albumin (HSA) in HBSS with Ca^{2+} and Mg^{2+} and 10 mM HEPES at pH 7.4, to a final concentration of 0.5 x 10^6 cells/mL. A digital video camera was used to record cells interacting with the substrate at various positions along the gradient while being subjected to defined amounts of wall shear stress. Shear stress was calculated using the equation $\tau = 6\mu Q/a^2 b$, where μ is the apparent viscosity of the media, Q is the volumetric flow rate, and a and b are the height and width of the flow chamber, respectively. To calculate wall shear stress, the viscosity of buffer was assumed equal to water at room temperature (1.0 centipoise, 24 °C).

Phase contrast microscopy was utilized to maximize contrast between interacting cells and the substrate, which was necessary to perform analyses with ImageJ software (National Institutes of Health). Using the MTrack2 plugin, the average velocity of rolling cells was determined (reported in μm/sec). To distinguish between interacting and non-interacting cells during the analysis, the critical velocity (v_{crit}) was determined for each flow rate.[40] To determine v_{crit}, videos of non-interacting cells in shear flow near the wall of the flow chamber were acquired and analyzed.[40] Cells moving slower than the v_{crit} for at minimum of 1 sec (30 frames) were defined as rolling. To determine rolling flux, cells were manually counted in the first 2

seconds of each video (reported as # rolling cells/mm^2). The field of view (FOV) for the microscope with a 20x objective was 0.174 mm^2.

In this study, initial attachment assays were performed to assess the ability of cells to initiate tethering and rolling while experiencing a defined level of wall shear stress. Cells were first introduced into the flow chamber at 3 mL/min (18.6 dyn/cm^2) for 1 min; the flow rate was then dropped to achieve the desired shear stresses occurring from 10 to 500 μL/min. The pre-determined shear stresses were 0.062, 0.16, 0.31, 0.47, 0.62, 0.93, 1.55 and 2.17 dyn/cm^2. After 1 min at each flow rate, videos (10 to 30 sec) were acquired at each position along the gradient (5 to 7 positions per substrate). Between each shear stress that was investigated, the interacting cells were stripped from the surface by applying a high shear (3 mL/min, 18.6 dyn/cm^2) and the process was repeated at the next flow rate.

3.4.6 Statistical analysis

For leukocyte flow assays, three replicates of each gradient substrate were generated for each of the two sets of assays, which were performed on different days. Data are reported as the average with error bars representing the standard error of the mean (SEM) for n=3 substrates, unless otherwise noted. To determine if a set of data showed correlation between dependent and independent variables (*i.e.*, rolling flux and site density), correlation and linear regression analyses were performed. To determine if two data points were statistically different, one-sided two-sample *t*-tests were performed (Microsoft Excel), assuming population variances to be equal. Two-dimensional plots were generated using OriginPro8 (OriginLab) and 3D surface plots were created with SigmaPlot (Systat Software, Inc.). Statistical significance was set at a value of $p<0.05$.

3.5 References

1. T. M. Keenan, A. Folch, *Lab on a Chip* **2008**, *8*, 34.
2. a) R. C. Gunawan, E. R. Choban, J. E. Conour, J. Silvestre, L. B. Schook, H. R. Gaskins, D. E. Leckband, P. J. A. Kenis, *Langmuir* **2005**, *21*, 3061; b) A. Lagunas, J. Comelles, E. Martinez, J. Samitier, *Langmuir* **2010**, *26*, 14154.
3. J. Y. Park, S. Takayama, S.-H. Lee, *Integrative Biology* **2010**, *2*, 229.
4. a) S. K. W. Dertinger, X. Jiang, Z. Li, V. N. Murthy, G. M. Whitesides, *Proceedings of the National Academy of Sciences* **2002**, *99*, 12542; b) J. Park, D.-H. Kim, G. Kim, Y. Kim, E. Choi, A. Levchenko, *Lab on a Chip* **2010**, *10*, 2130.
5. S. T. Plummer, Q. Wang, P. W. Bohn, R. Stockton, M. A. Schwartz, *Langmuir* **2003**, *19*, 7528.
6. W. S. Dillmore, M. N. Yousaf, M. Mrksich, *Langmuir* **2004**, *20*, 7223.
7. a) L. J. Millet, M. E. Stewart, R. G. Nuzzo, M. U. Gillette, *Lab on a Chip* **2010**, *10*, 1525; b) C. J. Wang, X. Li, B. Lin, S. Shim, G.-l. Ming, A. Levchenko, *Lab on a Chip* **2008**, *8*, 227.
8. a) G. Dorman, G. D. Prestwich, *Biochemistry* **1994**, *33*, 5661; b) L. F. Rozsnyai, D. R. Benson, S. P. A. Fodor, P. G. Schultz, *Angewandte Chemie International Edition in English* **1992**, *31*, 759; c) E. Delamarche, G. Sundarababu, H. Biebuyck, B. Michel, C. Gerber, H. Sigrist, H. Wolf, H. Ringsdorf, N. Xanthopoulos, H. J. Mathieu, *Langmuir* **1996**, *12*, 1997; d) W. W. Shen, S. G. Boxer, W. Knoll, C. W. Frank, *Biomacromolecules* **2001**, *2*, 70; e) X. Cao, M. S. Shoichet, *Journal of Biomaterials Science -- Polymer Edition* **2002**, *13*, 623; f) K. Abu-Rabeah, D. Atias, S. Herrmann, J. Frenkel, D. Tavor, S. Cosnier, R. S. Marks, *Langmuir* **2009**, *25*, 10384; g) N. Griep-Raming, M. Karger, H. Menzel, *Langmuir* **2004**, *20*, 11811; h) J. D. Jeyaprakash, S. Samuel, J. Ruhe, *Langmuir* **2004**, *20*, 10080; i) M. Y. Balakirev, S. Porte, M. Vernaz-Gris, M. Berger, J.-P. Arie, B. Fouque, F. Chatelain, *Analytical Chemistry* **2005**, *77*, 5474; j) T. L. Delaney, D. Zimin, M. Rahm, D. Weiss, O. S. Wolfbeis, V. M. Mirsky, *Analytical Chemistry* **2007**, *79*, 3220; k) T. Konry, M. Bouhifd, S. Cosnier, M. Whelan, A. Valsesia, F. Rossi, R. S. Marks, *Biosensors and Bioelectronics* **2007**, *22*, 2230; l) S. Szunerits, N. Shirahata, P. Actis, J. Nakanishi, R. Boukherroub, *Chemical Communications* **2007**, 2793; m) L. Y. Hwang, H. Gotz, W. Knoll, C. J. Hawker, C. W. Frank, *Langmuir* **2008**, *24*, 14088; n) Y. Jung, J. M.

Lee, J.-w. Kim, J. Yoon, H. Cho, B. H. Chung, *Analytical Chemistry* **2009**, *81*, 936; o) L. Marcon, M. Wang, Y. Coffinier, F. Le Normand, O. Melnyk, R. Boukherroub, S. Szunerits, *Langmuir* **2009**, *26*, 1075.

9. a) C. R. Toh, T. A. Fraterman, D. A. Walker, R. C. Bailey, *Langmuir* **2009**, *25*, 8894; b) T. A. Martin, C. T. Herman, F. T. Limpoco, M. C. Michael, G. K. Potts, R. C. Bailey, *ACS Applied Materials & Interfaces* **2011**, *3*, 3762.
10. C. S. Bonder, P. Kubes, in *Leukocyte Trafficking* (Eds.: A. Hamann, B. Engelhardt), WILEY-VCH Verlag GmbH &Co. KGaA, Weinhein, Germany, **2005**, pp. 14.
11. a) M. Bevilacqua, E. Butcher, B. Furie, B. Furie, M. Gallatin, M. Gimbrone, J. Harlan, K. Kishimoto, L. Lasky, R. McEver, J. Paulson, S. Rosen, B. Seed, M. Siegelman, T. Springer, L. Stoolman, T. Tedder, A. Varki, D. Wagner, I. Weissman, G. Zimmerman, *Cell* **1981**, *67*, 233; b) L. Lasky, *Science* **1992**, *258*, 964; c) R. P. McEver, *Current Opinion in Immunology* **1994**, *6*, 75; d) R. P. McEver, *Current Opinion in Cell Biology* **2002**, *14*, 581.
12. E. C. Butcher, in *Leukocyte Trafficking* (Eds.: A. Hamann, B. Engelhardt), WILEY-VCH Verlag GmbH &Co. KGaA, Weinhein, Germany, **2005**, pp. 3.
13. G. W. Schmid-Schonbein, *Annual Review of Biomedical Engineering* **2006**, *8*, 93.
14. a) D. A. Hammer, D. K. Brunk, in *Tissue Engineering Methods and Protocols*, **1999**, pp. 543; b) K. Moore, K. Patel, R. Bruehl, F. Li, D. Johnson, H. Lichenstein, R. Cummings, D. Bainton, R. McEver, *Journal of Cell Biology* **1995**, *128*, 661; c) T. Yago, A. Leppanen, H. Y. Qiu, W. D. Marcus, M. U. Nollert, C. Zhu, R. D. Cummings, R. P. McEver, *Journal of Cell Biology* **2002**, *158*, 787; d) U. Schaff, P. E. Mattila, S. I. Simon, B. Walcheck, *Journal of Leukocyte Biology* **2008**, *83*, 99; e) M. B. Lawrence, D. F. Bainton, T. A. Springer, *Immunity* **1994**, *1*, 137; f) U. H. von Andrian, S. R. Hasslen, R. D. Nelson, S. L. Erlandsen, E. C. Butcher, *Cell* **1995**, *82*, 989.
15. A. W. Greenberg, D. K. Brunk, D. A. Hammer, *Biophysical Journal* **2000**, *79*, 2391.
16. E. Woolf, I. Grigorova, A. Sagiv, V. Grabovsky, S. W. Feigelson, Z. Shulman, T. Hartmann, M. Sixt, J. G. Cyster, R. Alon, *Nature Immunology* **2007**, *8*, 1076.
17. a) L. S. Wong, F. Khan, J. Micklefield, *Chemical Reviews* **2009**, *109*, 4025; b) M. Mrksich, *Chemical Society Reviews* **2000**, *29*, 267.

18. G. Cinamon, V. Grabovsky, E. Winter, S. Franitza, S. Feigelson, R. Shamri, O. Dwir, R. Alon, *Journal of Leukocyte Biology* **2001**, *69*, 860.
19. D. K. Brunk, D. A. Hammer, *Biophysical Journal* **1997**, *72*, 2820.
20. M. Dore, R. J. Korthuis, D. N. Granger, M. L. Entman, C. W. Smith, *Blood* **1993**, *82*, 1308.
21. M. Sperandio, M. L. Smith, S. B. Forlow, T. S. Olson, L. Xia, R. P. McEver, K. Ley, *The Journal of Experimental Medicine* **2003**, *197*, 1355.
22. a) R. F. Bargatze, S. Kurk, E. C. Butcher, M. A. Jutila, *The Journal of Experimental Medicine* **1994**, *180*, 1785; b) R. Alon, R. C. Fuhlbrigge, E. B. Finger, T. A. Springer, *The Journal of Cell Biology* **1996**, *135*, 849.
23. K. Ley, T. Tedder, *Journal of Immunology* **1995**, *155*, 525.
24. M. B. Lawrence, G. S. Kansas, E. J. Kunkel, K. Ley, *Journal of Cell Biology* **1997**, *136*, 717.
25. R. P. McEver, in *Leukocyte Recruitment, Endothelial Cell Adhesion Molecules, and Transcriptional Control: Insights for Drug Discovery* (Ed.: T. Collins), Kluwer Academic Publishers, Boston, **2001**, pp. 1.
26. M. B. Lawrence, T. A. Springer, *Cell* **1991**, *65*, 859.
27. R. Alon, H. Rossiter, X. Wang, T. A. Springer, T. S. Kupper, *The Journal of Cell Biology* **1994**, *127*, 1485.
28. a) A. Atherton, G. V. R. Born, *Journal of Physiology* **1973**, *233*, 157; b) J. C. Firrell, H. H. Lipowsky, *American Journal of Physiology: Heart and Circulatory Physiology* **1989**, *256*, H1667.
29. S. Chen, T. A. Springer, *The Journal of Cell Biology* **1999**, *144*, 185.
30. S. M. Barry, D. G. Zisoulis, J. W. Neal, N. A. Clipstone, G. S. Kansas, *Blood* **2003**, *102*, 1771.
31. a) D. K. Brunk, D. J. Goetz, D. A. Hammer, *Biophysical Journal* **1996**, *71*, 2902; b) A. O. Eniola, P. J. Willcox, D. A. Hammer, *Biophysical Journal* **2003**, *85*, 2720.
32. T. G. Diacovo, S. J. Roth, C. T. Morita, J. P. Rosat, M. B. Brenner, T. A. Springer, *The Journal of Experimental Medicine* **1996**, *183*, 1193.
33. a) M. Lawrence, T. Springer, *Journal of Immunology* **1993**, *151*, 6338; b) S. Chen, R. Alon, R. C. Fuhlbrigge, T. A. Springer, *Proceedings of the National Academy of Sciences*

of the United States of America **1997**, *94*, 3172; c) T. Yago, J. Wu, C. D. Wey, A. G. Klopocki, C. Zhu, R. P. McEver, *Journal of Cell Biology* **2004**, *166*, 913.

34. G. Constantin, M. Majeed, C. Giagulli, L. Piccio, J. Y. Kim, E. C. Butcher, C. Laudanna, *Immunity* **2000**, *13*, 759.

35. a) S. Simon, A. Burns, A. Taylor, P. Gopalan, E. Lynam, L. Sklar, C. Smith, *The Journal of Immunology* **1995**, *155*, 1502; b) V. Evangelista, S. Manarini, R. Sideri, S. Rotondo, N. Martelli, A. Piccoli, L. Totani, P. Piccardoni, D. Vestweber, G. de Gaetano, C. Cerletti, *Blood* **1999**, *93*, 876; c) Y.-Q. Ma, E. F. Plow, J.-G. Geng, *Blood* **2004**, *104*, 2549.

36. a) J. A. DiVietro, M. J. Smith, B. R. E. Smith, L. Petruzzelli, R. S. Larson, M. B. Lawrence, *Journal of Immunology* **2001**, *167*, 4017; b) K. Ley, M. Allietta, D. C. Bullard, S. Morgan, *Circulation Research* **1998**, *83*, 287.

37. M. B. Kim, I. H. Sarelius, *American Journal of Physiology: Heart and Circulatory Physiology* **2004**, *287*, H2705.

38. ***Caution!*** *Piranha solutions are extremely dangerous, reacting explosively with trace quantities of organics*.

39. C. S. R. Gooden, in *Diagnostic and Therapeutic Antibodies* (Eds.: A. J. T. George, C. E. Urch), Humana Press, Inc., New Jersey, **2000**, pp. 339.

40. A. J. Goldman, R. G. Cox, H. Brenner, *Chemical Engineering Science* **1967**, *22*, 653.

Chapter 4

Bromelain Cleaves P-selectin Glycoprotein Ligand-1 and Decreases Neutrophil Recruitment on Immobilized P-selectin *In Vitro*

Notes and Acknowledgments

This work was funded by the Roy J. Carver Charitable Trust, the Camille and Henry Dreyfus Foundation, and by a predoctoral fellowship from the National Institutes of Health, National Center for Complementary and Alternative Medicine awarded to CTH (Award Number F31AT006286). The content is solely the responsibility of the authors and does not necessarily represent the official views of the National Center for Complementary & Alternative Medicine or the National Institutes of Health.

4.1 Introduction

Inflammation is a complex physiological process involving numerous receptor-ligand interactions between leukocytes and the endothelial lining of the blood vessel that ultimately lead to the trafficking of leukocyte subsets throughout the body.[2] Numerous diseases are associated with dysregulated inflammation, including rheumatoid arthritis, asthma, psoriasis, thrombotic disorders, cancer, and autoimmune disease.[3]

Bromelain is composed of several cysteine proteases isolated from pineapple extracts, and is currently marketed as an alternative or complementary medication for treating inflammation.[4] Bromelain has been shown to alter multiple cell surface molecules involved in the adhesion and activation leukocytes,[5] and while it has demonstrated anti-inflammatory, fibrinolytic, and anti-thrombotic effects *in vivo* and *in vitro*,[6] the mechanisms by which bromelain attenuates leukocyte recruitment during inflammation remains poorly understood.

Amongst the enzymes present in bromelain extract is stem bromelain, which was used in this study and will be referred to as bromelain herein.

Endothelial-expressed P-selectin and E-selectin play a central role during the initiation of an inflammatory response. When the endothelium receives distress signals from underlying tissue, P-selectin is the first biomolecule deployed as it is mobilized from intracellular storage pools to the luminal surface of the endothelium.[7] The interaction between P-selectin and its primary leukocyte-expressed ligand, P-selectin glycoprotein ligand-1 (PSGL-1), supports neutrophil rolling along the surface of the blood vessel.[8] E-selectin, which binds to PSGL-1

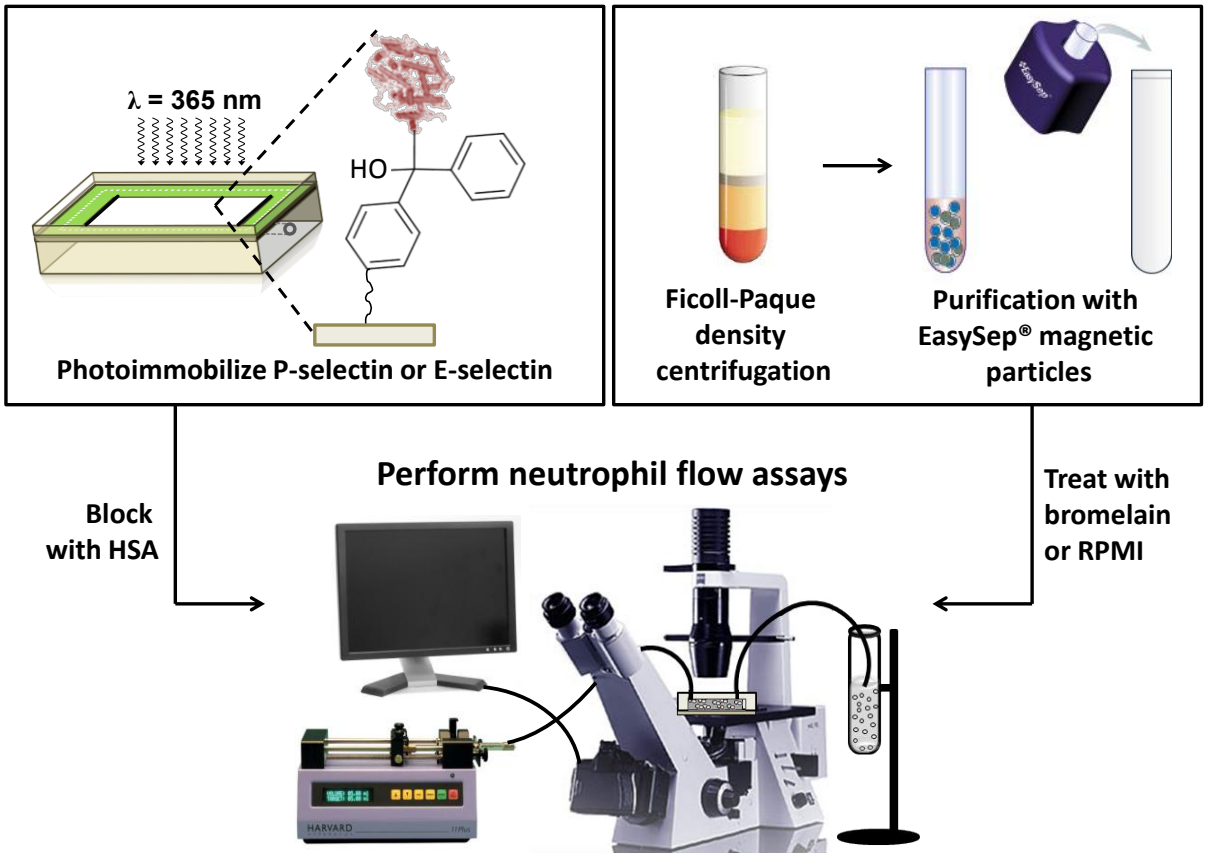

Figure 4.1 Schematic of neutrophil flow assay setup. To determine the effects of bromelain treatment on neutrophil interactions with immobilized P-selectin or E-selectin under physiological shear stress, substrates presenting photoimmobilized P-selectin or E-selectin were prepared, characterized, and utilized in neutrophil flow assays with human neutrophils isolated from whole blood.

among other ligands,[9] is also presented on the endothelium during the inflammatory response, but its expression is largely controlled by translation (*i.e.*, it is not stored intracellularly),[10] and its presentation temporally lags behind that of P-selectin *in vivo*. I felt it would be beneficial to independently probe bromelain's effects on neutrophil interactions with substrates presenting each of these glycoproteins, so I applied a photochemical surface patterning strategy developed in our lab[11] to generate substrates presenting P-selectin or E-selectin. I determined the site density of immobilized proteins using data from a previously reported radioimmunoassay,[1] and interfaced the substrates with human neutrophils in flow assays to investigate the effect of bromelain treatment on the ability of human neutrophils to tether to and roll on P-selectin or E-selectin (Figure 4.1). I chose to work with neutrophils amongst all the leukocyte subsets because they are among the first responders that rapidly accumulate at sites of inflammation.[12] I used flow cytometry to analyze the expression of two ligands involved in leukocyte recruitment mediated by P-selectin and E-selectin: PSGL-1 and cutaneous lymphocyte antigen (CLA). The purpose of these studies was to determine the effects of bromelain treatment on the ability of neutrophils to interact with P-selectin and E-selectin under conditions of physiological shear stress and to shed light on the mechanisms underlying these effects.

4.2 Results and Discussion

Bromelain treatment of neutrophils nearly eliminates their ability to interact with P-selectin presented on substrates *in vitro*, while E-selectin-mediated interactions are unaffected. The observations from neutrophil flow assays are complemented by a dose-dependence analysis of the effect of bromelain treatment on the expression of P-selectin and E-selectin ligands using flow cytometry, and suggest that bromelain's anti-inflammatory effects may be attributed in part to its ability to cleave PSGL-1 and reduce the number of cells interacting with the inflamed endothelium.

4.2.1 Bromelain treatment decreases tethering of human neutrophils to immobilized P-selectin, has no effect on neutrophil interactions with immobilized E-selectin

Using a method I previously developed for the photochemical immobilization of biomolecules on planar substrates,[11] I generated and characterized substrates presenting "high"

and “low” levels of P-selectin or E-selectin on BP-modified substrates (Figure 4.2). Substrates were characterized with fluorescence imaging and average fluorescence intensity values (Table 4.1) were converted into site densities using fluorescence-radioactivity correlation data that was previously reported data for P-selectin[1] and determined for E-selectin for this study (Figure 4.3).

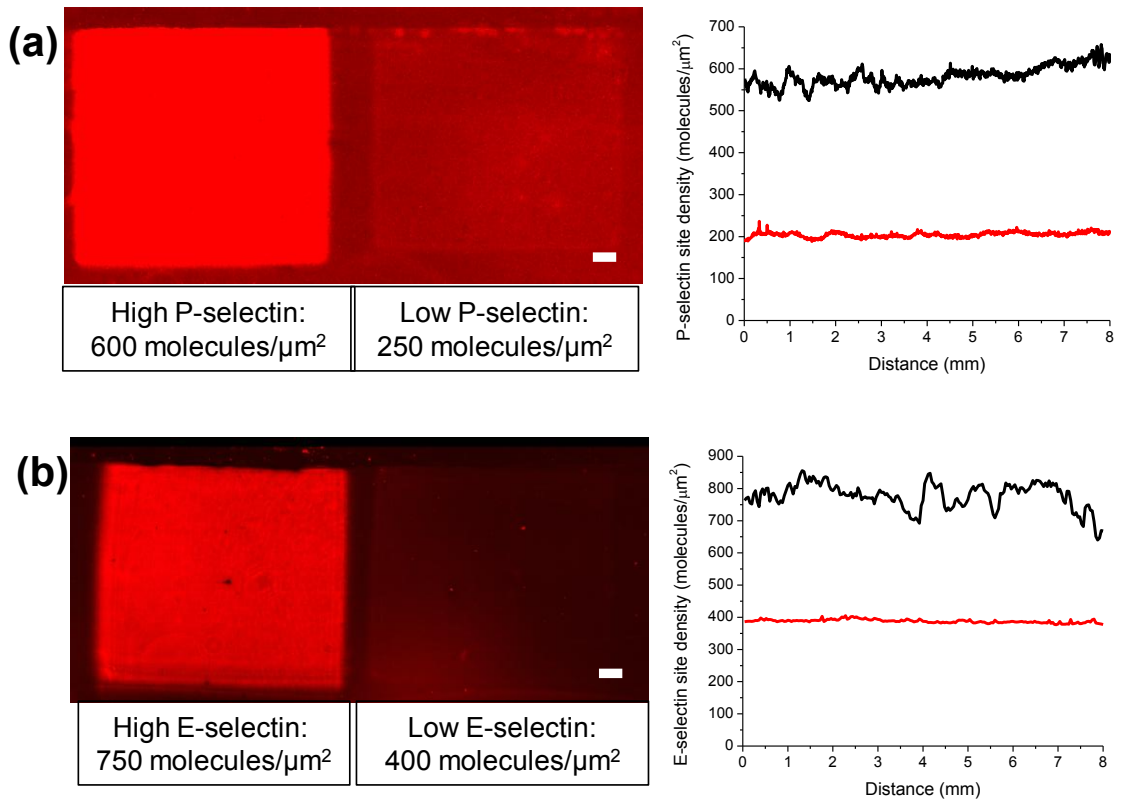

Figure 4.2 Fluorescence images and linescans from substrates presenting high and low levels of photoimmobilized (a) P-selectin or (b) E-selectin. Scale bar = 1 mm. Sites densities for P-selectin substrates were determined using data from a previously reported radioimmunoassay.[1] Data from a radioimmunoassay for E-selectin (see SI) were used to determine site densities of E-selectin substrates.

The data from the neutrophil flow assay experiments are presented in Figure 4.4. In the first set of neutrophil flow assays with P-selectin-presenting substrates, human neutrophils were isolated (>90% pure, >95% viable) and flowed at a constant shear stress (1.28 dyn/cm^2) over

substrates presenting immobilized P-selectin at two different site densities (700 and 250 molecules/μm^2). I observed that the number of interacting cells is significantly lessened when neutrophils are treated with 50 μg mL^{-1} bromelain, compared to the RPMI-treated control sample (p<0.05). Incubation of control cells with saturating levels of anti-PSGL-1 clone KPL-1 (30 μg mL^{-1}), which recognizes an epitope encompassing three sulfated tyrosines in PSGL-1's active site (Figure 4.5), also resulted in a decrease in the number of interacting cells, suggesting that the altered behavior following bromelain treatment is the result of bromelain cleaving off this portion of the PSGL-1's active site, which is required for interactions with P-selectin but not E-selectin.[13]

In a separate set of experiments involving E-selectin-presenting substrates, human neutrophils were flowed at 1.28 dyn/cm^2 over substrates presenting two different site densities of immobilized E-selectin (750 and 400 molecules/μm^2). In contrast to flow assay experiments on

For **P-selectin**:
Site density = 2.96(F.I.)-194.07, R^2 = 0.92

P-selectin				
Substrate	F.I., low-3 sec	Molecules /μm²	F.I., High-30 sec	Molecules /μm²
P1	679.00	295.36	2978.00	1073.10
P2	475.00	226.34	1316.00	510.85
P3	506.00	236.83	1187.00	467.21
P4	434.00	212.47	1164.00	459.43
P5	268.00	156.32	1131.00	448.26
Average	**472.40**	**225.46**	**1555.20**	**591.77**
stdev	**147.54**	**49.91**	**798.46**	**270.11**
SEM	**65.98227**	**22.32**	**357.08**	**120.80**

Approximations:
Low P-selectin: 250 molecules/μm^2
High P-selectin: 600 molecules/μm^2

For **E-selectin**:
Site density = 5.97(F.I.)-1597.20, R^2 = 0.91

E-selectin				
slide	F.I., Low-6 sec	Molecules /μm²	F.I., High-60 sec	Molecules /μm²
E1	618.70	371.27	1088.00	449.90
E2	812.00	403.66	6805.00	1407.78
E3	541.00	358.25	801.00	401.82
Average	657.23	**377.73**	2898.00	**753.17**
stdev	139.55	**23.38**	2765.15	**567.42**
SEM	**62.40811**	**13.50**	**1236.61**	**327.60**

Approximations:
Low E-selectin: 400 molecules/μm^2
High E-selectin: 750 molecules/μm^2

Table 4.1 Average fluorescence intensity and site density determination for P-selectin and E-selectin substrates. Substrates were incubated with fluorescently labeled antibodies, and fluorescence intensity units were converted to site density (molecules/μm^2) using a previous reported calibration curve (see Figure 3.2) for P-selectin, and newly reported data for E-selectin (Figure 4.3).

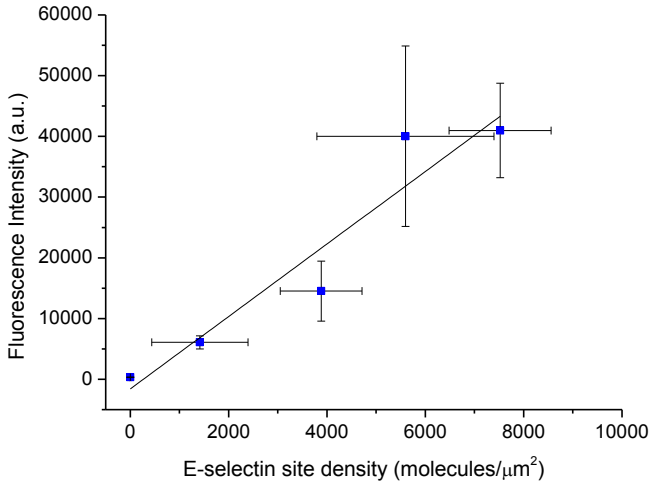

Figure 4.3 The relationship between fluorescence intensity and site density was determined for photoimmobilized E-selectin on BP-modified substrates. Substrates were generated in triplicate via flood UV exposures in the presence of protein solution, resulting in homogeneous substrates presenting a wide range protein site density levels. Fluorescence measurements were acquired after incubating substrates with fluorescently labeled antibodies. For site density determination, substrates were incubated with saturating concentrations of primary monoclonal antibody (mAb) and [^{125}I]-labeled secondary polyclonal antibody (pAb). Control substrates were used to account for non-specific mAb and pAb binding. Data is plotted as the average (± 95% C.I.) for n=3 substrates.

P-selectin-presenting substrates, bromelain treatment had no significant effect on the ability of neutrophils to tether to immobilized E-selectin. I did observe that a greater number of cells interacted with the region of the substrate presenting E-selectin at a site density of 750 molecules/μm^2 compared to 400 molecules/μm^2 (p<0.05). These findings suggest that bromelain is not able to cleave E-selectin ligands to reduce or eliminate E-selectin-mediated interactions. Incubation of neutrophils with saturating levels of HECA-452 (30 μg mL^{-1}), which recognizes a glycan moiety known as cutaneous lymphocyte antigen (CLA) that is present on several E-selectin ligands, did not significantly decrease neutrophil interactions on immobilized

E-selectin. These findings suggesting that E-selectin-mediated neutrophil rolling occurs via interactions with ligands in addition to those presenting the CLA carbohydrate epitope.

As a control experiment, I tested whether neutrophils would interact with BP-modified substrates blocked with HSA without P-selectin or E-selectin. Neutrophils did not interact with

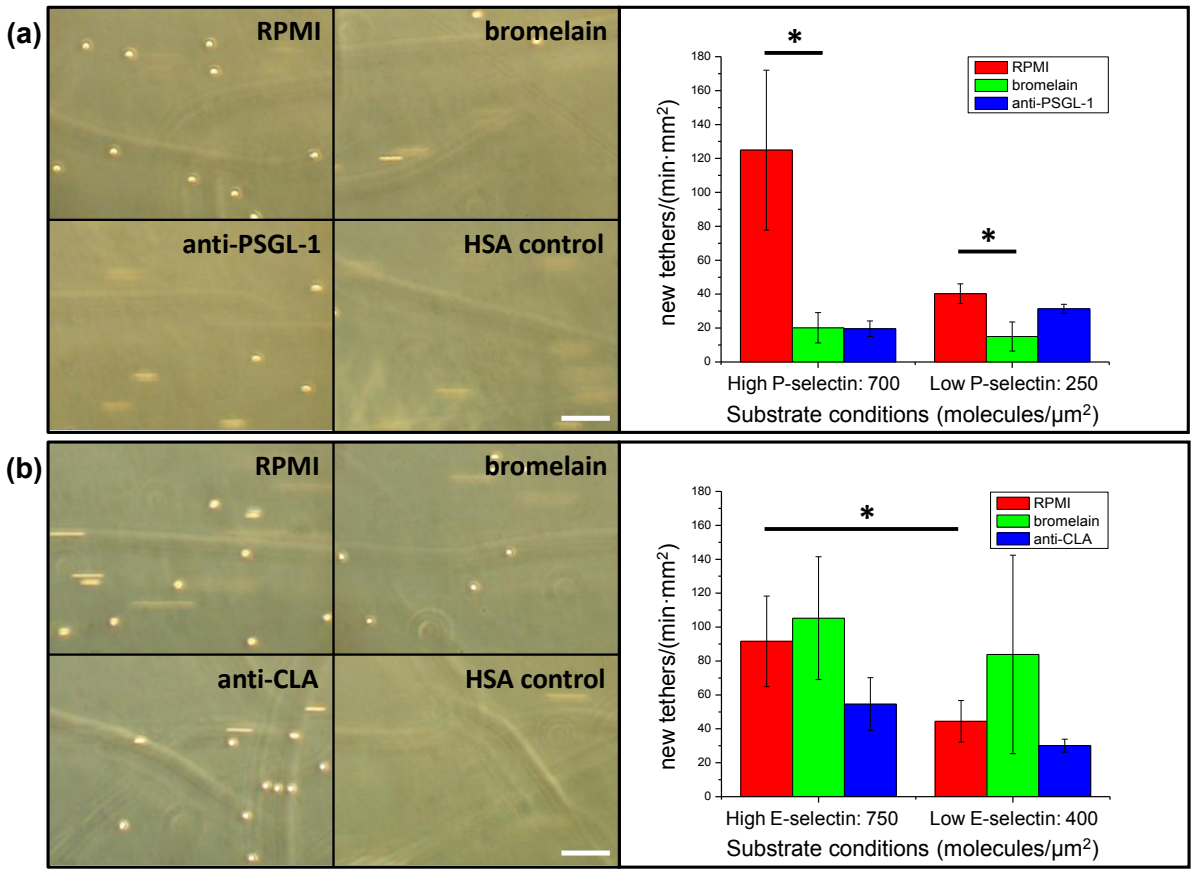

Figure 4.4 Data from neutrophil flow assays reveals that treatment of neutrophils with 50 μg mL^{-1} bromelain (a) decreases the formation of new tethers on immobilized P-selectin substrates relative to RPMI-treated neutrophils ($p<0.05$), but (b) has no effect on neutrophil interactions with immobilized E-selectin. Treatment of neutrophils with saturating concentrations of anti-PSGL-1 (clone KPL-1) decreased neutrophil tethering of neutrophils to immobilized P-selectin substrates, suggesting that the mechanism by which bromelain decreases tethering to P-selectin substrates is by cleaving a portion of the PSGL-1 active site required for P-selecting binding. Neutrophils failed to interact with HSA-blocked control substrates. Scale bar: 80 μm.

HSA-blocked substrates (data not shown), which suggests that the observed cell-substrate interactions were the result of specific receptor-ligand interactions.

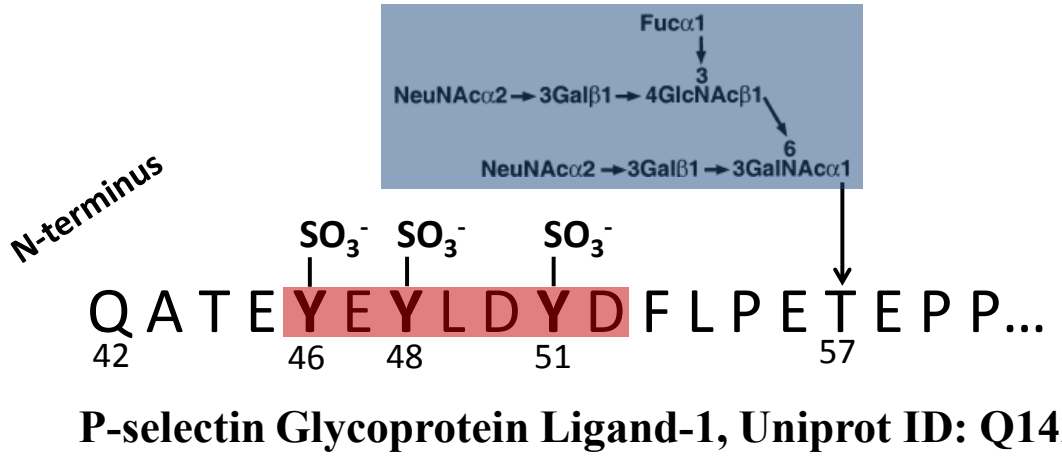

Figure 4.5 Two portions of the N-terminal active site of PSGL-1 are responsible for P-selectin binding—sulfated tyrosine residues (Tyr46, Tyr48 and Tyr51) and a glycosylated threonine residue (Thr57).

Results from the described neutrophil flow assays suggest that bromelain cleaves PSGL-1 in a manner that abolishes its ability to recognize P-selectin. However, bromelain appears to have no effect on the ability of neutrophils to interact with immobilized E-selectin, suggesting that E-selectin ligands, or at least the regions of E-selectin's ligands that are required for E-selectin binding, are not cleaved by bromelain.

4.2.2 Bromelain cleaves PSGL-1 near N-terminal active site and causes a dose-dependent decrease in PSGL-1 expression on human neutrophils.

In order to determine what is going on at the molecular level when neutrophils are treated with bromelain, I set out to perform flow cytometry analysis of human neutrophils to determine how expression levels of ligands for P-selectin and E-selectin, namely PSGL-1 and CLA, are affected by bromelain treatment (Figure 4.6). I obtained three antibodies that recognize well-characterized epitopes that are present on PSGL-1 and CLA. Then I treated human neutrophils

with various doses of bromelain (from 10 to 100 μg mL^{-1}) or RPMI and used flow cytometry analysis to determine how bromelain treatment affects surface expression of PSGL-1 and CLA.

To analyze PSGL-1 expression, I used monoclonal antibody (mAb) clones CHO131 and KPL-1. Clone CHO131 recognizes the sialyl-Lewis^x–bearing core 2 O-glycan structures

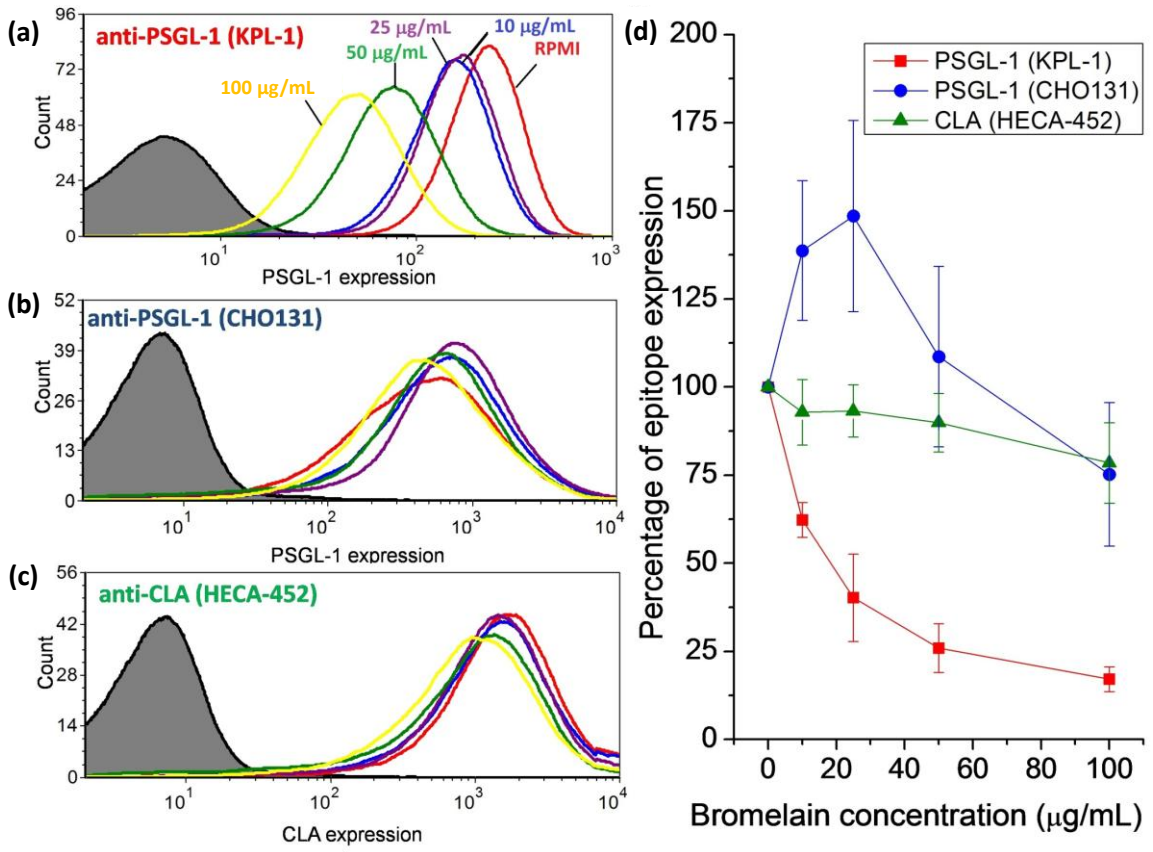

Figure 4.6 Bromelain treatment decreases expression levels of surface-expressed PSGL-1 and CLA in a dose-dependent manner. (a,b) To determine expression levels of PSGL-1, the primary ligand for P-selectin, following bromelain treatment, two anti-PSGL-1 antibodies that recognize distinct regions within the protein's active site were used. The epitope for clone KPL-1 (red) is closer to the N-terminal tip of the extracellular portion of PSGL-1 than the epitope for clone CHO131 (blue). The data suggest that the primary site of bromelain cleavage is between the two epitopes within PSGL-1's active site. (c) The effect of bromelain treatment on expression of a carbohydrate epitope CLA, which is required for recognition of some ligands by E-selectin, was assessed with anti-CLA, clone HECA-452 (green).

presented at PSGL-1's active site. This glycan structure is one of the two regions known to be required for high-affinity P-selectin binding.[14] The epitope for clone KPL-1 has been mapped to a site that includes the tyrosine sulfation motifs that comprise the second of the two regions known to be essential for interaction with P-selectin, and the antibody has been reported to completely block interactions with P-selectin without affecting leukocyte recognition of E-selectin.[15]

The data suggest that bromelain treatment reduces PSGL-1 expression on human neutrophils by directly cleaving PSGL-1 at a site between the epitopes for clones KPL-1 and CHO131 (Figure 4.6). Flow cytometry analysis with clone KPL-1 reveals that the level of the PSGL-1 tyrosine sulfation motif, which is required for recognition by P-selectin but not E-selectin,[13] sharply drops to about 20% as the bromelain dose increases from 0 to 100 μg mL^{-1}. Flow cytometry analysis with clone CHO131, however, shows that PSGL-1 expression levels either increase or remain roughly the same at all concentrations of bromelain tested (Figure 4.6).

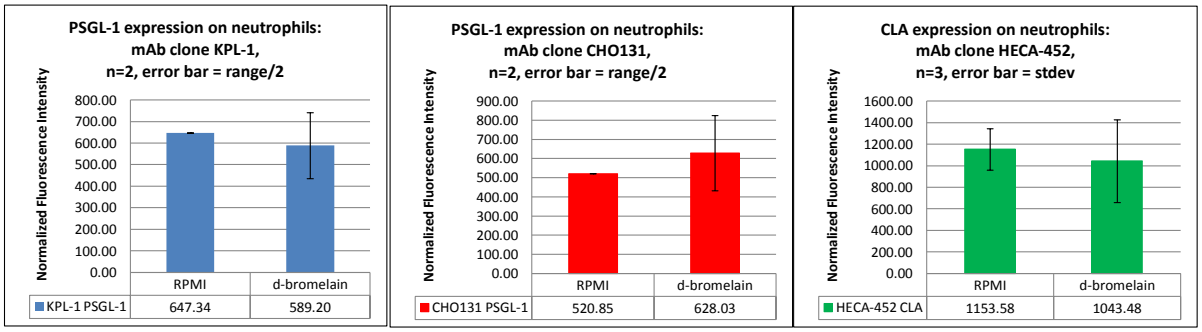

Figure 4.7 Flow cytometry analysis of PSGL-1 and CLA expression on neutrophils treated with RPMI or deactivated bromelain reveals that deactivated bromelain has no significant effect on PSGL-1 or CLA expression levels.

These data suggest that bromelain may be causing two things to happen to neutrophils simultaneously: Bromelain may trigger an increase in PSGL-1 surface expression through an outside-in mechanism at low doses, while at the same time cleaving PSGL-1 on the surface at a position within the N-terminal active site, yet upstream of the sialyl-Lewis^x–bearing core 2 O-glycan structures. Treatment of human neutrophils with deactivated bromelain had no significant

effect on neutrophil expression of PSGL-1 (Figure 4.7), suggesting that enzyme activity is required to induce the changes in surface expression of PSGL-1 that I observed following treatment with active bromelain.

PSGL-1 is P-selectin's primary ligand *in vivo* and is also one of several known ligands for E-selectin.[9] Previous studies involving mouse models revealed that when PSGL-1 is knocked out or blocked, P-selectin-mediated leukocyte rolling is completely eliminated, while E-selectin-mediated rolling still occurs.[16] Since P-selectin is the first selectin expressed on the endothelial lining of the blood vessel immediately in response to proinflammatory signals, interactions between P-selectin and PSGL-1 are among the first receptor-ligand interactions that initiate tethering and rolling of leukocytes during an inflammatory response.[7] It is interesting to note that at the doses used in this study, bromelain cleaves off one of the two motifs in PSGL-1's active site that are required for P-selectin recognition, while leaving the region required for E-selectin recognition intact.

I also determined the effects of bromelain treatment on expression levels of CLA, a carbohydrate epitope shared by sialyl-Lewis^x and sialyl-Lewis^a structures that has been found to be present on PSGL-1 and other E-selectin ligands,[17] and plays a role in leukocyte tethering and rolling mediated by E-selectin.[18] To characterize CLA expression on neutrophils, I used clone HECA-452, a widely used monoclonal antibody for CLA detection.

The data reveal that the average CLA expression declines in a nearly linear fashion to about 80% as the dose of bromelain increases from 0 to 100 μg mL^{-1}. Similar to flow cytometry analysis of PSGL-1 expression, treatment of human neutrophils with deactivated bromelain caused minimal changes in the surface expression of CLA (Figure 4.7).

It is interesting to note that although both PSGL-1 active site epitopes are required for P-selectin recognition, only the Thr O-glycan moiety recognized by mAb CHO131 is required for E-selectin recognition.[13] This could explain why although bromelain cleaves off the sulfated tyrosine residues that are required for P-selectin binding and significantly attenuates neutrophil interactions with immobilized P-selectin under shear stress, there is not a significant change in neutrophil interactions with immobilized E-selectin following bromelain treatment.

While other research labs have investigated the effects of bromelain treatment on neutrophil migration in response to chemokines,[5,19] this report represents the first to reveal that bromelain cleaves PSGL-1, P-selectin's primary ligand that is involved in the onset of selectin-mediated leukocyte rolling during inflammation, and results in an attenuation of rneutrophil recruitment on immobilized P-selectin *in vitro*. These findings suggest that a potential mechanism by which bromelain exerts its anti-inflammatory effects *in vivo* is by cleaving PSGL-1, one of the key ligands responsible for the initial tethering and rolling of leukocytes to P-selectin on the inflamed endothelium. Additional studies will be needed to investigate if bromelain exerts similar effects on neutrophils *in vivo*. Further investigations into the molecular details of bromelain's effects on neutrophil-selectin interactions may help shed additional light on how bromelain exerts its anti-inflammatory effects *in vivo* and lay the foundation for the development of more effective anti-inflammatory treatments.

4.3 Materials and Methods

4.3.1 Preparation and characterization of substrates presenting P-selectin or E-selectin

Substrates presenting immobilized P-selectin or E-selectin were prepared using a previously reported photochemical immobilization method I developed.[11] All chemicals were purchased from Sigma-Aldrich, unless otherwise noted.

Briefly, glass microscope slides were cleaned with Piranha solution (3:1 v/v concentrated H_2SO_4/30% H_2O_2),[20] reacted with 4-(triethoxysilyl)butyl aldehyde (Gelest) under reduced pressure for 2.5 hr, cured at 120 °C for 1 hr, then soaked in 200 proof EtOH for 30 min and dried under a stream of nitrogen. Substrates were then incubated with 20 mM 4-benzoyl benzylamine hydrochloride (Matrix Scientific) and 200 mM $NaCNBH_3$ in PBS (pH 7.4) for 4 hr, followed by immersion in aldehyde-blocking buffer (200 mM ethanolamine, 0.1 M Tris, pH 7) for 1 hr. The resulting BP-modified slides were rinsed with water, MeOH, EtOH, dried under a stream of nitrogen, and stored in a dessicator until use. P-selectin and E-selectin (R&D Systems) were freshly diluted from concentrated stocks into PBS with Ca^{2+} and Mg^{2+} (Sigma) to a final concentration of 2.5 μg mL^{-1}. BP-modified substrates were assembled into a rectangular parallel-plate flow chamber (GlycoTech) with a silicone gasket (127 μm thickness). Protein solutions were flowed through the chamber at 3 mL/min until filled, then flow was ceased. Protein

photoimmobilization was enabled through the use of an Ar ion laser (Coherent Innova 90-4, Laser Innovations, 351.1-363.8 nm), whose Gaussian beam profile was converted to a flat-top profile using a π-Shaper (MT-Berlin), and expanded to a 1 cm^2 area using beam-expanding optics (ThorLabs). The final output power was adjusted to 14 mW/cm^2 for protein photoimmobilization. Exposure conditions were optimized to generate binary substrates presenting a 1 cm^2 area of high protein site density (650-750 molecules/μm^2) and a 1 cm^2 area of low protein site density (250-400 molecules/μm^2) on each substrate. The two separate areas of each substrate were subjected to UV exposure for 3 or 30 seconds (for P-selectin) and for 6 or 60 seconds (for E-selectin), and a total of 7 or 8 replicates substrates were generated with each protein. Substrates for flow assay experiments were stored in 0.5% HSA in HBSS with Ca^{2+} and Mg^{2+} and 10 mM HEPES (pH 7.4, HBSS/HEPES) until use, while the remaining replicate substrates were characterized with fluorescence and converted to site density.

Data for quantitation of P-selectin substrates has been previously reported,[1] while data for E-selectin quantitation was obtained for this study (Figure 4.3). I generated substrates presenting varying levels of immobilized E-selectin in a defined area on BP-modified substrates, and split the substrates into two groups: one group for fluorescence analysis and the other for radioactivity analysis. The data from both studies were correlated to determine the relationship between fluorescence intensity (F.I.) and site density for each protein. Using the equation from the linear regression for the resulting calibration curves, binary substrates were quantified by converting data from fluorescence analyses to site density. The procedure for correlating fluorescence units to site density has been previously reported.[1] Briefly, a solution of E-selectin (R&D Systems) was freshly diluted from a concentrated stock into PBS with Ca^{2+} and Mg^{2+} to a final concentration of 5 μg/mL. A BP-modified substrate was assembled with a silicone gasket into a rectangular parallel-plate flow chamber. Protein solutions were flowed through the chamber at 3 mL/min until filled (about 200 μL required), then flow was stopped. A UV LED (365 nm, 17 mW/cm^2, Clearstone Technologies) was employed to perform flood exposures of each substrate for various times (0, 15, 30, 60, or 120 sec) in the presence of E-selectin solution. Following protein photoimmobilization, the flow chamber was disassembled and substrates transferred to a solution of 1% BSA/0.5% Tween 20/PBS with Ca^{2+} and Mg^{2+} for 1 hr, and blocked in 1% BSA in PBS with Ca^{2+} and Mg^{2+} for an additional 1 hr. For each set of exposure conditions, six replicates were generated, three of which were subjected to fluorescence analysis,

and three of which were analyzed for radioactivity and site density quantification. One set of substrates was incubated with a fluorescently labeled binding partner (1 μg/mL unlabeled anti-E-selectin from R&D Systems and 0.5 μg/mL AlexaFluor647-labeled secondary mAb from Invitrogen), and imaged on a fluorescence microarray scanner (GenePix 4000B, MDS Analytical Technologies). The other set was incubated with a saturating concentration (20 μg/mL) unlabeled anti-E-selectin from R&D Systems at rt overnight, followed by incubation with [^{125}I]-labeled secondary goat anti-mouse IgG/IgM polyclonal antibody (pAb, Amersham Biosciences, 30 μg/mL, 0.69 μCi/μg, 4.42% free ^{125}I) in BSA/PBS at rt for 30 min, followed by analysis with a scintillation counter (LS 6500 Multi-Purpose Scintillation Counter, Beckman). Under the conditions used, I observed a linear relationship between the fluorescence intensity (F.I.) and corresponding radioactivity signal (converted from cpm to site density using a standard curve of known amounts of [^{125}I]-labeled goat anti-mouse IgG/IgM pAb) was linear for each set of immobilized protein substrates. The reported site densities are an estimate based on the ability of antibodies to detect the proteins. For simplicity, I assume a 1:1 binding relationship between the [^{125}I]-labeled secondary polyclonal antibody (pAb) and primary monoclonal antibody (mAb), which likely results in an overestimate of protein loading, since each primary mAb might be recognized by multiple secondary [^{125}I]-labeled pAbs. I also assume a 1:1 binding relationship between the primary mAb and the immobilized surface proteins, although each primary mAb has two antigen binding sites. Similar methods and assumptions have been previously made for substrates used in quantitative selectin-ligand assays.[21]

4.3.2 Neutrophil flow assays on P-selectin and E-selectin

Substrates presenting P-selectin or E-selectin were utilized in flow assays with human neutrophils, shown schematically in Figure 1. While immersed in HBSS/HEPES, substrates were assembled into a rectangular parallel-plate flow chamber with a silicone gasket (254 μm thickness). Solution flow through the chamber was controlled by a syringe pump (Harvard Apparatus). The flow chamber assembly was positioned on top of an optical microscope (Zeiss 40C Invertiskop, Carl Zeiss, Inc.).

Human neutrophils were isolated from whole blood by density centrifugation using Ficoll-Paque, followed by red blood cell lysis and negative selection with magnetic particles

from the EasySep Human Neutrophil Enrichment Kit, following the manufacturer's protocols (STEMCELL Technologies). Blood was obtained from healthy adults, who were recruited as blood donors and gave informed consent for participation. All protocols for human subjects research were approved by the Institutional Review Board at the University of Illinois at Urbana-Champaign (IRB Protocol Number: 11117).

To assess the purity of isolated neutrophils, cells were blocked with 3% HSA and incubated with two antibodies against neutrophil cell surface markers: PE-labeled anti-CD16 and FITC-labeled anti-CD66b monoclonal antibodies (STEMCELL Technologies). Neutrophil purity

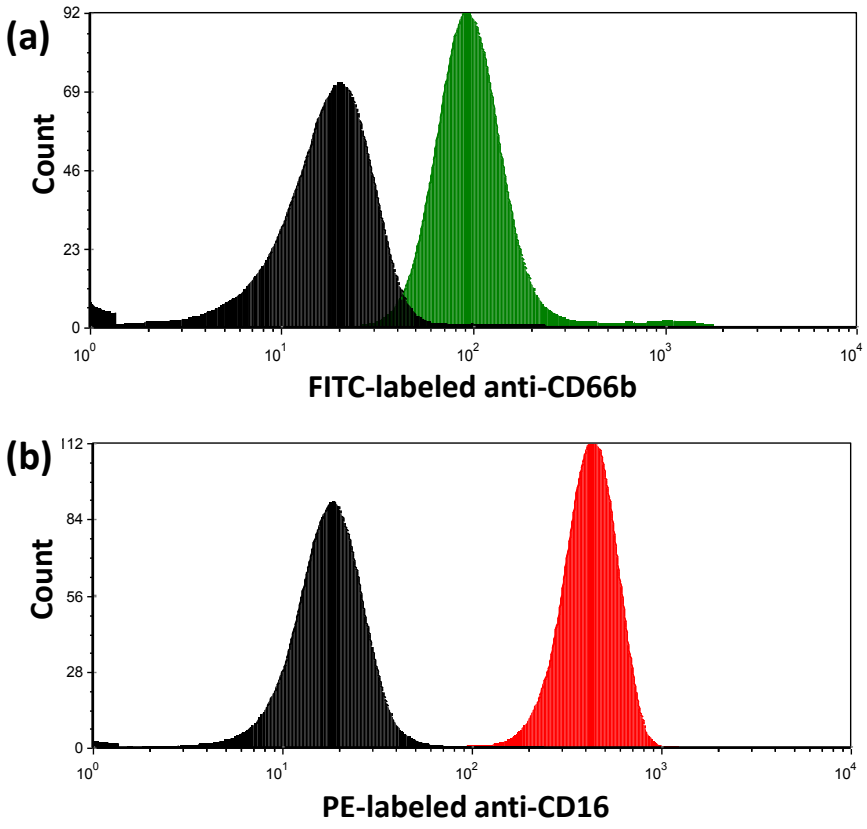

Figure 4.8 Flow cytometry analysis of human neutrophils for neutrophil markers (a) CD66b and (b) CD16 revealed >90% neutrophil purity in all cell samples isolated for neutrophil flow assay experiments (representative data shown). Neutrophils were isolated using traditional Ficoll-Paque density centrifugation followed by magnetic bead separation. Control sample (black) were incubated with fluorescently labeled isotype control antibodies.

was analyzed with flow cytometry (Figure 4.8) and cell viability was determined with standard trypan blue staining and counting. The remaining neutrophils were split into three separate tubes and pelleted for 5 min at 500 rcf. One sample was resuspended in a solution of 50 μg mL^{-1} bromelain in RPMI, and the other two samples were resuspended in RPMI alone. All samples were incubated for 30 min at 37 °C, at which point samples were washed with HSA/HBSS/HEPES and cells were pelleted for 5 min at 500 rcf. One of the RPMI-treated neutrophil samples was resuspended in 30 μg mL^{-1} anti-PSGL-1 (clone KPL-1, for experiments with P-selectin substrates) or anti-CLA (clone HECA-452, for experiments with E-selectin substrates) and incubated at rt for 30-60 min before being diluted to 0.5 E 6 cells/mL for flow assay experiments. The remaining two samples' cell pellets were immediately resuspended in HBSS/HEPES containing 0.5% HSA to a final concentration of 0.5 E 6 cells/mL. All samples were used in flow assay experiments within 2 hours of bromelain or RPMI treatment.

Neutrophils were introduced into the chamber at a high flow rate (3 mL/min, 9.3 dyn/cm^2) for 1 min, then the flow rate was then dropped to 400 μL/min (1.28 dyn/cm^2). After 1 min, 20-30 sec videos were acquired at 4-5 positions in each area of the substrate (high site density and low site density). For each set of flow assay experiments (involving P-selectin or E-selectin substrates), neutrophils from three donors were used to perform independent experiments on three replicate substrates. For each substrate, the number of new tethers formed per unit area and time was determined by counting the number of cells that interacted with the surface. Cells that were already rolling or adhered upon the surface were not included in the analysis. HSA-blocked BP-modified substrates were used as control substrates to verify that the observed interactions were due to neutrophil interactions with immobilized P-selectin or E-selectin. Data from neutrophil flow assays are reported as the average (±SEM) for n=3 substrates.

4.3.3 Flow cytometry analysis of bromelain's effect on the expression of cell surface molecules

Human neutrophils were isolated from whole blood as described above. Neutrophils were prepared for analysis of expression of PSGL-1 and CLA following treatment with 0, 10, 25, 50, or 100 μg mL^{-1} bromelain in RPMI cell cultre medium for 30 min at 37 °C. In some experiments, an additional aliquot of cells were treated with deactivated bromelain, which was prepared by reacting bromelain with dithiothreitol and iodoacetamide and removing excess reagents with a

Zeba spin filter column (Pierce), followed treatment with a proteinase cocktail inhibitor solution containing the cysteine-protease deactivating molecule E-64, according to manufacturer's protocols. Following incubation with bromelain or RPMI, cell samples were washed with HSA/HBSS/HEPES and cells were pelleted for 5 min at 500 rcf. After aspirating the supernatant, neutrophils were blocked for 15 min with 3% HSA in HBSS/HEPES, followed by incubation for 30 min with primary monoclonal antibodies and fluorescently labeled secondary antibodies at final concentrations of 10 and 20 μg mL^{-1}, respectively, in HSA/HBSS/HEPES. For detection of cell-surface PSGL-1, I used mouse anti-human PSGL-1 clone KPL-1 (Millipore), and mouse anti-human PSGL-1 clone CHO131 (R&D Systems). For detection of CLA, the HECA-452 clone (BioLegend) was used. For all samples, I used a fluorescently labeled secondary antibody: phycoerythrin (PE)-conjugated goat anti-mouse IgG (Invitrogen). Cell samples were stained for only one antigen at a time. Control samples were incubated with the PE-labeled secondary antibody only. Solutions composed of primary and secondary antibodies were preincubated for at least 1 hr prior to incubation with cells. Cells were analyzed with BD FACSCanto II cytometer (BD Biosciences).

Flow cytometry data was processed using FCS Express (BD Biosciences). Fluorescence data from neutrophil populations were plotted in histogram form, and the average fluorescence intensity from each sample was plotted as the percentage of the antigen expression from the RPMI-treated sample as a function of bromelain concentration. Data are reported as the average (±SEM) for n=3-6 donors.

4.3.4 Statistical Analysis

Student's unpaired *t* test was used to determine *p* values and compare differences between groups. Statistical significance was set at a value of $p<0.05$.

4.4 References

1. C. T. Herman, G. K. Potts, M. C. Michael, N. V. Tolan, R. C. Bailey, *Integrative Biology* **2011**, *3*, 779.
2. A. Hamann, B. Engelhardt, WILEY-VCH Verlag GmbH &Co. KGaA, Weinheim, Germany, **2005**.
3. a) G. W. Schmid-Schonbein, *Annual Review of Biomedical Engineering* **2006**, *8*, 93; b) A. Ekbom, C. Helmick, M. Zack, H. Adami, *New England Journal of Medicine* **1990**, *323*, 1228.
4. H. R. Maurer, *Cellular and Molecular Life Sciences* **2001**, *58*, 1234.
5. L. P. Hale, P. K. Greer, G. D. Sempowski, *Clinical Immunology* **2002**, *104*, 183.
6. a) D. J. Fitzhugh, S. Shan, M. W. Dewhirst, L. P. Hale, *Clinical Immunology* **2008**, *128*, 66; b) L. P. Hale, P. K. Greer, C. T. Trinh, M. R. Gottfried, *Clinical Immunology* **2005**, *116*, 135; c) F. Pirotta, C. de Guili-Morghen, *Drugs Exp. Clin. Res.* **1978**, *4*, 1.
7. R. P. McEver, J. H. Beckstead, K. L. Moore, L. Marshall-Carlson, D. F. Bainton, *The Journal of Clinical Investigation* **1989**, *84*, 92.
8. M. Sperandio, *Febs Journal* **2006**, *273*, 4377.
9. X. Zou, V. R. Shinde Patil, N. M. Dagia, L. A. Smith, M. J. Wargo, K. A. Interliggi, C. M. Lloyd, D. F. J. Tees, B. Walcheck, M. B. Lawrence, D. J. Goetz, *American Journal of Physiology - Cell Physiology* **2005**, *289*, C415.
10. M. P. Bevilacqua, J. S. Pober, D. L. Mendrick, R. S. Cotran, M. A. Gimbrone, *Proceedings of the National Academy of Sciences of the United States of America* **1987**, *84*, 9238.
11. C. R. Toh, T. A. Fraterman, D. A. Walker, R. C. Bailey, *Langmuir* **2009**, *25*, 8894.
12. V. Witko-Sarsat, P. Rieu, B. Descamps-Latscha, P. Lesavre, L. Halbwachs-Mecarelli, *Laboratory Investigation*, *80*, 617.
13. V. Ramachandran, M. U. Nollert, H. Qiu, W.-J. Liu, R. D. Cummings, C. Zhu, R. P. McEver, *Proceedings of the National Academy of Sciences* **1999**, *96*, 13771.
14. B. Walcheck, A. Leppanen, R. D. Cummings, R. N. Knibbs, L. M. Stoolman, S. R. Alexander, P. E. Mattila, R. P. McEver, *Blood* **2002**, *99*, 4063.
15. K. R. Snapp, H. Ding, K. Atkins, R. Warnke, F. W. Luscinskas, G. S. Kansas, *Blood* **1998**, *91*, 154.

16. J. Yang, T. Hirata, K. Croce, G. Merrill-Skoloff, B. Tchernychev, E. Williams, R. Flaumenhaft, B. C. Furie, B. Furie, *The Journal of Experimental Medicine* **1999**, *190*, 1769.
17. E. Borges, G. Pendl, R. Eytner, M. Steegmaier, O. Zöllner, D. Vestweber, *Journal of Biological Chemistry* **1997**, *272*, 28786.
18. R. Alon, H. Rossiter, X. Wang, T. A. Springer, T. S. Kupper, *The Journal of Cell Biology* **1994**, *127*, 1485.
19. J. E. Onken, P. K. Greer, B. Calingaert, L. P. Hale, *Clinical Immunology* **2008**, *126*, 345.
20. ***Caution!*** *Piranha solutions are extremely dangerous, reacting explosively with trace quantities of organics*.
21. D. K. Brunk, D. A. Hammer, *Biophysical Journal* **1997**, *72*, 2820.

Chapter 5

Future Outlook

In this work, I have presented a summary of my progress toward the development of a direct, photochemical method for the generation of biomolecular interfaces for applications in leukocyte biology. I have described my work toward applying the developed methodology to the investigation of selectin-mediated leukocyte rolling and studies on the mode of action of a natural anti-inflammatory agent, bromelain.

Future work will include investigations into the molecular mechanism underlying the reduction in selectin-mediated rolling *in vitro* caused by bromelain treatment. The investigation will also be extended to consider the effect of bromelain treatment on the subsequent stages of leukocyte recruitment, such as leukocyte adhesion and migration in response to both immobilized and soluble biochemical cues.

Both biochemical and bioanalytical tools will be used in addition to, or in conjunction with, the biointerface generation methodology, to tease out the molecular details behind bromelain's anti-inflammatory properties. Future work will also involve substrates that simultaneously present multiple ligands to cells, both on the surface and in solution, in order to probe synergistic biomolecular interactions that control leukocyte rolling. Finally, future work will include studies on bromelain's effects on leukocyte interactions with cytokine-stimulated endothelial cell monolayers, which better mimic the physiological environment of the inflamed blood vessel. These studies will serve to fully illuminate the cooperative effects of the biomolecular interactions that facilitate leukocyte tethering, rolling, and adhesion to the endothelium during an inflammatory response, and the molecular details underlying the anti-inflammatory properties of bromelain.

5.1 Bioanalytical characterization: What is the molecular mechanism underlying bromelain's cleavage of neutrophil-expressed PSGL-1?

In the results presented in Chapter 4, I observed that bromelain treatment of neutrophils results in a decrease in neutrophil tethering and rolling on substrates presenting immobilized P-selectin, but has no effect on neutriphil interactions with substrates presenting immobilized E-selectin (Fig. 4.7). Flow cytometry analysis of P-selectin expression on neutrophils with antibodies recognizing two epitopes within P-selectin's active site revealed that bromelain treatment results in a decrease in the presence of one the two epitopes, leaving the other epitope largely intact (Fig. 4.2). In combination, these data support the hypothesis that bromelain cleaves neutrophil-expressed PSGL-1 *in vitro* at a site within its N-terminal active site.

To further probe this hypothesis, future work will include performing molecular analyses to determine exactly where bromelain is cleaving PSGL-1. This will include three different experiments involving (a) a synthetic peptide representing PSGL-1's active site, (b) recombinantly expressed PSGL-1, and (c) cell surface-bound PSGL-1 expressed on human neutrophils.

5.1.1 Studies involving a synthetic peptide representing PSGL-1's active site

A 19-amino acid synthetic peptide representing PSGL-1's active site (Figure 5.1) will be obtained. The peptide will include the sulfated tyrosines (Tyr46, Tyr48, Tyr51) located near the N-terminus, which encompasses the region that appears to be cleaved off following bromelain treatment. The peptide extends several amino acids past the threonine residue, which in the native protein presents the sulfation moiety that is recognized my mAb CHO131 that does not appear to be cleaved off with bromelain treatment (Figure 4.2). Although the synthetic peptide will not include the glycosylation moiety at Thr57 and may not have the same tertiary structure as native PSGL-1, the results from these studies will show whether bromelain is able to cleave PSGL-1 at some (or many) position(s) between these two components of the active site. The peptide (1 mg/mL) will be incubated with bromelain (100 μg/mL) in ammonium acetate buffer (pH 7), and remove and quench aliquots at pre-determined time points with 0.5% trifluoroacetic acid (TFA). Ammonium acetate buffer will be used because of its compatibility with mass spectrometry analysis due to its low volatility.[2] Samples will be prepared for analysis with

matrix-assisted laser desorption ionization time-of-flight mass spectrometry (MALDI-TOF-MS, or MALDI). MALDI data from the analysis of the untreated peptide will be compared to the bromelain-treated peptide and see if a specific cleavage site is observed. I predict the results of these studies will reveal that bromelain cleaves PSGL-1 within its active site.

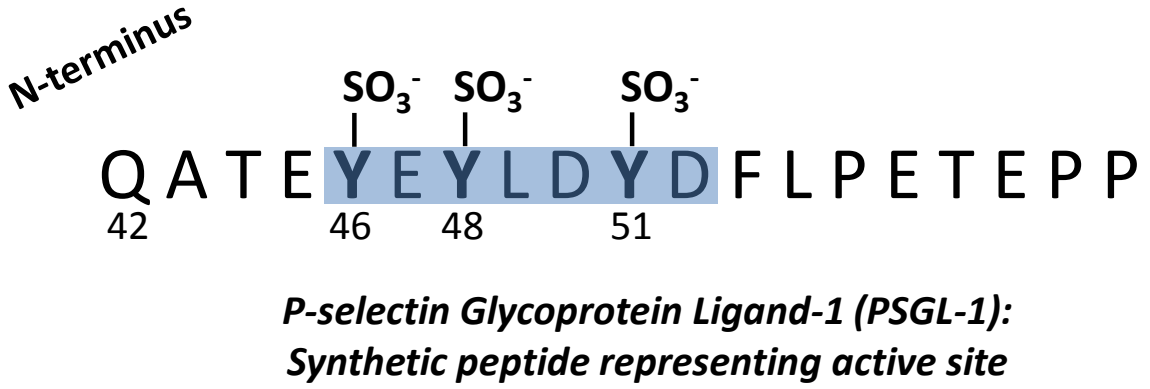

Figure 5.1 The 19-amino acid peptide shown above represents PSGL-1's N-terminal active site and will be used in bromelain digestion studies to see if bromelain is capable of cleaving off the epitope recognized by monoclonal antibody clone KPL-1 (shown in blue), which is required for P-selectin recognition.

The limitations of bioanalytical studies with a synthetic peptide include that the peptide may not have the tertiary structure that it has when it is presented in its native context, and thus bromelain may not act upon the PSGL-1 active site peptide in the same way it is able to act upon native PSGL-1 expressed on the surface of neutrophils. Furthermore, while peptide studies can reveal that bromelain is able to cleave within the active site, these studies will not be able to determine that bromelain is *not* cleaving PSGL-1 elsewhere. Thus, peptide studies will need to be supported by other studies involving native PSGL-1.

5.1.2 Studies involving recombinant human PSGL-1

Following analyses of bromelain digestions of the peptide active site, a recombinantly expressed human PSGL-1 (R&D Systems) will be obtained and incubated with bromelain to see

if the data reveals the expected peptides are cleaved from the N-terminal active site. The active site of the recombinant form of PSGL-1 has all the native modifications, including the tyrosine sulfations and the gycosylation moiety at Thr57, so it should be a more accurate model of what bromelain "sees" on the neutrophil surface when it cleaves PSGL-1, compared to the synthetic peptide. Digestion studies will be performed, samples will be prepared for analysis, and finally MALDI-TOF-MS analyses will be carried out to determine which peptide fragments were cleaved off during bromelain treatment. Tandem mass spectrometry (MS/MS) will be used to confirm the amino acid sequences of expected fragments observed in the initial MALDI analysis.

However, even these studies with recombinant PSGL-1 may be limited by the fact that the soluble protein may interact differently with bromelain than the cell surface-bound protein. PSGL-1 is expressed as a homodimer on the surface of leukocytes,[3] whereas the recombinant form exists as a monomer that is expressed attached to a mouse F_c chimera. In preliminary studies, I observed bromelain cleave recombinantly expressed PSGL-1 in more places than expected. For this reason, it is apparent that to concretely determine bromelain's effects on PSGL-1 at the molecular level, one will need to perform these bromelain digestion experiments with cell-surface-bound PSGL-1.

5.1.3 Studies involving neutrophil-expressed PSGL-1

To concretely confirm, at a molecular level, that bromelain is acting on PSGL-1 by cleaving the N-terminal portion of the active site as is suggested by results presented in Chapter 4, neutrophils will be treated with bromelain and the supernatant will be analyzed using mass spectrometry.

Mass spectrometry analysis of cell supernatant following bromelain treatment will be much more involved than studies on enzymatic digestion of a recombinant protein or peptide in solution. Bromelain is able to cleave synthetic peptides most efficiently with Arg-Arg sites and is able to preferentially cleave glycyl and alanyl bonds,[4] but unlike certain proteolytic enzymes that require specific consensus sequences to enable protein cleavage, bromelain does not appear to have a consensus sequence for cleavage. This makes it difficult to predit protein sensitivity based on the primary amino acid sequence alone.[5] Previous studies have shown that bromelain alters the expression levels of several cell-surface-bound proteins that are involved in cell adhesion and

migration.[5a,6] It is not unreasonable, therefore, to suspect that bromelain is able to cleave hundreds of cell surface bound proteins, which could result in the supernatant containing hundreds or thousands of different peptide fragments, which will make identifying the PSGL-1 fragments like finding a needle in a haystack.

Because the sample is a complex biological sample, high-performance liquid chromatography (HPLC) will be needed to help separate out the various components present in the sample. An LC/MS instrument that couples the separating power of HPLC with an electrospray ionization (ESI) source will be used to allow each peak that elutes off the column to be analyzed by mass spectrometry.

While LC/MS is a robust technique and is broadly used for analysis of biological samples,[7] considerable user time will be spent optimizing the experimental conditions, the sample preparation procedure, and the LC/MS method parameters.

At the experimental level, one will need to optimize the bromelain concentration and digestion time such that enzymatic cleavage of PSGL-1 occurs without over-digesting the peptide of interest to the point where it is no longer detectable in the supernatant. To start, the optimized digestion conditions from the studies with the synthetic PSGL-1 active site peptide and with the recombinantly expressed PSGL-1 protein will be used. However, I anticipate a higher concentration of enzyme and longer digestion time may be needed in the experiments with neutrophils for two reasons: Cells have a much lower diffusion rate than proteins or peptides, therefore the probability of bromelain-neutrophil interactions will be lower, and since bromelain is able to cleave many different proteins on the cell surface, I suspect it will take longer to cleave cell surface-bound PSGL-1, compared to the solution-phase protein or peptide. After treating neutrophils with bromelain, the neutrophils will be pelleted at a speed that causes minimal damage to the cells (to prevent cell lysis and membrane disruption) but also is sufficient for the removal of the majority of cellular components from the supernatant. Following centrifugation, the supernatant will be removed and prepared for LC/MS analysis.

The sample preparation stage will be critical to the success of the LC/MS analysis. The supernatant will be run though a molecular weight cut-off filter (5 kDa) to remove high-molecular weight proteins and peptides that are not of interest to the analysis and that could clog

the chromatography column. Next, the salts will need to be removed from the sample by performing a standard procedure for trichloracetic acid precipitation of proteins and peptides from the solution.[8] Following several rinse steps, the peptide will be resuspended in an appropriate mobile phase.

Finally, numerous aspects of the LC/MS analytical method will need to be optimized. These include the contents of the mobile phase, flow rate, and column type and size, as well as the voltage for sample ionization. The goal in optimizing these parameters will be to allow sufficient separation of the various components in the samples to achieve efficient sample ionization and obtain a clean MS spectrum for each time-resolved LC peak.

I expect that knowledge from prior mass spectrometry analyses of bromelain-treated recombinant PSGL-1 and bromelain-treated synthetic peptide will help us optimize the conditions for the analysis of the cell supernatant from bromelain-treated neutrophils. If it is known where bromelain cleaves PSGL-1, solid-phase synthesis can be used to synthesize the peptide fragment and the peptide can be run on LC/MS to determine what time it elutes. Then when the cell supernatant is run on the LC/MS, the elution time of the expected peptide fragment can be anticipated in order to collect MS data on that peak. If the peak for the PSGL-1 peptide fragment is time-resolved, it will also be possible to use standards of the pure PSGL-1 fragment to create a calibration curve that can be used to quantitatively determine the peptide levels in the supernatant. Overall, these studies will help us confirm, at a molecular level, how bromelain is acting upon PSGL-1 expressed on primary neutrophils *in vitro*.

5.2 A more physiologically relevant model system: How does bromelain affect neutrophil recruitment to cytokine-stimulated endothelial cell monolayers?

During an immune response, dying cells and bacteria secrete chemicals, such as cytokines that stimulate the endothelial lining of the blood vessel. Cytokine stimulation causes the endothelial cells to express P-selectin and E-selectin, among numerous other biomolecules that participate in the leukocyte adhesion cascade (Scheme 1.1).[9]

For decades, researchers have isolated and cultured human umbilical vein endothelial cells (HUVECs, Figure 5.2) for biological studies—in fact, most of the current understanding of the functioning of human endothelial cells is derived from experiments with cultured HUVECs.[10] A portion of these experiments have been applications of HUVECs in leukocyte flow assays with parallel-plate flow chambers.[10] In the work described in Chapters 3 and 4, I used parallel-plate flow chambers to study leukocyte interactions with substrates presenting proteins, P-selectin or E-selectin, which are responsible for the initial tethering and rolling of leukocytes to the inflamed endothelium. The advantage of using photochemistry to generate substrates for leukocyte flow assays is the ability to immobilize multiple components and control the density of biomolecules presented. Leukocyte flow assays with substrates generated in this manner can assess the unique role that the individual components play in the process of leukocyte rolling. The primary shortcoming of using this method for generating biomolecular substrates that serve as models of the blood vessel, however, is that such substrates present proteins in a non-native context and in a highly simplified environment. In other words, a protein that is chemically

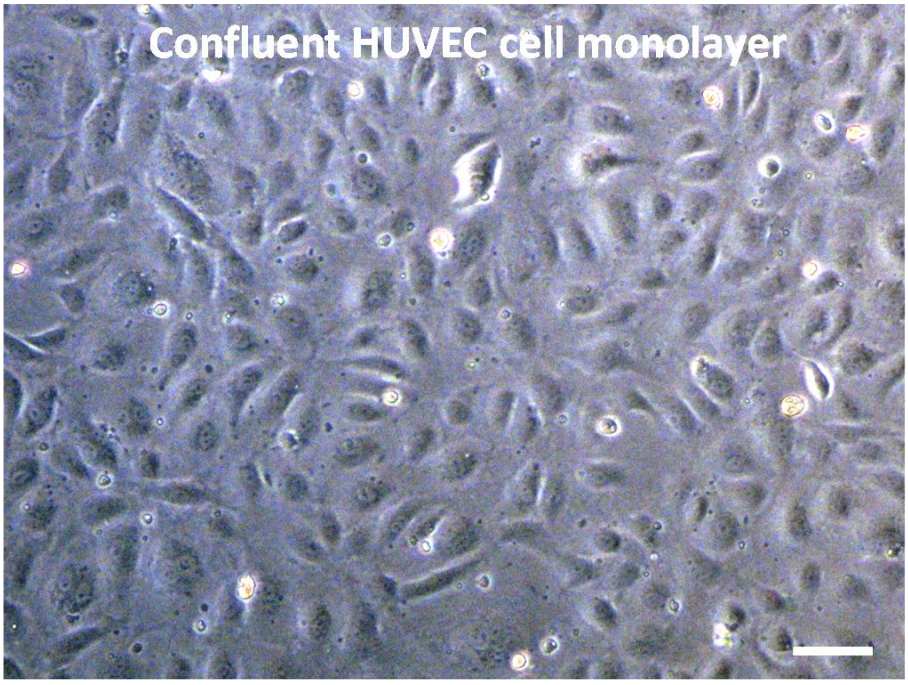

Figure 5.2 Cytokine-stimulated monolayers of human umbilical vein endothelial cells (HUVECs) will be used as a model of the inflamed endothelium in future neutrophil flow assays. Scale bar: 30 μm.

attached to a surface will appear very different to leukocytes than a protein presented on the surface of endothelial cells in a blood vessel.

Experiments on HUVECs have yielded a wealth of information regarding the effect of cytokine stimulation on the expression of biomolecules involved in the leukocyte adhesion cascade, including P-selectin,[9a,11] E-selectin,[9a,11c,12] ICAM-1,[13] and VCAM-1.[11b] Of greatest relevance to these studies, numerous reports show the use of HUVECs as a model of the inflamed endothelium in flow assays with leukocytes.[14] By using a parallel-plate flow chamber in conjunction with cytokine-stimulated HUVECs, researchers have studied leukocyte rolling and adhesion under conditions of physiological shear stress, with a substrate that is a more physiologically similar to the inflamed endothelium than simple biomolecules attached to a surface. Arguably, the most physiologically relevant environment is that which is inside a live animal, but while *in vivo* studies have been of enormous utility to the current understanding of the inflammatory response, they are limited by the lack of ability to control various experimental parameters, such as vessel diameter and flow rate. By using HUVECs for *in vitro* leukocyte flow assays, researchers strike a balance between physiological accuracy and experimental control.

Previous studies have shown that certain inflammatory mediators cause specific proteins to be upregulated without affecting the expression of others. More specifically, histamine-stimulated HUVECs have been found to upregulate P-selectin expression while E-selectin expression is unaffected,[14a] and studies in rabbit models of inflammation suggest that stimulation with IL-1β causes an upregulation in E-selectin expression without affecting P-selectin levels.[15]

These previous research studies suggest that it may be possible to independently control the expression P-selectin and E-selectin, the two endothelial-expressed selectins responsible for leukocyte tethering and rolling, on cultured monolayers of HUVECs. Given this ability, I envision that one could extend the *in vitro* studies on the role of bromelain treatment on selectin-mediated neutrophil recruitment to substrates presenting cytokine-stimulated HUVECs, which are more physiologically relevant than proteins immobilized on glass substrates.

One could carry out the following experiments with cultured HUVECs. First, it will need to be confirmed that given the reported conditions, HUVECs can independently upregulate either P-selectin or E-selectin through cytokine stimulation with histamine or IL-1β, respectively.

HUVECs will be cultured to confluency in a 96-well plate. At 2 days post-confluency, cells will be stimulated for 24 hours in the presence of 20 ng/mL of IL-4 or TNF-α. Following stimulation, cells will be fixed, blocked, and stained with fluorescently labeled antibodies that recognize P-selectin or E-selectin. The following controls will be performed: unstimulated cells will be stained with fluorescently labeled antibodies against P-selectin and E-selectin, and histamine- or IL-1β- stimulated cells will be stained with fluorescently labeled isotype control antibodies to account for nonspecific antibody binding. Data will be analyzed to confirm that histamine upregulates P-selectin independently of E-selectin, and IL-1β upregulates E-selectin independently of P-selectin.

Once it is confirmed that cytokine stimulation upregulates P-selectin or E-selectin in the expected manner, HUVECs will be cultured in 35-mm culture dishes and use the same conditions used in the 96-well plate assays to stimulate cells to express P-selectin or E-selectin. Then neutrophils will be isolated from whole blood, characterize them for purity and viability, and use them in leukocyte flow assays to determine the role of bromelain treatment on the ability of neutrophils to tether to and roll on stimulated HUVECs. In preparation for leukocyte flow assays, neutrophils will be treated with bromelain or buffer, as described in Chapter 4. Briefly, neutrophils will be incubated for 30 min at 37 °C in 50 μg/mL bromelain in HBSS with Ca^{2+} and Mg^{2+}, or in HBSS buffer alone. Cells will be rinsed, pelleted, and resuspended in HBSS with Ca^{2+} and Mg^{2+} and 0.5% human serum albumin (HSA) at 0.5 E 6 cells/mL. A 35-mm circular parallel plate flow chamber will be assembled with the 35-mm culture dishes containing cytokine-stimulated HUVECs. Neutrophils will be introduced into the chamber with the flow rate at a predetermined flow rate that will be controlled by a syringe pump. Videos of neutrophils interacting with HUVECs will be recorded and analyzed using ImageJ software to determined the number of new tethers formed per unit time and area. The fully processed data will be compared to the results from Chapter 4's flow assay studies that involved the use of benzophenone-immobilized P-selectin and E-selectin substrates, to see if the same trends are observed in both sets of data.

5.3 Biomolecular gradient studies: How do neutrophils process solution-phase and surface-bound biomolecular signals simultaneously *in vitro*?

My previous studies on the leukocyte adhesion cascade have focused on the first step of the process: selectin-mediated tethering and rolling, and on the effects that bromelain treatment has on the ability of leukocytes to be recruited to surfaces presenting immobilized P-selectin and E-selectin. Another interesting component of leukocyte recruitment that is still not completely understood is the process of cell migration to the site of infection in response to immobilized and soluble-phase cues. The process of cell migration has been previously studied involving both leukocytes[16] and other adhesive cells.[1,17]

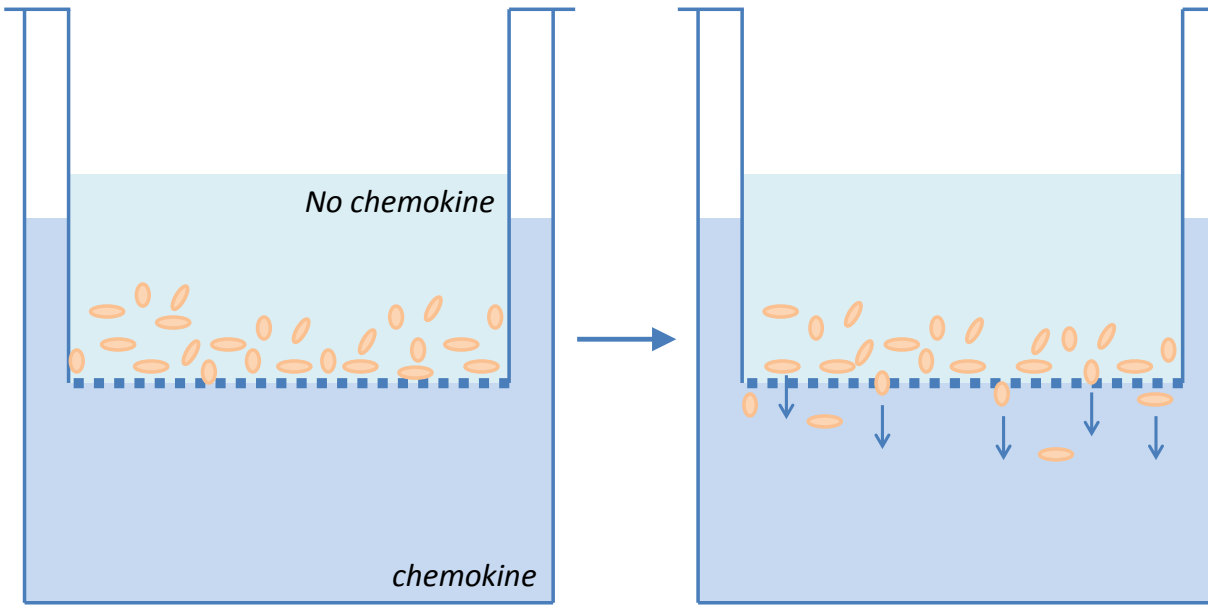

Figure 5.3 Schematic representation of a Transwell migration assay. Cells are suspended in solution in the absence of chemokine and placed in a well which has a permeable membrane base. Over time, cells are observed to migrate through the membrane in response to the soluble chemokine gradient.

A traditional approach to studying leukocyte migration in response to chemokines involves the use of Transwell migration assays. Cells are placed inside a well whose base is composed of a permeable membrane (Figure 5.3). The well is placed inside a solution containing

a cytokine, and cells respond by moving in the direction of the higher concentration of cytokine and migrate through the membrane. The extent of migration is characterized by determining the number of cells that transmigrated through the permeable membrane.[16b] Transwell migration assays have been used by researchers to study the effect of bromelain treatment on the ability of neutrophils to migrate in response to two different chemotaxis-inducing molecules, a bacterial peptide formyl-Met-Leu-Phe (fMLP) and IL-8, showing that bromelain treatment abolishes migration in response to IL-8 but not fMLP.[16b]

The Transwell migration assay, due to the relative ease of the experiment, is a good starting point for basic studies on cell migration in response to biological cues. The primary limitation of the Transwell assay, however, is that it does not present the cells or the cues in a physiologically relevant setting. For example, a prerequisite to cell migration through the extracellular matrix (ECM) is the ability of the migrating cell to adhere to ECM proteins—this is true of both adhesive cells and leukocytes.[18] But in a Transwell assay, cells are suspended in a solution, and the mechanism by which the cells migrate through the permeable membrane in response to soluble cues is independent of adhesion to ECM proteins, and therefore not representative of the mechanism by which cells undergo chemotaxis in a physiological environment.

In an effort to improve upon the Transwell migration assay, researchers have turned to hydrogels, Matrigel, and collagen matrices, each composed of cross-linked biological polymers.[19] For example, a protein gradient can be made in a three-dimensional collagen matrix by placing two reservoirs, one with protein solution and the other with buffer or a second protein component, on each site of the hydrogel. The resulting solution-phase gradients presented within the hydrogel can be used to study cell migration in response to soluble gradient cues.[20] It is possible to generate immobilized gradients of proteins within a hydrogel construct by tailoring the hydrogel to present a photochemical crosslinker, such as benzophenone, creating a solution-phase gradient within the hydrogel, and then using light to immobilize the solution-phase gradient to the hydrogel.[19b] In this way, hydrogels have been demonstrated to be applicable to probing migration in response to both soluble and immobilized cues.

A third approach to studying cell migration utilizes microfluidics to generate a solution-phase gradient of biomolecules. In some demonstrations, the solution-phase gradients are converted into immobilized gradients by using a surface chemistry tethering approach, such as EDC/NHS coupling.[21] Other approaches, such as electrochemical desorption,[22] photochemical deprotection,[23] and diffusion-guided surface adsorption[24] have also previously been used to generate surface-immobilized gradients for applications in cell biology. It is also possible to generate solution-phase gradients through diffusion[16g] or through the use of microfluidic gradient generation devices.[25] These demonstrations of solution-phase gradient generation with microfluidics are part of the necessary groundwork for studying the interplay between immobilized biomolecules and solution-phase gradients.

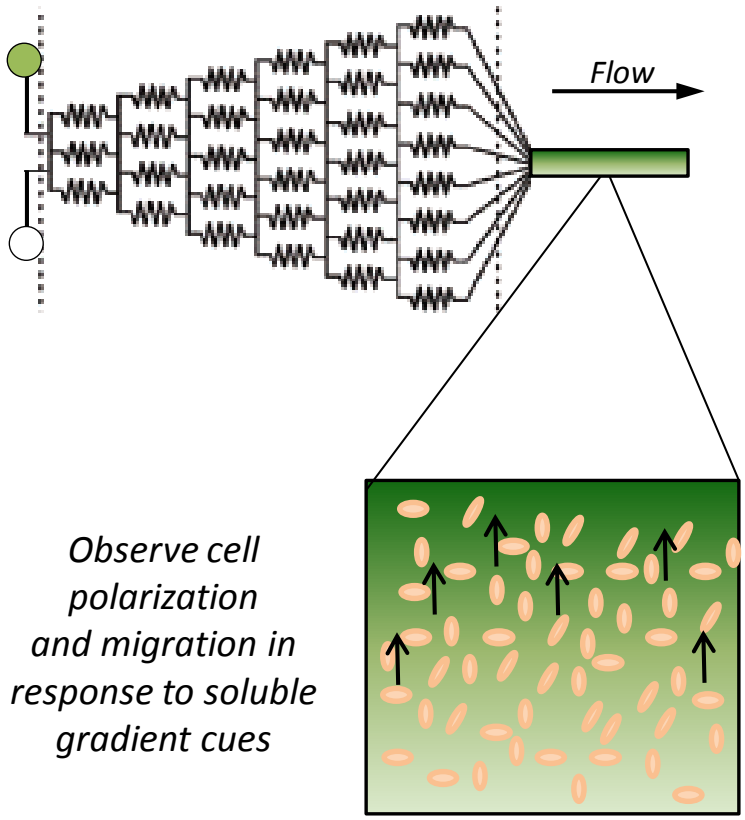

Figure 5.4 Schematic of microfluidic gradient generation device that will be used to create a solution-phase gradient. Adherent cells will be observed under a microscope to see if they migrate in response to the soluble gradient, and the effects of bromelain on cell adhesion and migration will be investigated. Adapted from reference.[1]

I envision that one could couple the methodology I developed for the generation of immobilized gradients with microfluidic gradient generation to study the interplay between immobilized biomolecular signals and soluble biomolecular signals (Figure 5.4). I could generate a surface-immobilized biomolecular gradient on a BP-modified substrate and then assemble the substrate with a microfluidic device that will allow the introduction of a solution-phase gradient[25c] on top of the immobilized gradient.

As a proof-of-concept demonstration of the technique, one could generate BP-modified substrates presenting immobilized fibronectin. After allowing neutrophils to adhere to the native ECM protein, the substrate will be rinsed to remove non-adherent neutrophils and assemble the substrate with a microfluidic gradient generation device. A one-component solution-phase gradient of fMLP or IL-8 will be generated over the immobilized neutrophils, and time-lapse microscopy will be used to visualize the migration of neutrophils in response to each individual biomolecular cue. To assess the effect of bromelain treatment on the ability of neutrophils to both adhere to fibronectin and migrate in response to fMLP or IL-8, neutrophils will be treated with bromelain before seeding them onto fibronectin substrates. In contrast to the Transwell migration assays that have been previously reported to assess the affect of bromelain treatment on migration in response to fMLP and IL-8,[16b] this new approach will take into consideration that under physiological conditions, migrating cells must first adhere to ECM proteins before they undergo polarization in response to chemotactic molecules. These initial studies could lead to a better understanding of the mechanism underlying bromelain's anti-inflammatory properties by assessing the effect of bromelain treatment on neutrophil adhesion *and* subsequent migration in response to inflammatory signals..

Following these studies, one could perform experiments combining solution-phase and immobilized biomolecular gradients to determine the effect of presenting a cell with both immobilized and solution-phase gradients of chemotactic molecules. A substrate presenting a uniform density of fibronectin will be generated and an overlapping immobilized gradient of IL-8 or fMLP. These substrates will be characterized with fluorescence analysis as described in Chapter 2. The microfluidic setup will then be used to create a solution-phase gradient of fMLP or IL-8, either in the same direction as the immobilized gradient, or in the opposite direction. Subsequent cell adhesion and migration studies will reveal if adherent neutrophils migrate at a

faster rate in the presence of both a solution-phase and immobilized gradient. In the case of the opposing gradients, the studies will reveal which of the two types of gradients—the solution-phase or immobilized—is able to out-compete the other to cause cells to migrate in one direction or the other. These studies will help shed light on the interplay between solution-phase and immobilized biomolecular cues during leukocyte migration.

Dual-gradient experiments can also be extended to study the effects of bromelain on neutrophil adhesion and migration. Experiments will be performed with substrates presenting fibronectin plus an immobilized fMLP or IL-8 gradient in the absence of a solution-phase gradient, and with substrates presenting fibronection in the presence of a solution-phase fMLP or IL-8 gradient only. These studies will help determine if bromelain's ability to reduce migration is dependent on the nature of the biomolecular gradient (solution-phase vs. immobilized). Data from these experiments will assist in the design of additional *in vitro* experiments on bromelain's effects on cell migration in response to biomolecular cues.

5.4 Conclusion

The proposed work described in this chapter will serve to elucidate the molecular details underlying bromelain's effects on various aspects of the leukocyte adhesion cascade, and will also shed light on the interplay of multiple biomolecular cues on neutrophil adhesion and migration. All in all, the photochemical methodology for the generation of biomolecular interfaces, in conjunction with the future work described in this chapter, will result in a better understanding of bromelain's mode of action and will lay the groundwork for the development of more effective anti-inflammatory treatments.

5.5 References

1. R. C. Gunawan, J. Silvestre, H. R. Gaskins, P. J. A. Kenis, D. E. Leckband, *Langmuir* **2006**, *22*, 4250.

2. H. Sterling, J. Batchelor, D. Wemmer, E. Williams, *Journal of the American Society for Mass Spectrometry* **2010**, *21*, 1045.

3. Y. Huo, L. Xia, *Trends in Cardiovascular Medicine* **2009**, *19*, 140.

4. H. R. Maurer, *Cellular and Molecular Life Sciences* **2001**, *58*, 1234.

5. a) L. P. Hale, P. K. Greer, G. D. Sempowski, *Clinical Immunology* **2002**, *104*, 183; b) A. D. Rowan, D. J. Buttle, A. J. Barrett, *Archives of Biochemistry and Biophysics* **1988**, *267*, 262.

6. L. Hale, B. Haynes, *Journal of Immunology* **1992**, *149*, 3809.

7. N. Takahashi, T. Isobe, *Proteomic Biology Using LC-MS*, John Wiley & Sons, Inc., Hoboken, New Jersey, **2008**.

8. L. Jiang, L. He, M. Fountoulakis, *Journal of Chromatography A* **2004**, *1023*, 317.

9. a) L. Yao, J. Pan, H. Setiadi, K. D. Patel, R. P. McEver, *The Journal of Experimental Medicine* **1996**, *184*, 81; b) S. L. Cuvelier, K. D. Patel, *The Journal of Experimental Medicine* **2001**, *194*, 1699.

10. C. D. Helgason, C. L. Miller, Humana Press, Totowa, New Jersey, **2005**, pp. 315.

11. a) Y. Khew-Goodall, C. Butcher, M. Litwin, S. Newlands, E. Korpelainen, L. Noack, M. Berndt, A. Lopez, J. Gamble, M. Vadas, *Blood* **1996**, *87*, 1432; b) K. D. Patel, *Blood* **1998**, *92*, 3904; c) K. D. Patel, *The Journal of Immunology* **1999**, *162*, 6209; d) G. Woltmann, C. A. McNulty, G. Dewson, F. A. Symon, A. J. Wardlaw, *Blood* **2000**, *95*, 3146; e) S. Kukreti, K. Konstantopoulos, C. W. Smith, L. V. McIntire, *Blood* **1997**, *89*, 4104.

12. a) L. H. Ulfman, D. P. H. Joosten, J. A. M. van der Linden, J.-W. J. Lammers, J. J. Zwaginga, L. Koenderman, *The Journal of Immunology* **2001**, *166*, 588; b) J. Kitayama, C. R. Mackay, P. D. Ponath, T. A. Springer, *The Journal of Clinical Investigation* **1998**, *101*, 2017.

13. G. Constantin, M. Majeed, C. Giagulli, L. Piccio, J. Y. Kim, E. C. Butcher, C. Laudanna, *Immunity* **2000**, *13*, 759.

14. a) A. Burns, R. Bowden, Y. Abe, D. Walker, S. Simon, M. Entman, C. Smith, *Journal of Leukocyte Biology* **1999**, *65*, 299; b) M. Lawrence, L. McIntire, S. Eskin, *Blood* **1987**, *70*, 1284.

15. A. Olofsson, K. Arfors, L. Ramezani, B. Wolitzky, E. Butcher, U. von Andrian, *Blood* **1994**, *84*, 2749.

16. a) N. Agrawal, M. Toner, D. Irimia, *Lab on a Chip* **2008**, *8*, 2054; b) D. J. Fitzhugh, S. Shan, M. W. Dewhirst, L. P. Hale, *Clinical Immunology* **2008**, *128*, 66; c) E. F. Foxman, E. J. Kunkel, E. C. Butcher, *Journal of Cell Biology* **1999**, *147*, 577; d) G. E. Rainger, C. Buckley, D. L. Simmons, G. B. Nash, *Current Biology* **1997**, *7*, 316; e) D. A. Steeber, M. L. K. Tang, N. E. Green, X.-Q. Zhang, J. E. Sloane, T. F. Tedder, *Journal of Immunology* **1999**, *163*, 2176; f) E. Berthier, J. Surfus, J. Verbsky, A. Huttenlocher, D. Beebe, *Integrative Biology* **2010**, *2*, 630; g) D. Kim, M. A. Lokuta, A. Huttenlocher, D. J. Beebe, *Lab on a Chip* **2009**, *9*, 1797.

17. a) K. C. Chaw, M. Manimaran, F. E. Tay, S. Swaminathan, *Microvascular Research* **2006**, *72*, 153; b) B. N. Goguen, B. Imperiali, *ACS Chemical Biology* **2011**, *6*, 1164; c) X. Y. Jiang, D. A. Bruzewicz, A. P. Wong, M. Piel, G. M. Whitesides, *Proceedings of the National Academy of Sciences of the United States of America* **2005**, *102*, 975; d) D. Jowhar, G. Wright, P. C. Samson, J. P. Wikswo, C. Janetopoulos, *Integrative Biology* **2010**, *2*, 648.

18. D. Wedlich, WILEY-VCH Verlag GmbH & Co., KGaA, Weinheim, **2005**.

19. a) D. S. W. Benoit, K. S. Anseth, *Acta Biomaterialia* **2005**, *1*, 461; b) X. Cao, M. S. Shoichet, *Journal of Biomaterials Science -- Polymer Edition* **2002**, *13*, 623; c) V. Chan, P. Zorlutuna, J. H. Jeong, H. Kong, R. Bashir, *Lab on a Chip*, *10*, 2062; d) J. Y. Wong, A. Velasco, P. Rajagopalan, Q. Pham, *Langmuir* **2003**, *19*, 1908; e) H. Y. Yoshikawa, F. F. Rossetti, S. Kaufmann, T. Kaindl, J. Madsen, U. Engel, A. L. Lewis, S. P. Armes, M. Tanaka, *Journal of the American Chemical Society* **2011**, null.

20. V. V. Abhyankar, M. W. Toepke, C. L. Cortesio, M. A. Lokuta, A. Huttenlocher, D. J. Beebe, *Lab on a Chip* **2008**, *8*, 1507.

21. R. C. Gunawan, E. R. Choban, J. E. Conour, J. Silvestre, L. B. Schook, H. R. Gaskins, D. E. Leckband, P. J. A. Kenis, *Langmuir* **2005**, *21*, 3061.

22. S. T. Plummer, Q. Wang, P. W. Bohn, R. Stockton, M. A. Schwartz, *Langmuir* **2003**, *19*, 7528.

23. W. S. Dillmore, M. N. Yousaf, M. Mrksich, *Langmuir* **2004**, *20*, 7223.

24. a) L. J. Millet, M. E. Stewart, R. G. Nuzzo, M. U. Gillette, *Lab on a Chip* **2010**, *10*, 1525; b) C. J. Wang, X. Li, B. Lin, S. Shim, G.-l. Ming, A. Levchenko, *Lab on a Chip* **2008**, *8*, 227.

25. a) T. M. Keenan, A. Folch, *Lab on a Chip* **2008**, *8*, 34; b) T. Ahmed, T. S. Shimizu, R. Stocker, *Integrative Biology* **2010**, *2*, 604; c) Y. He, A. Kapoor, S. Cook, S. Liu, Y. Xiang, C. V. Rao, P. J. A. Kenis, F. Wang, *Journal of Cell Science* **2011**, *124*, 2153.